Chapter 5

Conformational Study of Substance P through Molecular Dynamics and NMR Spectroscopy in Different Solvents

5.1 Summary

The present study is a combined approach using nuclear magnetic resonance (NMR) and molecular dynamics (MD) on the amidated and the free acid forms of substance P. The results obtained from both techniques have been compared in order to rationalize the structural characteristics of both peptide analogs in solution. From the NMR experiments it can be derived that the free acid form of the peptide adopts an extended conformation at the N-terminus and a helical conformation in the central and the C-terminus segments of the peptide in both water and methanol. These structural features are in agreement with the results obtained using MD. No remarkable differences have been observed between the amidated and the free acid forms of substance P in the MD simulations of both peptides in water, thus suggesting that differences in the activity of both peptide analogs are not due to their conformational preferences and could be due to the different interaction of the peptides with the receptor. A MD trajectory of the free acid form of the peptide within a box containing dymethyl sulfoxide (DMSO) molecules has also been carried out. In DMSO the peptide adopts an extended and rigid conformation in agreement with other studies that suggest that DMSO has a breaking effect on the weakly hydrogen bonded structures and decreases the number of backbone conformers. Finally, structures obtained from all the MD trajectories have been classified with in house developed software, CLASICO and CLUSTERIT. This software is suitable for the study of the evolution and comparison of the folding process through MD of peptides and proteins.

5.2 Introduction

Although characterizing the whole folding mechanism of proteins through molecular dynamics (MD) has remained elusive until now (Duan et al. 1998a, Duan et al. 1998b), folding studies of peptides through MD are within the reach for currently available computational power. The reversible folding of peptides through MD has been described in past years (Daura et al., 1998, Daura et al., 1999, Daura et al., 2001). Given that secondary structural motif formation seems to occur in the nanosecond timescale (Hummer et al., 2001), a 10-residue peptide is expected to fold during a 5 to 10 ns trajectory. Given the flexibility of peptides, from that point onwards the peptide fluctuates among a pool of folded and partially folded states. Regarding the solvent differences in the structural behavior arise when the peptide is placed in water or in organic solvents, such as methanol or DMSO. It is generally accepted that organic solvents rigidify the

peptide and favor secondary structure (Bodkin et al., 1995, Brooks III et al., 1993), whereas water allows for greater flexibility.

In the present study we have addressed the folding mechanism of, substance P, an 11-residue long neuropeptide of sequence Arg^{1}-Pro^{2}-Lys^{3}-Pro^{4}-Gln^{5}-Gln^{6}-Phe^{7}-Phe^{8}-Gly^{9}-Leu^{10}-Met^{11} and its amide, in different solvents using MD. The C-terminal residue of Substance P suffers a post-translational modification *in vivo*, and the carboxylic group of Met^{11} is amidated in order to attain the its active form (Fournier et al., 1982). Accordingly, substance P has been studied in the present work in both its native form, i.e. amidated in the C-terminus (SP) and its free acidic form (SPOH), i.e. with the terminal methionine deamidated. Since the latter exhibits no biological activity (Murokoshi et al., 1983) the characterization of the conformational profile of the peptides, may identify structural differences that may provide insights into the structural requirements for activity of the neuropeptide.

Although the folding of peptides can be reproduced using MD simulations, experimental validation is still required. NMR experiments have shown to be of great importance to validate the folding of peptides (Daura et al. 2001). Therefore, NMR experiments with substance P in methanol and water were carried out concomitantly with the simulations and the results are compared.

Regarding the structural features of SP and SPOH, several reports both experimental and theoretical, devoted to discuss the conformational profile of SP have appeared in the past, however none of them can be considered as definitive. Different spectroscopic studies were carried out in water and organic solvents using diverse techniques, including NMR studies (Chassaing et al., 1986, Sumner et al. 1990, Shukla et al., 1991, Patel et al., 2001), circular dichroism, Raman and IR spectroscopy (Mehlis et al. 1975, Mehlis et al., 1980). Other studies were undertaken in model membranes and surfactants using NMR spectroscopy (Miyazawa, 1984, Schwyzer et al., 1986, Erne et al, 1986, Rolka et al., 1986, Williams et al., 1990, Young et al., 1994). Moreover, substance P was also studied by energy calculations (Nikiforovich, et al. 1981, Manavalan et al., 1981, Manavalan et al., 1982) and more recently, by limited simulations using molecular dynamics (Wymore et al., 1999a, Wymore et al., 1999b, Coutinho et al, 1998).

This series of studies clearly point out the dependence of the conformation of the peptide with the environment. Thus, whereas in DMSO and pyridine the peptide exhibits an extended conformation, in water, NMR studies suggest *some degree of folding* in the region between residues 5 to 11 (Chassaing et al., 1986). Furthermore, in methanol, the same authors proposed that the peptide attains a certain structure consisting in either a 3_{10}-helix along the segment Gln^{5}-Gln^{6}-Phe^{7}-Phe^{8} or a α-helix along the segment Pro^{4}-Gln^{5}-Gln^{6}-Phe^{7}-Phe^{8}, with the N-terminus region segment Arg^{1}-Pro^{2}-Lys^{3} being a flexible region and the C-terminal segment Gly^{9}-Leu^{10}-Met^{11} is oriented towards the side chains of Gln^{5} and Gln^{6}. Other studies suggest (Schwyzer et al.,

1986, Miyazawa, 1984, Rolka et al., 1986, Williams et al., 1990, Erne et al, 1986) that in lipid membranes and sodium dodecylsulfate, SP adopts a α-helical structure. Interestingly, a NMR study reported the comparison of the structures of a segment of the β-amyloid peptide (25-35) (Aβ25-35) and substance P showing a similar α-helical structure in their C-terminal regions in a trifluoroethanol (TFE)/water solution (Lee et al., 1999).

5.3 Methods

5.3.1 NMR experiments

5.3.1.1. NMR structure determination in water

Sample: 0.75 mg of substance P in its free acidic form (from SIGMA-ALDRICH S2136, purity > 99%) was dissolved in 0.5 mL of H_2O/D_20 (9:1). The pH of the sample was adjusted to 5.05 by additions of acetate buffer. Sodium azide (0.02% in weight) was added for sample conservation. One TOCSY (miximg time 70 ms) and a series of NOESY spectra at increasing miximg times (100, 200 and 400 ms) were acquired in a Bruker Avance 600. The spectra were processed with the software package NMRpipe, whereas the assignment of the resonances was carried out using NMRVIEW.

5.3.1.2. NMR structure determination in methanol

Sample: 0.75 mg of substance P in its free acidic form (from SIGMA-ALDRICH S2136, purity > 99%) was dissolved in 0.7 mL of CD_3OH (from SDS with isotropic enrichment >99.8). One TOCSY (mixing time 70 ms) and a series of NOESY spectra at increasing mixing times (100, 200 and 400 ms) were acquired in a Bruker Avance 600 .The spectra were processed with the software package NMRpipe, whereas the assignment of the resonances was carried out using NMRVIEW.

5.3.2. Molecular dynamics

All the calculations were carried out within the molecular mechanics framework by means of the AMBER 5 package (Case et al., 1997) using the Cornell force field (Cornell et al., 1995). The missing RESP charges were obtained by *Ab initio* calculations performed with the GAUSSIAN94 package (Frisch et al., 1995).

5.3.2.1. Molecular dynamics of SP in water

In order to simulate SP in its native form, the peptide was generated with its methionine amidated (Men) using the PREP module of AMBER 5 package. RESP charges of the Men residue were computed by the combined use of the GAUSSIAN94 package and the RESP module of AMBER 5. The former was used to fit the molecular electrostatic potential (MEP) to point charges located on the nuclei. MEPs were computed at Hartree-Fock level with a 6-31G* basis set. The RESP module of AMBER was used to adjust the electrostatic potential with the addition of hyperbolic restraints on charges on non-hydrogen atoms in two steps. In the second step equivalent hydrogen atoms are assigned the same charge (Cornell et al., 1995). The charges obtained are shown in Table 5.1.

The peptide was minimized with the module SANDER *in vacuo* using a dielectric constant of 80. 1500 cycles of steepest descent followed by the conjugated gradient method were applied until the RMS distance between two consecutive structures was smaller than 0.001 kcal·mol^{-1}·Å^{-1}. Subsequently, the peptide was soaked in a rectangular box containing 1233 TIP3P water molecules. The dimensions of the box were chosen in such a way that the minimum distance from the peptide in its extended conformation to the box wall was larger than 8 Å. The system was minimized fixing the coordinates of the peptide and allowing the water molecules to move. A dielectric constant ε =1 and a cutoff of 10 Å were used. A trajectory of 100 ps was carried out using periodic boundary conditions at constant temperature (300 K) and constant pressure (1 atm), with a cutoff of 10 Å. An integration step of 2 fs in conjunction with the use of the SHAKE algorithm to constrain the stretching of bonds involving hydrogen atoms was applied. The translation and rotational motion was removed after 1000 steps and at the beginning of each 500 ps fragment of MD. Then, the system was changed to Particle Mesh Ewald conditions with a grid spacing of 1 Å and a tolerance for the Ewald sum of 10^{-5}. A snapshot was recorded after each ps and the MD trajectory was extended for 40 ns.

Table 5.1.AMBER parameters computed for the amidated methionine residue.

ATOM				RADIUS (IJ)	ANGLE (IJK)	DIHEDRAL ANGLE (IJKL)	CHARGE	BACK-BONE ATOM TYPE	ATOM	
I	J	K	L						TYPE	NAME
1	0	-1	-2	0	0	0	0	M	DU	DUMM
2	1	0	-1	1.449	0	0	0	M	DU	DUMM
3	2	1	0	1.522	111.1	0	0	M	DU	DUMM
4	3	2	1	1.335	116.6	180	-0.3762	M	N	N
5	4	3	2	1.01	119.8	0	0.25	E	H	H
6	4	3	2	1.449	121.9	180	-0.0182	M	CT	CA
7	6	4	3	1.09	109.5	300	0.0967	E	H1	HA
8	6	4	3	1.525	111.1	60	-0.0012	3	CT	CB
9	8	6	4	1.09	109.5	300	0.0909	E	HC	HB2
10	8	6	4	1.09	109.5	60	0.0909	E	HC	HB3
11	8	6	4	1.525	109.47	180	-0.288	3	CT	CG
12	11	8	6	1.09	109.5	300	0.1335	E	H1	HG2
13	11	8	6	1.09	109.5	60	0.1335	E	H1	HG3
14	11	8	6	1.81	110	180	-0.2348	S	S	SD
15	14	11	8	1.78	100	180	-0.1041	3	CT	CE
16	15	14	11	1.09	109.5	60	0.0788	E	H1	HE1
17	15	14	11	1.09	109.5	180	0.0788	E	H1	HE2
18	15	14	11	1.09	109.5	300	0.0788	E	H1	HE3
19	6	4	3	1.522	111.1	180	0.4759	M	C	C
20	19	6	4	1.229	120.5	0	-0.5075	E	O	O
21	19	6	4	1.335	116.6	180	-0.6598	M	N	NA
22	21	19	6	1.01	119.8	180	0.3404	E	H	HA1
23	21	19	6	1.01	119.8	0	0.3404	E	H	HA2

5.3.2.2. Molecular dynamics of SPOH in water

The extended conformation of substance P in its free acid form (SPOH) was generated using the AMBER program. The peptide was minimized with the module SANDER *in vacuo* using a dielectric constant of 80. 1500 cycles of steepest descent followed by the conjugated gradient method were applied until the RMS distance between two consecutive structures was smaller than 0.001 kcal·mol^{-1}·Å^{-1}. This peptide was used as the starting point for the MD trajectories in explicit water, methanol and DMSO. Subsequently, the peptide was soaked in a rectangular box containing 1150 TIP3P water molecules. The dimensions of the box were chosen in such a way that the minimum distance from the peptide in its extended conformation to the box wall was larger than 8 Å. The system was minimized fixing the coordinates of the peptide and allowing the water molecules to move. A dielectric constant ε =1 and a cutoff of 10 Å were used. A trajectory of 100 ps was carried out using periodic boundary conditions at constant temperature (300 K) and

constant pressure (1 atm), with a cutoff of 10 Å. An integration step of 2 fs in conjunction with the use of the SHAKE algorithm to constrain the stretching of bonds involving hydrogen atoms was applied. The translation and rotational motion was removed after 1000 steps and at the beginning of each 500 ps fragment of MD. Then, the system was changed to Particle Mesh Ewald conditions with a grid spacing of 1 Å and a tolerance for the Ewald sum of 10^{-5}. A snapshot was recorded after each ps and the MD trajectory was carried out for 40 ns.

5.3.2.3. Molecular dynamics of SPOH in methanol

The methanol OPLS-AA parameters (Jorgensen et al., 1996) (listed in Table 5.2) derived from a gas phase optimization carried out with BOSS Version 4.2 (Jorgensen, 2000) were kindly provided by Prof. Bill Jorgensen. In the Lennard-Jones potential equation the *collision diameter* σ (the separation between two atoms whose energy is equal to zero) is related to the minimum of the Lennard-Jones potential (R*) by the equation:

$$R_{ij}^{*} = 2^{\frac{1}{6}} \cdot \sigma_{ij} \tag{5.1}$$

The collision diameter for two atoms can be estimated by the equation:

$$\sigma_{ij} = \sigma_{i} + \sigma_{j} \tag{5.2}$$

Moreover, in order to obtain a minimum of the Lennard-Jones potential valid for all the possible interactions of a given atom (R_i^*), the following equation can be used:

$$R_{i}^{*} = \frac{1}{2} R_{ii}^{*} \tag{5.3}$$

Equations (5.1-5.3) were used in order to transform OPLS-AA parameters into parameters readable by the AMBER package. The rotational barrier used for methanol was 1.36 kcal·mol^{-1} (Jorgensen et al., 1996). A methanol molecule was generated with the AMBER package and was minimized *in vacuo* with the sander module in order to obtain a good starting geometry. A dielectric constant ε = 32.63, corresponding to the experimental value for methanol was used (Lide et al., 1995a). A box containing 65 methanol molecules was generated. In order to obtain a good starting density for the box the maximum distance from the central methanol molecule to the borders of the box was estimated to be 8.2 Å. This was done assigning the density its value obtained from tables at 20º C, 0.7914 g·cm^{-3} (Lide et al., 1995b). A 10 ps MD trajectory simulation at 300 K was

followed with 40 ps at constant volume. Subsequently, the system was placed for 40 ps at constant pressure of 1 atm. Finally, the MD trajectory was extended for 490 ps using Particle Mesh Ewald conditions. For the latter fragment of the MD trajectory an average density equal to 0.749 $g \cdot cm^{-3}$ was obtained. This is in relative good agreement with the experimental data. This box was used as the building block in order to obtain a box of methanol molecules containing 1800 methanol molecules. In order to equilibrate the new box a heating MD trajectory for one ps with an integration step of 0.1 fs was carried out. After that, the integration step was increased to 0.5 fs and the trajectory was extended for 9 ps. The integration step was increased to 2 fs for a 40 ps trajectory. All these steps were done using the NVT ensemble. Subsequently, the system was placed in the NPT ensemble with a pressure equal to 1 atm and its trajectory extended for 40 ps. Keeping the same pressure, Particle Mesh Ewald conditions were applied to the system for 410 ps with an integration step of 2 fs. An average density of 0.724 $g \cdot cm^{-3}$ was obtained for the last 300 ps of the latter part of the trajectory (Figure 5.1.A).

Table 5.2. OPLS-AA methanol parameters used for the MD trajectories of SPOH.

I ATOM	SYMBOL	J ATOM	RADIUS (IJ)	K ATOM	ANGLE (IJK)	L ATOM	DIHEDRAL ANGLE (IJKL)
1	O	0	0	0	0	0	0
2	DUM	1	0.5	0	0	0	0
3	DUM	2	0.5	1	90	0	0
4	H	1	0.9457	2	90	3	180
5	C	1	1.4119	4	108.9898	2	180
6	HC	5	1.0904	1	110.239	4	180
7	HC	5	1.0904	1	110.54935	6	119.8507
8	HC	5	1.0904	1	110.5495	6	240.1493

ATOM NAME	ATOM NUMBER	A(II)	B(II)	CHARGE	SIGMA	EPSILON	R*
OH	1	578580.8	627.4	-0.6830	3.12	0.170	1.7510
	2	0.0	0.0	0.0000	0.00	0.000	All Solutes
	3	0.0	0.0	0.0000	0.00	0.000	All Solutes
HO	4	0.0	0.0	0.4180	0.00	0.000	0.0000
CT	5	892114.2	485.30	0.1450	3.50	0.066	1.9643
HC	6	7152.6	29.30	0.0400	2.50	0.030	1.4031
HC	7	7152.6	29.30	0.0400	2.50	0.030	1.4031
HC	8	7152.6	29.30	0.0400	2.50	0.030	1.4031

(A)

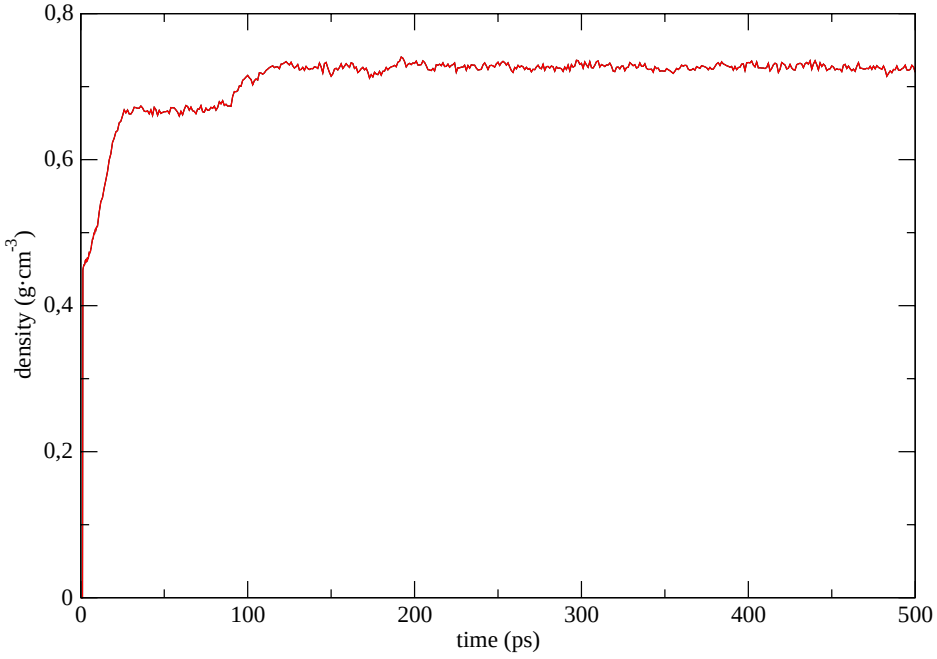

(B)

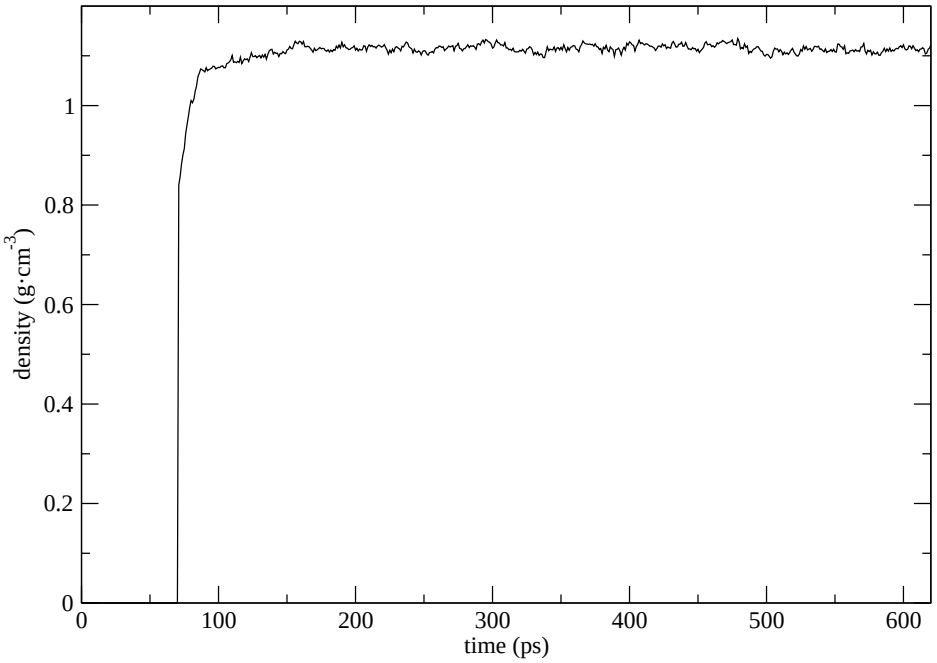

Figure 5.1. Density evolution for the equilibration phase of the MD trajectory of the box containing 1800 molecules of methanol (A) and the box containing 226 molecules of DMSO (B).

The equilibrated box of methanol molecules was used to carry out a MD trajectory with the peptide in its zwitterionic form. The peptide was minimized *in vacuo* with a dielectric constant of 80 as described above. Subsequently, the minimized peptide was soaked in a rectangular box containing 1796 methanol molecules. The system was minimized fixing the coordinates of the peptide and allowing the methanol molecules to move. A dielectric constant ε =1 and a cutoff of 10 Å were used. A trajectory of 100 ps was carried out using periodic boundary conditions at constant temperature (300 K) and constant pressure (1 atm), with a cutoff of 10 Å. An integration step of 2 fs in conjunction with the use of the SHAKE algorithm to constrain the stretching of bonds involving hydrogen atoms was applied. The translation and rotational motion was removed after 1000 steps and at the beginning of each 500 ps fragment of MD. Then, the system was changed to Particle Mesh Ewald conditions with a grid spacing of 1 Å and a tolerance for the Ewald sum of 10^{-5}. A snapshot was recorded after each ps and the trajectories were extended for more than 20 ns.

5.3.2.4. Molecular dynamics of SPOH in DMSO

DMSO molecule was generated using RESP parameters present in the literature (Fox et al, 1998) (Table 5.3). The DMSO molecule was minimized with the module SANDER *in vacuo* using a dielectric constant of 4.70. 1500 cycles of steepest descent followed by the conjugated gradient method were applied until the RMS distance between two consecutive structures was smaller than 0.001 kcal·mol^{-1}·Å^{-1}. The molecule was included in a box containing 226 molecules of DMSO. The system was minimized with 500 cycles of steepest descent plus 19500 cycles of conjugate gradient. A dielectric constant ε =1 and a cutoff of 12 Å were used for the entire trajectory. The system was heated from 0 to 300 K by running 5000 cycles with integration step of 2 fs in conjunction with the use of the SHAKE algorithm to constrain the stretching of bonds involving hydrogen atoms that was applied for the rest of the trajectory. Initial velocities were assigned from a Maxwellian distribution at temperature 0 K, periodic boundary conditions with constant volume were applied. Then, the system was kept in the same conditions for 60 ps. After that, the system was changed to constant pressure conditions at 1 atm and a compressibility of $52.5 \cdot 10^{-6}$ bar^{-1} (Liu et al., 1995) for 50 ps. Then, the system was changed to Particle Mesh Ewald conditions with a grid spacing of 1 Å and a tolerance for the Ewald sum of 10^{-5}. The system was kept for 500 ps under these conditions. The density was kept fairly constant for the later part of the trajectory (500 ps) with an average value of 1.11 g·cm^{-3} being the DMSO density listed in tables 1.1014 g·cm^{-3} (Figure 5.1.B) (Lide et al., 1995b).

The peptide used in its minimized conformation for water and methanol, containing the N-terminus and C-terminus in their charged form, was soaked in a box containing 588 DMSO molecules that was built using the equilibrated box obtained before. The system was placed under the same conditions used to equilibrate the box containing only DMSO molecules, i.e. following the

minimization, heating and equilibration protocols described above. A snapshot was recorded after each ps and the trajectories were extended for more than 20 ns.

Table 5.3. AMBER parameters used for the DMSO molecule (Parameters were taken from Fox et al., 1998).

ATOM		COORDINATES			CHARGE
No.	Name	X	Y	Z	
1	C1	1.366	-1.3	0.758	-0.324
2	1H1	2.419	-1.659	0.846	0.142
3	2H1	0.972	-1.612	-0.235	0.142
4	3H1	0.776	-1.828	1.542	0.142
5	S	1.347	0.432	0.91	0.315
6	O1	1.612	0.713	2.35	-0.521
7	C2	-0.351	0.727	0.678	-0.324
8	1H2	-0.533	1.828	0.709	0.142
9	2H2	-0.999	0.268	1.458	0.142
10	3H2	-0.685	0.346	-0.313	0.142

ANGLES	K_Q (kcal mol^{-1} rad^{-2})	Q_0 (DEG)
H1-CT-SZ	50.0	109.5
CT-SZ-CT	62.0	97.4
O-SZ-CT	80.0	106.75
H1-CT-H1	35.0	109.5

BONDS	K_B (kcal mol^{-1} Å^{-2})	R_0 (Å)
SZ-O	570.0	1.53
CT-SZ	227.0	1.81
CT-H1	340.0	1.09

DIHEDRALS	IDIVF	K_Q (kcal mol^{-1} rad^{-1})	PHASE (DEG)	PERIODICITY
H1-CT-SZ	3	0.85	109.5	3

5.3.2.5 Conformation classification

Conformations were classified using, the computer program CLASICO, developed in this laboratory and described in chapter 4. In order to compute the helical content and the helicity at each residue a modified version of the CLASICO program was run to compute the structures that attained α or 3_{10}-helical motifs at each residue without requiring that the criteria for the presence of helix was fulfilled by three consecutive residues.

5.3.2.6. Clustering of the structures

Patterns attained by the peptide are numerous and diverse. In order to tackle such diversity, we proceeded to group the conformations into clusters according to their similarity. Clusters were computed using an algorithm based on information theory. The algorithm considers that a pattern can be categorized unambiguously by the presence or absence of each of the secondary structure motifs. Therefore the pattern can be translated into a binary code and the number of bits or information contained in the pattern can be computed. For a detailed description of the method see chapter 4.

5.3.2.7 Transition analysis

The MD trajectory is translated for each structure into a pattern that is subsequently assigned to a cluster. It might be interesting to analyze the visiting sequence of the different clusters along the MD. This analysis may provide information about the intrinsic characteristics of the process. A *transition* is defined when a pattern belongs to a different cluster of the previous one already classified. The opposite can be considered as an *autotransition*. A cluster is defined as *stable* when the probability of suffering an autotransition is much higher than the probability of falling in that cluster in a random move, according to the size of the cluster. It is also possible to study the *reversibility* of transitions. Indeed, it is possible to determine whether the transitions taking place between two clusters occur with the same probability in both directions. A ratio of 1 is obtained when transitions in both directions are equally probable. However, this ratio must be higher than 1 for clusters that are sources, and smaller than 1 for clusters that are sinks. The percentage of transitions to a given cluster in regard to the total number of transitions of the cluster is called *local transitions.* Similarly, the percentage of transitions in regard to the total number of transitions is termed *global transitions* and provides a measure of the statistical relevance of such transition.

5.4. Results

5.4.1 NMR experiments

In order to assess the structural differences in solution, substance P has been studied in two different solvents, water and methanol. Furthermore, the data obtained are compared with the results obtained in the MD simulations. NMR assignment was done based upon the two-step procedure using a combination of TOCSY and NOESY spectra (Wüthrich, K, 1986).

5.4.1.1. Study of SPOH in water

The ^{1}H chemical shifts were assigned by the combination of TOCSY and NOESY experiments. Shifts for substance P in water are shown in Table 5.4 and a section of the TOCSY experiment is shown in Figure 5.4.A. Summary of the observed NOEs for SPOH in water are shown in Figure 5.2.A. Differences between the observed Hα proton chemical shifts and the random coil values described in Wüthrich (1986) are known as Hα conformational shifts (HαCS). Negative values of HαCS are indicative of helicity. The HαCS for each residue was calculated and plotted (Figure 5.3). The helical content of the peptide in water was estimated to be 10 %. These values were obtained by dividing the HαCS for each residue or the average HαCS (the sum of the HαCS for all the residues divided by the number of residues) by 0.38 ppm, considered to be the average shift for 100% helicity (Rizo et al., 1993, Wishardt, 1994). In the case of Gly^{9} the HαCS was computed in respect to the average values of the chemical shift for the two Hαs.

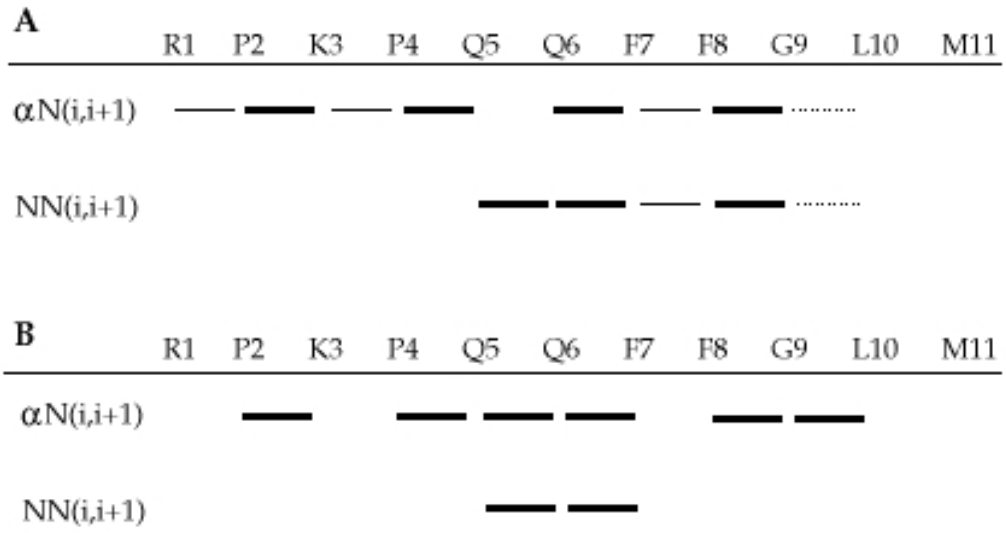

Figure 5.2. Summary of the observed NOEs for SPOH in A) water and B) methanol. Increasing line thickness represents increasing NOE intensity.

Table 5.4. Chemical shifts (ppm) of SPOH in water.

	NH	**αH**	**β_1H**	**β_2H**	**γ_1H**	**γ_2H**	**δ_1H**	**δ_2H**	**εH**
R1	7.26	4.42	1.98	1.98	1.75	1.75	3.27	3.27	
P2		4.52	2.05	2.36	2.06	2.06	3.78	3.60	
K3	8.57	4.57	1.85	1.85	1.54	1.54	1.72	1.72	3.02
P4		4.42	2.05	2.33	2.06	2.06			
Q5	8.50	4.22	1.97	1.97	2.32	2.32			
Q6	8.32	4.24	1.87	1.87	2.16	2.16			
F7	8.24	4.62	3.08	2.95					
F8	8.27	4.62	3.18	2.98					
G9	7.92	3.71,3.83							
L10	8.07	4.44	1.66	1.66	1.66	1.66			
M11	7.96	4.31	1.96	2.12	2.55	2.55			

5.4.1.2. Study of SPOH in methanol

Two different conformations arising due to slow isomerization around either the Arg-Pro or the Lys-Pro could be identified in the NMR spectrum. The chemical shifts for the most populated isomer are presented in Table 5.5 and a section of the TOCSY experiment is shown in Figure 5.4.B. The summary of the observed NOEs are shown in Figure 5.2.B. The HαCS for each residue was calculated and plotted (Figure 5.3). The average helical content (23 %) and the helical content for each residue (shown in Figure 5.5.B) for the most representative conformation were calculated.

Table 5.5. Chemical shifts (ppm) of SPOH in methanol.

	NH	αH	β_1H	β_2H	γ_1H	γ_2H	δ_1H	δ_2H
R1	7.62	4.25	1.92	1.92	1.76	1.76	3.21	3.21
P2		4.53					3.73	3.60
K3	8.52	4.57	1.96	1.96	1.72	1.72	1.53	1.53
P4		4.33			2.31	2.31	3.80	3.73
Q5	8.74	4.14	2.37	2.37	2.02	2.02		
Q6	8.14	4.23	2.22	2.22	1.99	1.99		
F7	7.92	4.41	2.99	2.99	2.86	2.86		
F8	7.93	4.46	3.26	3.26	3.00	3.00		
G9	7.97	3.69,3.96						
L10	7.80	4.46	1.62	1.62	1.62	1.62	0.92	0.92
M11	8.08	4.40	1.97	2.10	2.53	2.53		

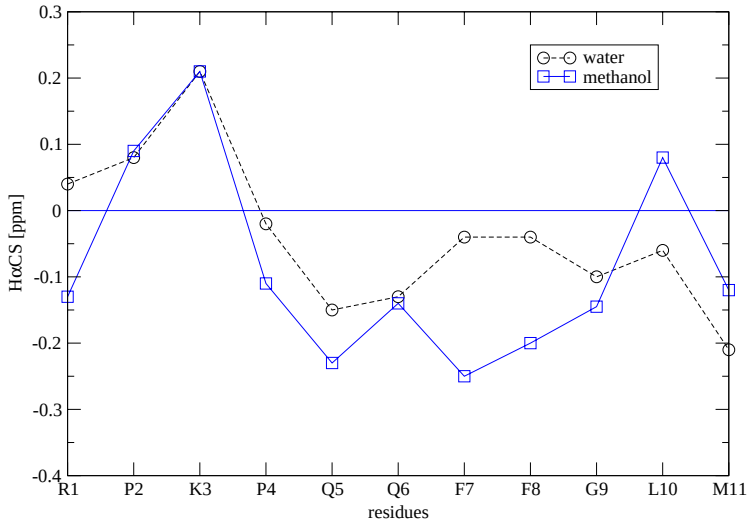

Figure 5.3. Hα conformational shifts SPOH in water (○) and methanol (□).

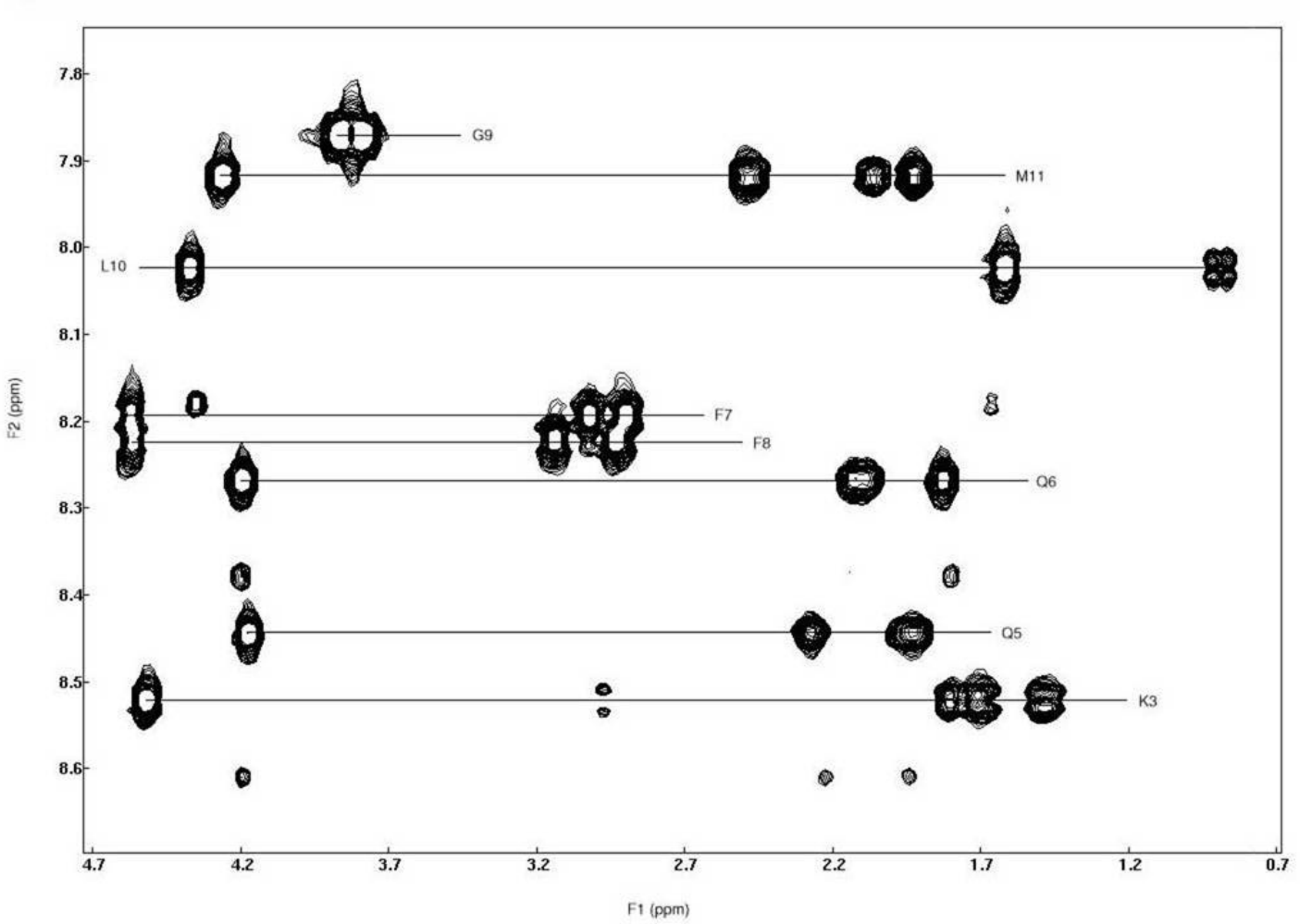

Figure 5.4.A. A section of the 600 MHz TOCSY spectrum of SPOH in water. The F2 axis represent the chemical shift of NH protons whereas in F1 axis the chemical shift of α-, β-, γ- and other protons are shohwn. Intraresiude spin system connectivities are shown by vertical lines with tags corresponding to the amino acid one letter code. The assignments have been determined by NOESY spectrum.

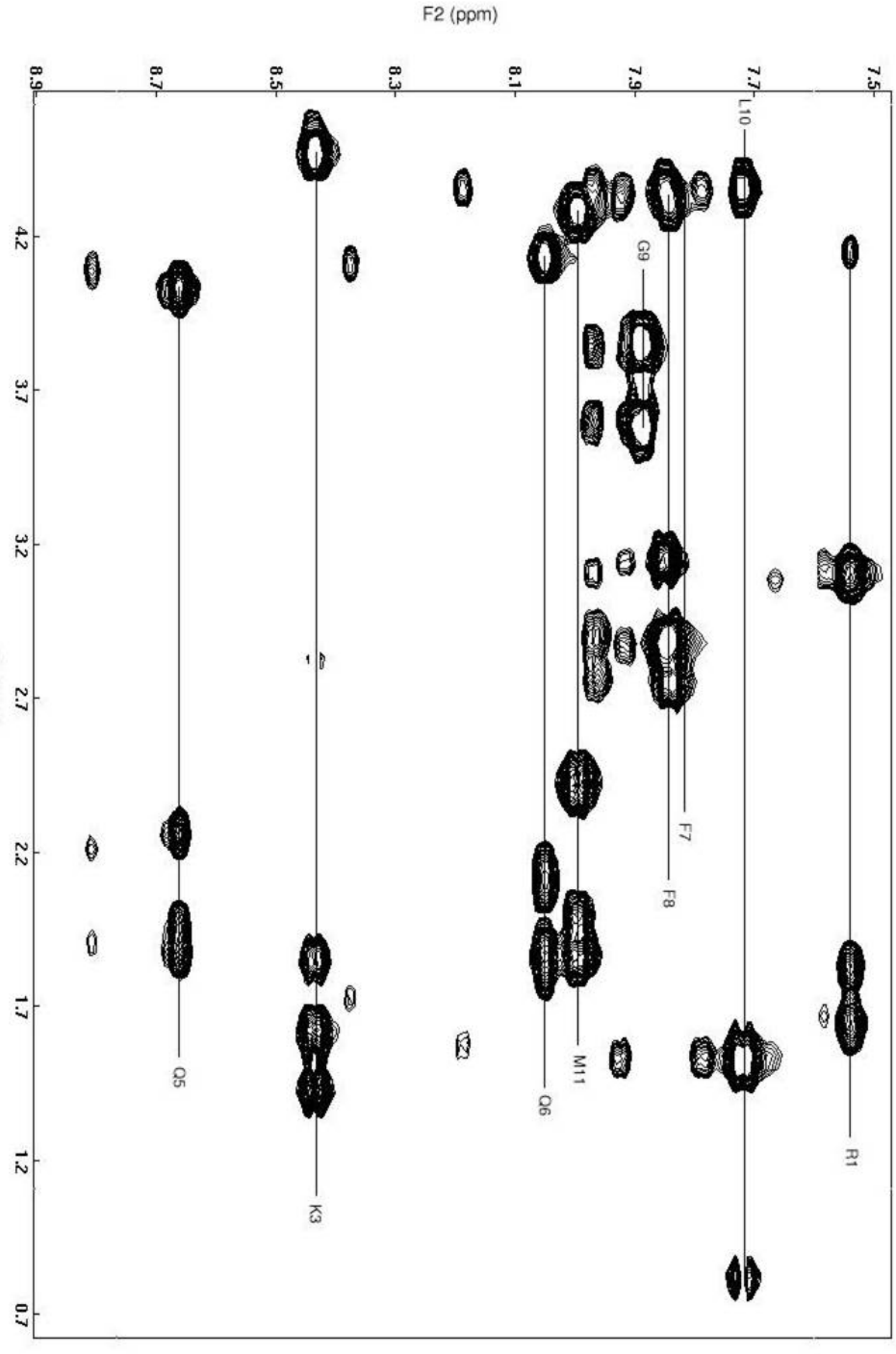

Figure 5.4.B. A section of the 600 MHz TOCSY spectrum of SPOH in methanol. The F2 axis represent the chemical shift of NH protons whereas in F1 axis the chemical shift of α-, β-, γ- and other protons are shohwn. Intraresiude spin system connectivities are shown by vertical lines with tags corresponding to the amino acid one letter code. The assignments have been determined by NOESY spectrum.

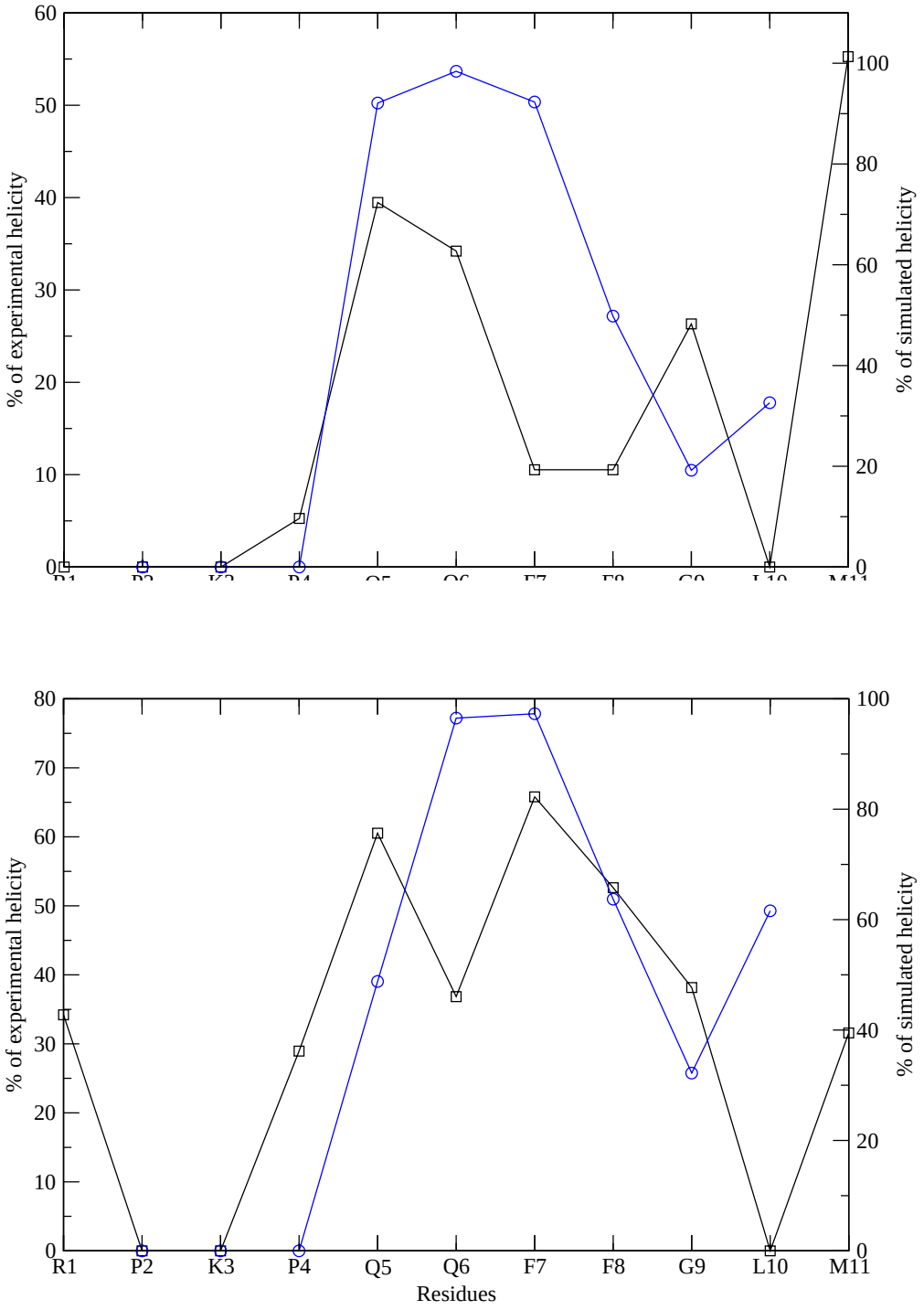

Figure 5.5. Percentage of computed helicity of SPOH in water (A) and methanol (B) obtained from MD simulations (○) and NMR experiments (□).

5.4.2. Molecular dynamics

5.4.2.1. Molecular dynamics of SP in water

A 40 ns MD trajectory of the peptide at 300 K was undertaken starting from its extended conformation soaked in a box of water molecules, using PBC and PME conditions as described in the methods section. The total energy and the density kept fairly constant at -9817 kcal·mol^{-1} and 0.962 g·cm^{-3}, respectively for the PME segment of the MD trajectory.

The CLASICO algorithm was used to analyze the structures of the MD simulation in water at 300 K in order to determine the conformational motifs attained by SP that are summarized in Table 5.6 and Figure 5.6. The average helical content for SP in water yielded 6.1% and was calculated as the sum of all the percentages of structures exhibiting α or 3_{10}-helical motifs and divided by 9, the number of residues that contain dihedral angle pairs. The different conformations were labeled according to the conformational motifs exhibited and classified into 196 different patterns. Figure 5.7.A shows the evolution of new patterns sampled along time. At the beginning of the trajectory the profile grows linearly until nanosecond 10. At nanosecond 9 there is a big increase in the number of new patterns. Then, from nanosecond 12 the pace of new pattern appearance decreases and the profile tends to a plateau. Thus for the 12 first nanoseconds 160 patterns are obtained whereas for the rest 28 nanoseconds of the MD trajectory only 36 new patterns are observed, thus indicating that we have thoroughly explored the conformational space that is attainable for the peptide under the experimental conditions.

Table 5.6. Summary of secondary structure motifs present in the MD trajectories of SP in water, and SPOH in water, methanol and DMSO. (Percentages from the total structures of each experiment are shown in brackets).

DIHEDRAL PAIR NO.	SP IN WATER	SPOH IN WATER	SPOH IN METHANOL	SPOH IN DMSO
1	S(73.5)	S(69.3)	S(95.0)	S(90.8)
2	S(73.5), II2(1.0)	S(69.3), II2(9.2)	S(95.2)	S(90.8)
3	S(73.9), I1(1.0)	S(69.4)	S(95.3)	S(90.9)

DIHEDRAL PAIR NO.	SP IN WATER	SPOH IN WATER	SPOH IN METHANOL	SPOH IN DMSO
4	H(6.1), 3_{10}(6.1), S(14.5), I1(81.1)	H(5.0), 3_{10}(5.1), S(40.3), I1(46.5)	H(0.9), 3_{10}(6.7), S(60.3), I1(26.5)	S(85.3)
5	H(7.3), 3_{10}(7.0), S(9.6), I1(2.5), I2(81.1)	H(6.1), 3_{10}(9.3), S(0.1), I1(48.8), I2(46.5), ii1(0.2)	H(4.1), 3_{10}(13.2), S(2.2), I1(57.4), I2(26.5)	S(79.3)
6	H(7.4), 3_{10}(7.1), S(9.5), I1(0.3), I2(71.2)	H(6.1), 3_{10}(9.4), S(0.1), I1(1.1), I2(92.9), ii2(0.2)	H(4.5), 3_{10}(15.7), S(5.4), I1(4.2), I2(83.7)	S(73.5)
7	H(4.6), 3_{10}(2.4), S(7.9), I1(2.3), I2(67.8), II1(5.8)	H(1.4), 3_{10}(6.0), S(0.1), I1(0.8), I2(86.8), i1(0.4), II1(0.1)	H(3.9), 3_{10}(14.3), S(5.1), I1(1.2), I2(82.1), II1(0.4)	S(1.3), I1(0.1)
8	H(2.6), 3_{10}(0.8), S(0.1), I1(13.0), I2(14.9), II2(5.8), ii1(0.3)	H(0.1), 3_{10}(1.3), I1(2.0), I2(13.3), i2(0.4), II2(0.1)	H(1.1), 3_{10}(8.2), S(4.2), I1(1.4), I2(48.7), II2(0.4), ii1(4.3)	S(0.1), I1(0.6), I2(0.1), ii1(0.1)
9	H(2.5), 3_{10}(0.6), I2(25.9), ii2(0.3)	3_{10} (1.1), I2(11.9)	H(0.2), 3_{10}(3.8), S(2.7), I2(38.0), ii2(4.3)	S(0.1), I2(0.7), ii2(0.1)

The first patterns to appear correspond to β-strand motifs expanding all the molecule that are partially replaced by type I β-turns at residues 5 and 6 and 9 and 10. The increase in the number of new patterns observed at nanosecond 9 is due to the appearance of helical motifs and

the type I β-turns expanding from residues 5 to 10. The patterns that are obtained from that moment on are combinations of structures exhibiting a β-strand or no structure for residues 2 to 4 and for the segment expanding from residues 5 to 10 exhibiting type I β-turns and in some cases α- or 3_{10} helices. A II2 motif in residue number 3 appears at pattern 185 giving rise to a small increase in the number of patterns, till pattern 194. These patterns lasts between nanoseconds 33.7 and 34.2.

In summary, the simulation points to the tendency of SP to attain a helical turn in the center of the molecule, however this turn is not stable and the molecule fluctuates around an ensemble of folded conformations characterized by the presence of two consecutive turns expanding residues 5 to 10.

A

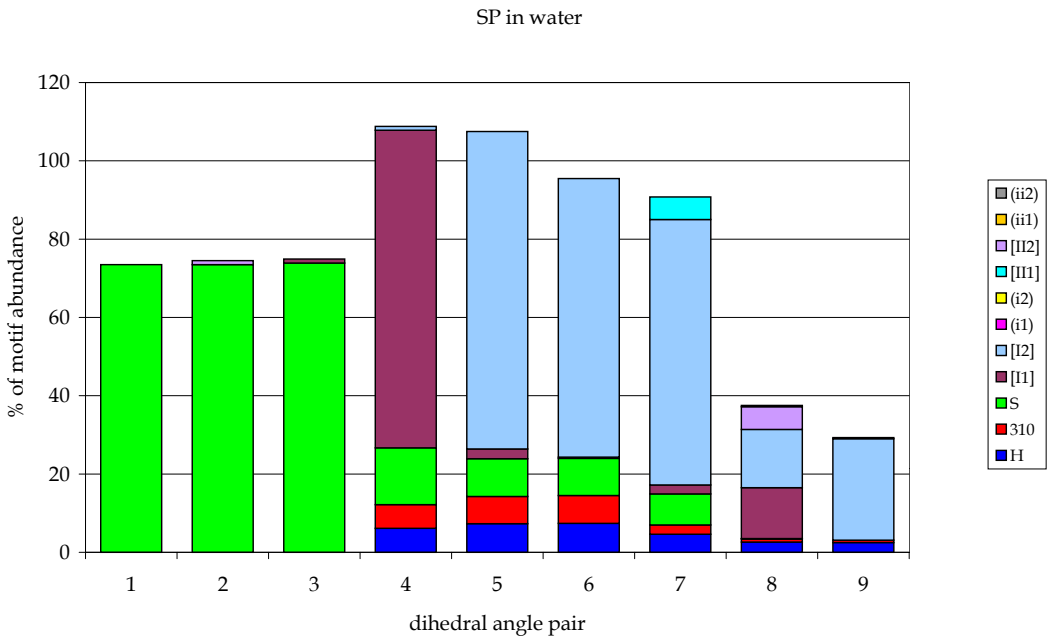

B

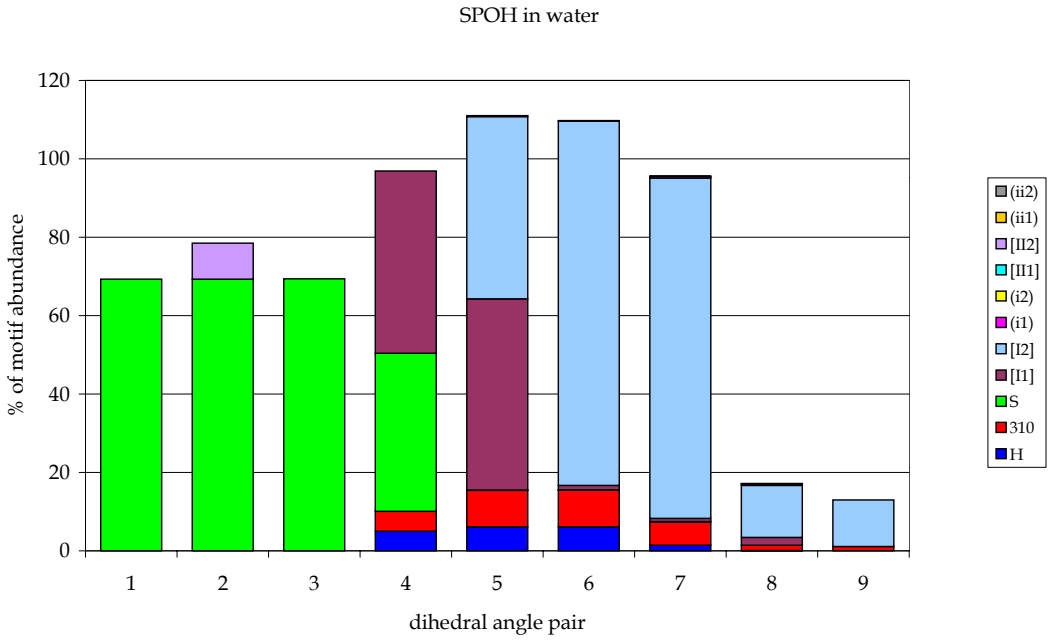

Figure 5.6. Cumulative statistics of conformational motifs for the MD trajectories of SP in water (A) and the MD trajectories of SPOH in water (B), methanol (C) and DMSO (D).

C

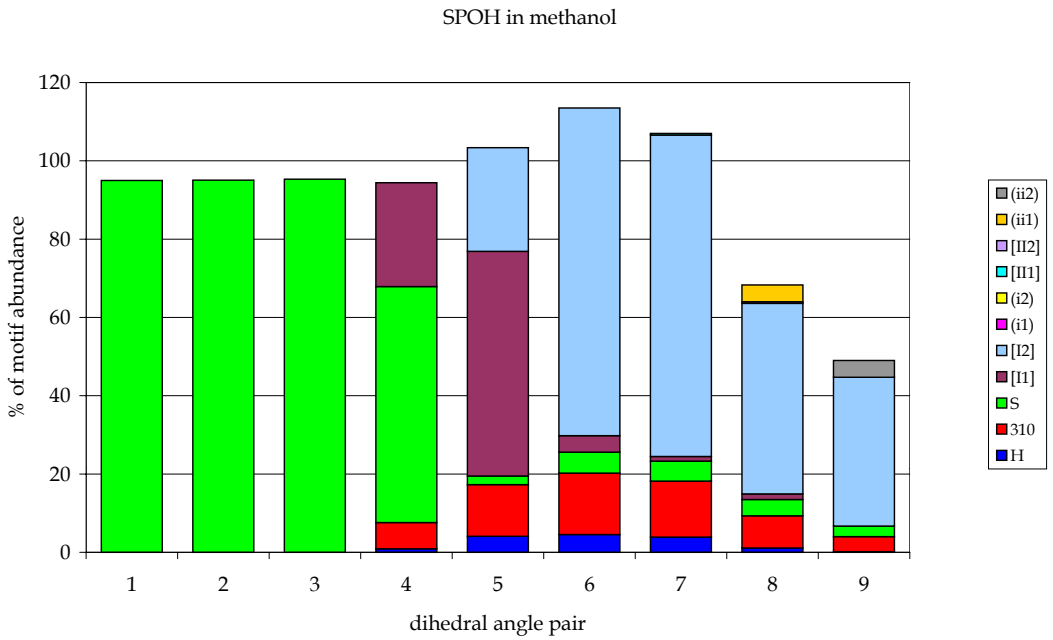

D

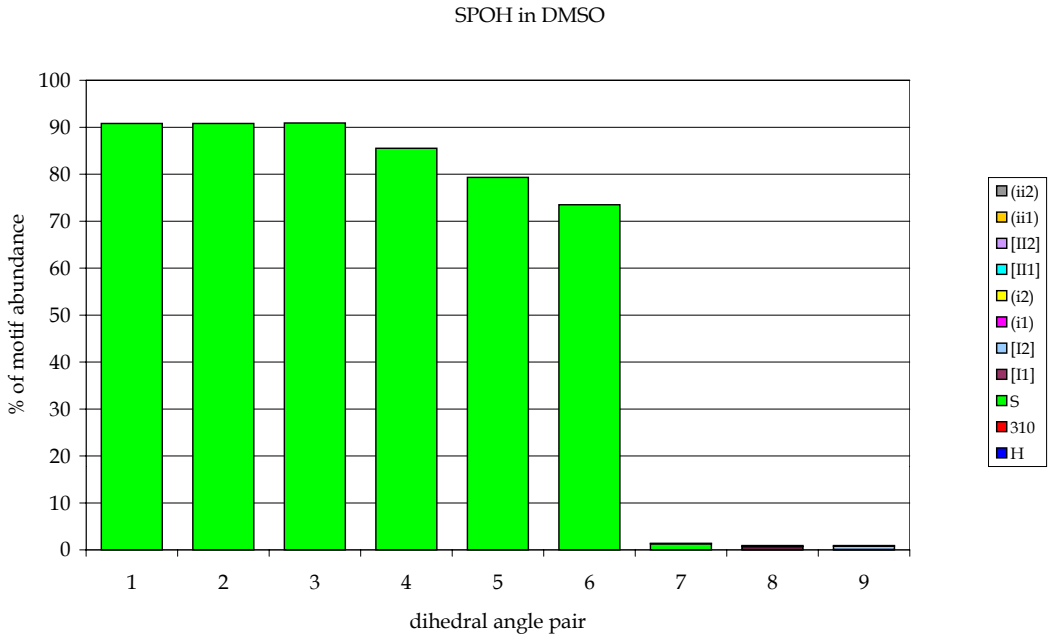

Figure 5.6. Cumulative statistics of conformational motifs for the MD trajectories of SP in water (A) and the MD trajectories of SPOH in water (B), methanol (C) and DMSO (D).

A

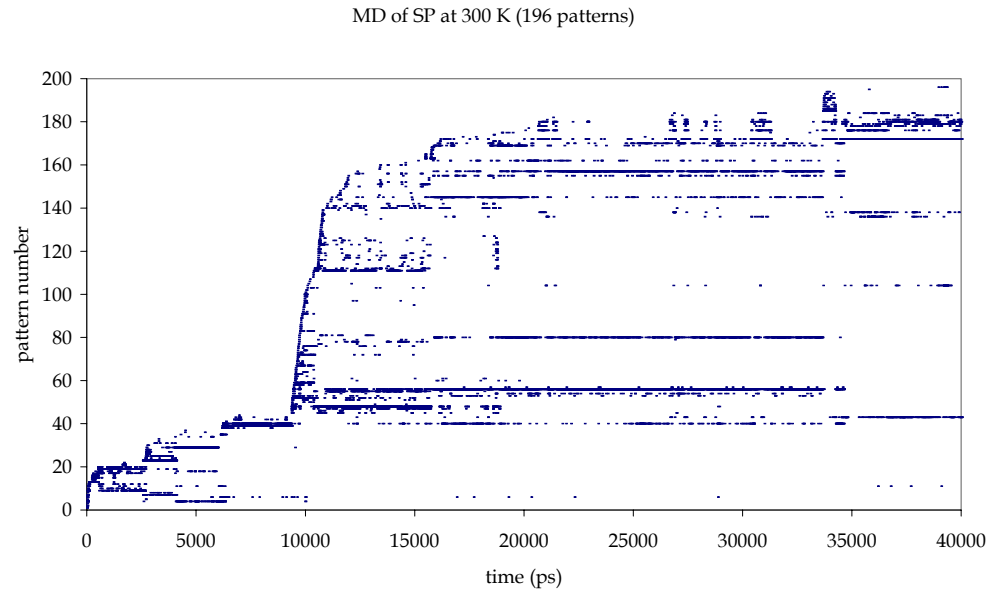

B

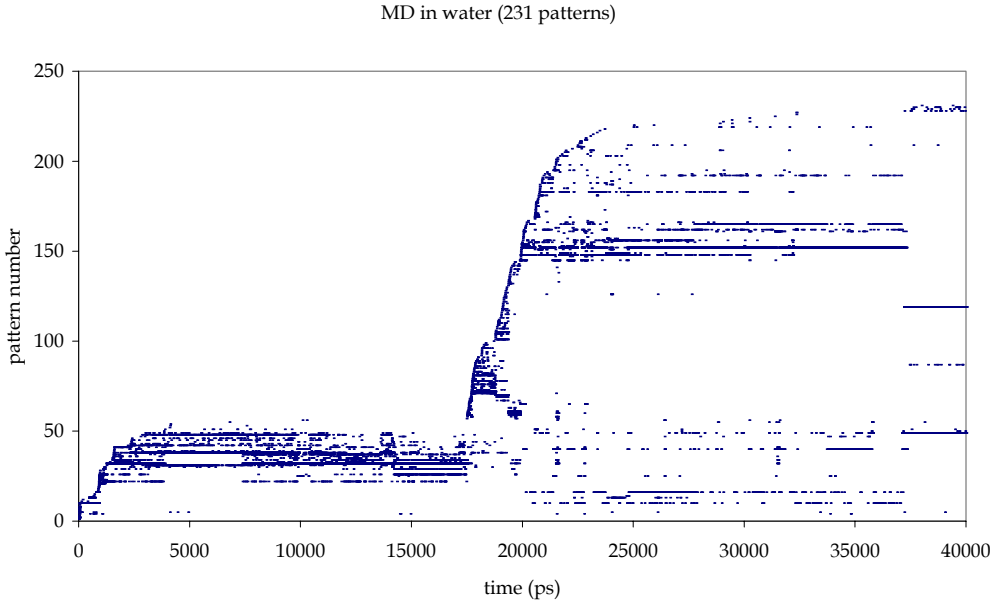

Figure 5.7. Evolution of patterns for the MD of SP in water (A) and the MD of SPOH in water (B), methanol (C) and DMSO (D).

C

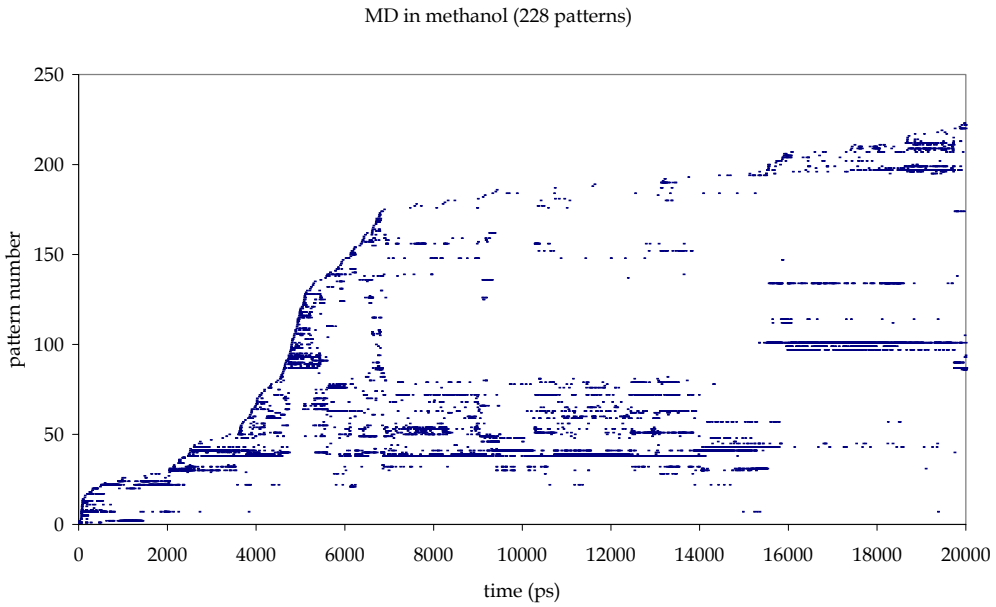

D

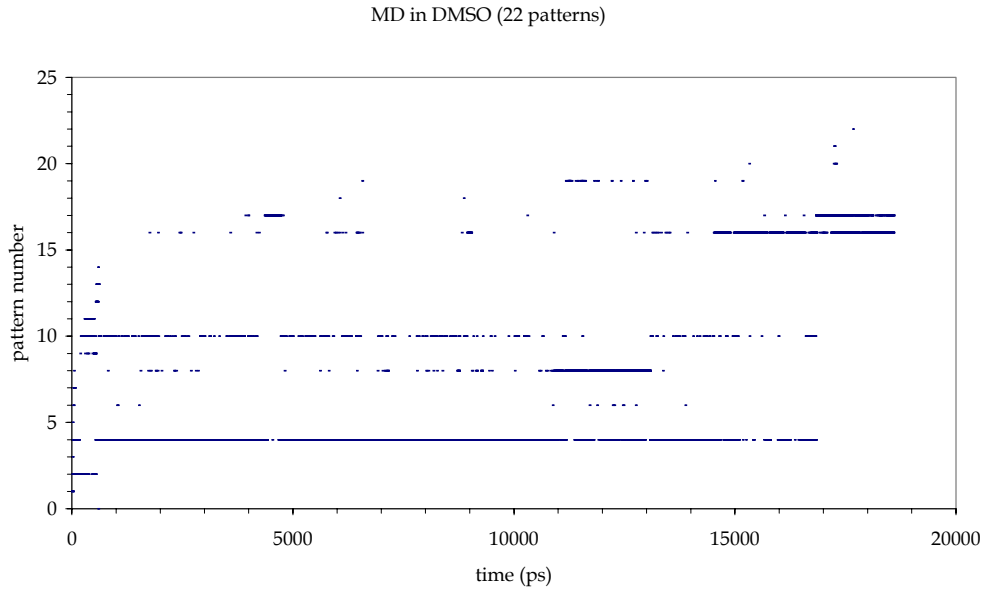

Figure 5.7. Evolution of patterns for the MD of SP in water (A) and the MD of SPOH in water (B), methanol (C) and DMSO (D).

The structures of SP previously characterized were classified into clusters using the CLUSTERIT algorithm, described in the previous chapter methods section. A criterion of $\Delta\overline{R} \geq 0.01$ (Figure 5.8) was adopted to stop the clustering process. Using this criteria 13 clusters remained (Figure 5.9). Table 5.7 summarizes the main structural features of the clusters found from the analysis of the MD trajectory of SP in water. The four most abundant clusters, represent 84% of the structures (shown in Figures 9.1 to 9.4) suggesting that the bulk of structures is grouped in a small number of clusters. The most abundant cluster (containing 51.8% of the total number of structures) exhibits β-strand dihedral angles for residues 2 to 4 and a type I β-turn on residues 5 to 10. The second most abundant cluster (16.9%) exhibits two consecutives type I β-turns extending from residues 5 to 8. Furthermore, it shows a α-helical turn extending from residues 5 to 7 and an II2 motif at residue 3 but both are present in a small proportion of the structures of the cluster. The third most abundant cluster (19.9%) exhibits β-strand values from residues 2 to 8 and a type I β-turn at residues 9 and 10. Cluster IV groups structures presenting β-strand dihedral angles at residue 2 to 4 and consecutive type I β-turns extending from residues 5 to 10. It also exhibits α-helical turns at residues 5 to 10. The rest of clusters, representing 16% of the structures exhibit less frequent structural features like β-strand dihedral angles at residue 2 to 5, instead of residues 2 to 4 or like in cluster VII not presenting the β-strand dihedral angles at the N-terminus and exhibiting a 3_{10}-helical turn at residues 5 to 8. Finally, cluster XIII amounting for 0.10% of the total number of structures is the cluster not showing any of the conformational motifs.

Transitions between clusters for the MD trajectory of SP in water were analyzed as described in the methods section and the data is presented in Table 5.8 and Figure 5.10. Only 9 clusters representing 98.6% of the structures and local transitions above 5% have been depicted for conciseness. However, transitions between cluster I and V are shown in order to make evident the low degree of connectivity between these two subgroups of clusters. For each snapshot in the MD trajectory of SP in water, its corresponding cluster has been assigned. The cluster number of each conformation has been plotted in Figure 5.11.

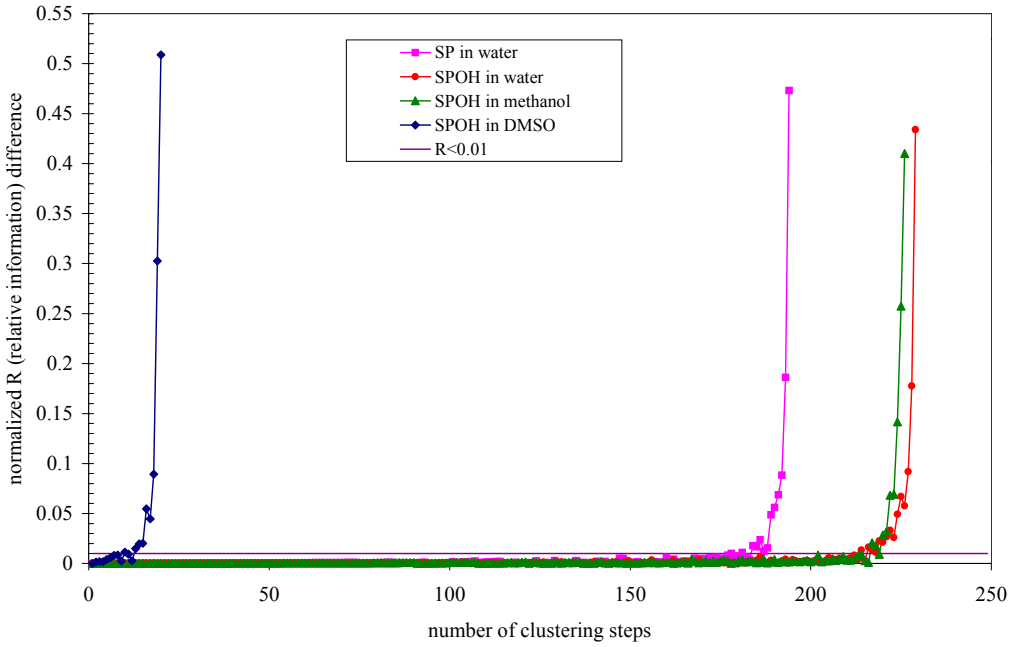

Figure 5.8. Evolution of the difference of normalized relative information $(\Delta\overline{R})$ between two consecutive clustering steps. The stopping condition of the clustering process, $\Delta\overline{R} \geq 0.01$, is also depicted.

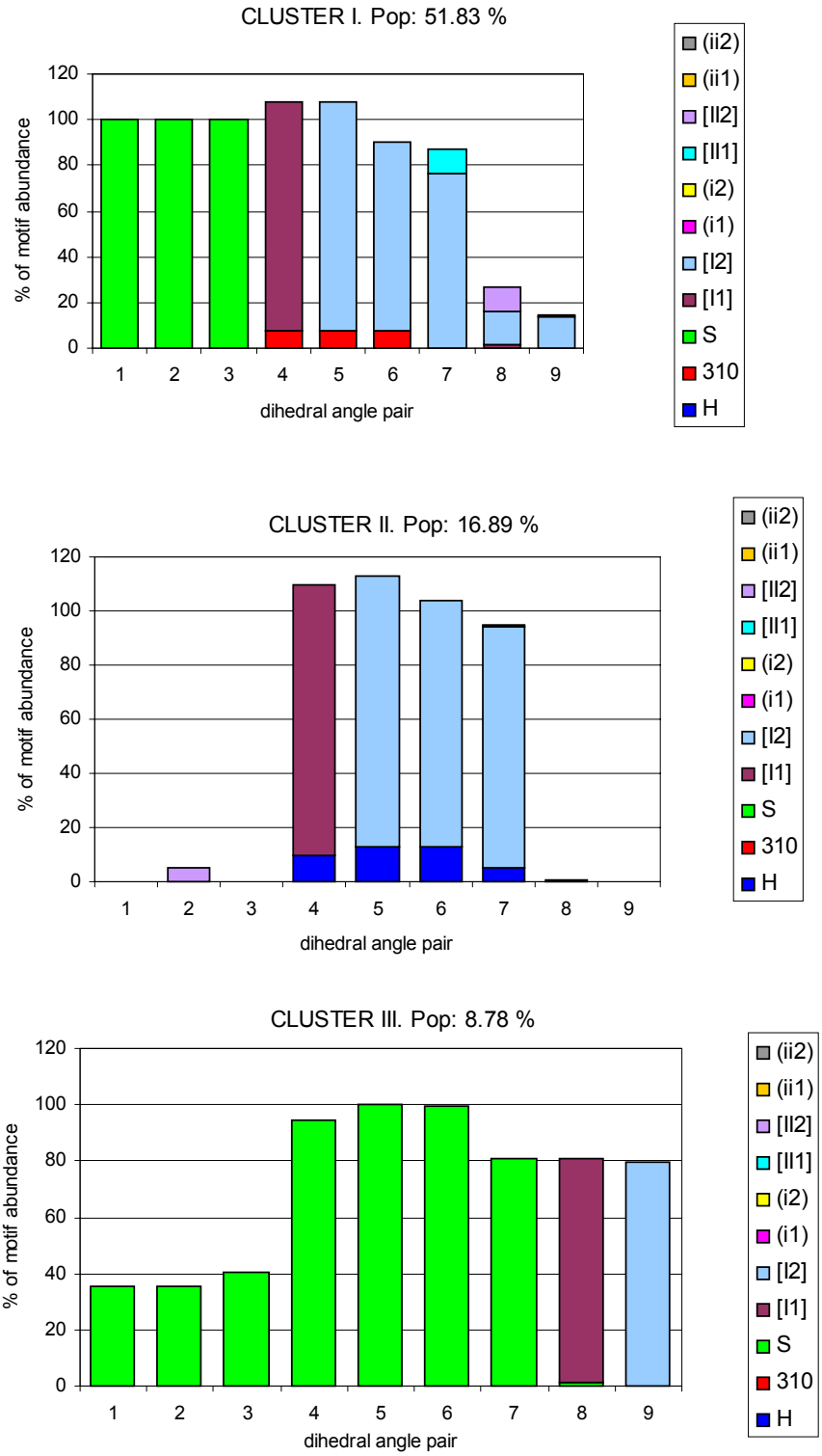

Figure 5.9. Clusters obtained for the MD trajectory of SP in water.

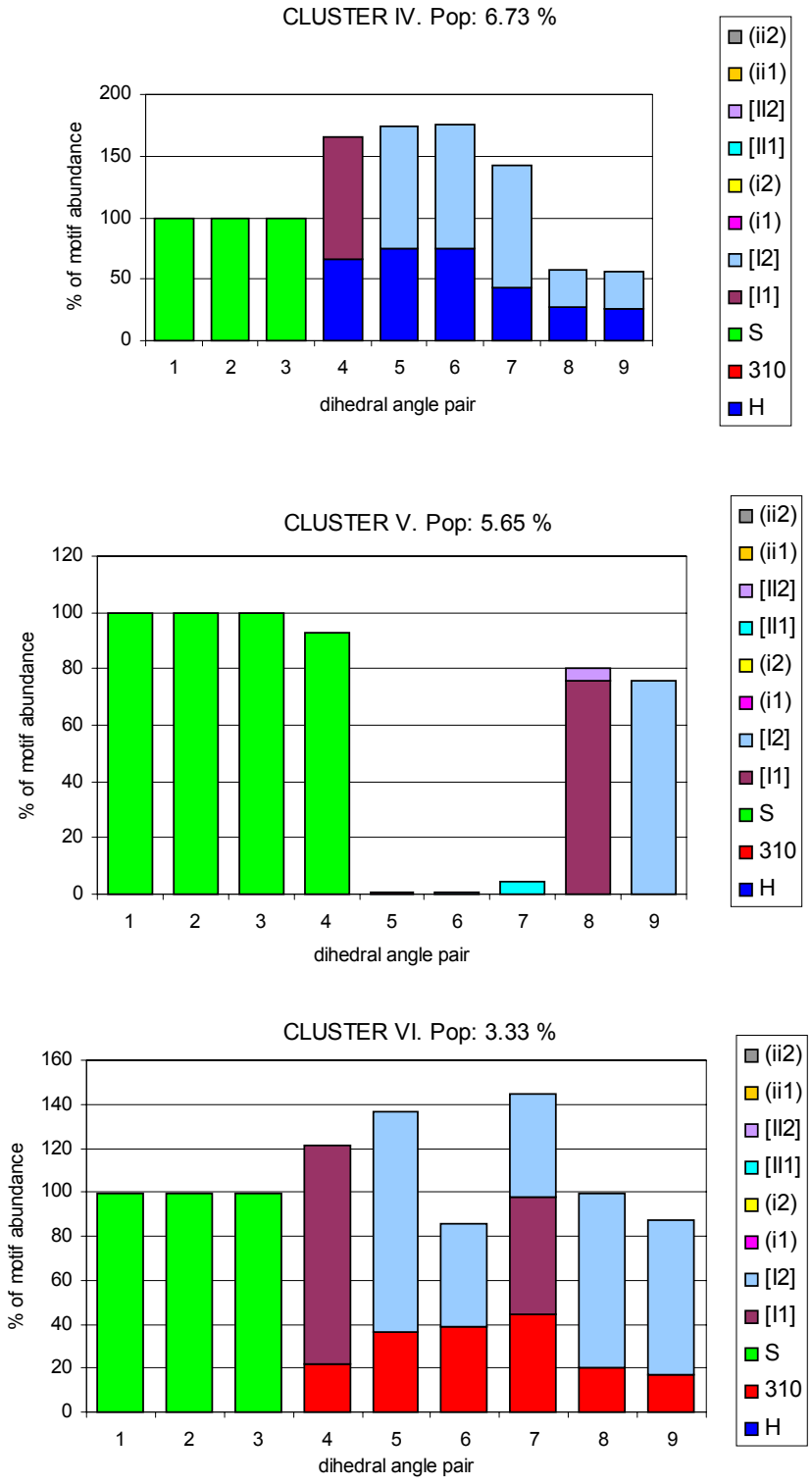

Figure 5.9. Clusters obtained for the MD trajectory of SP in water.

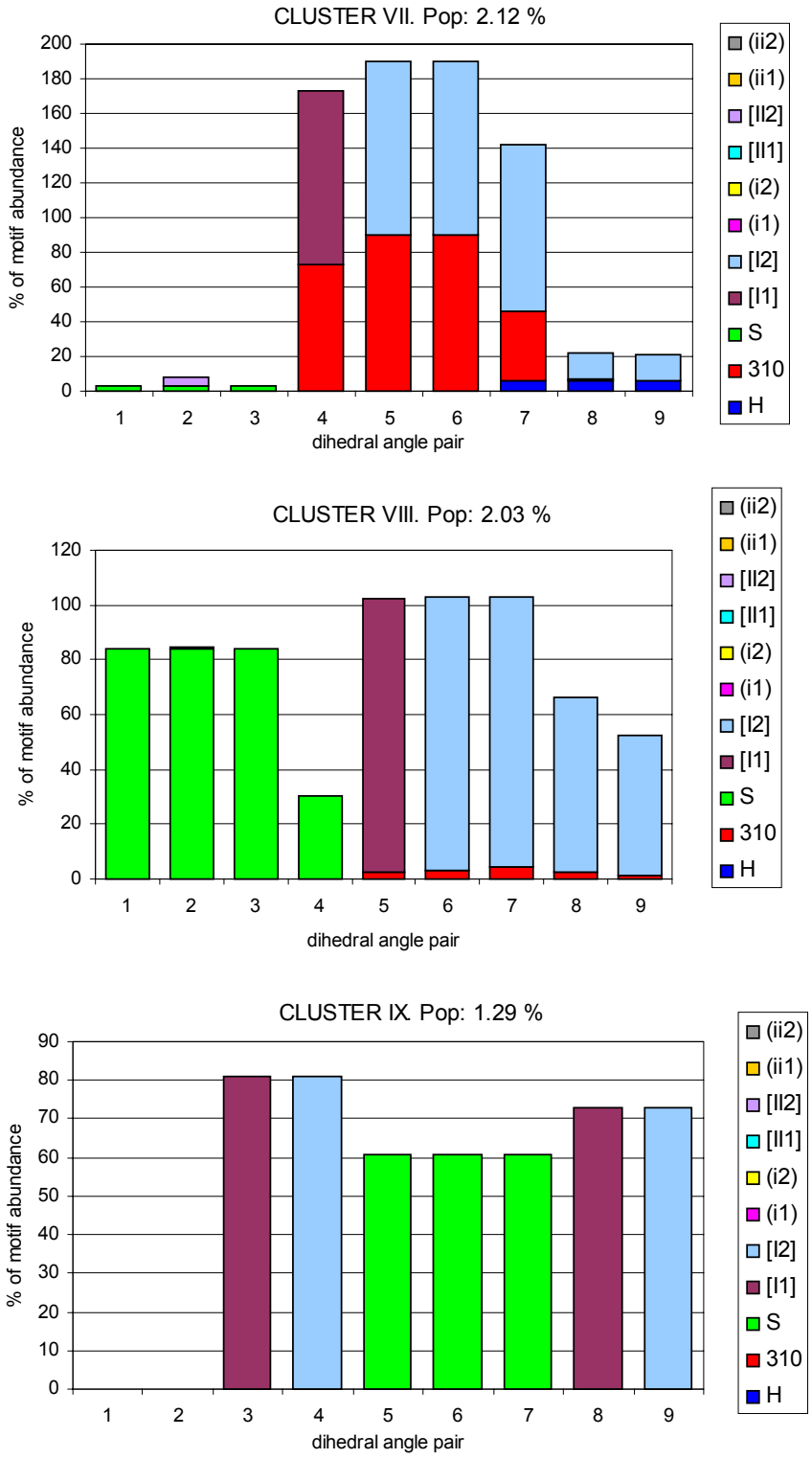

Figure 5.9. Clusters obtained for the MD trajectory of SP in water.

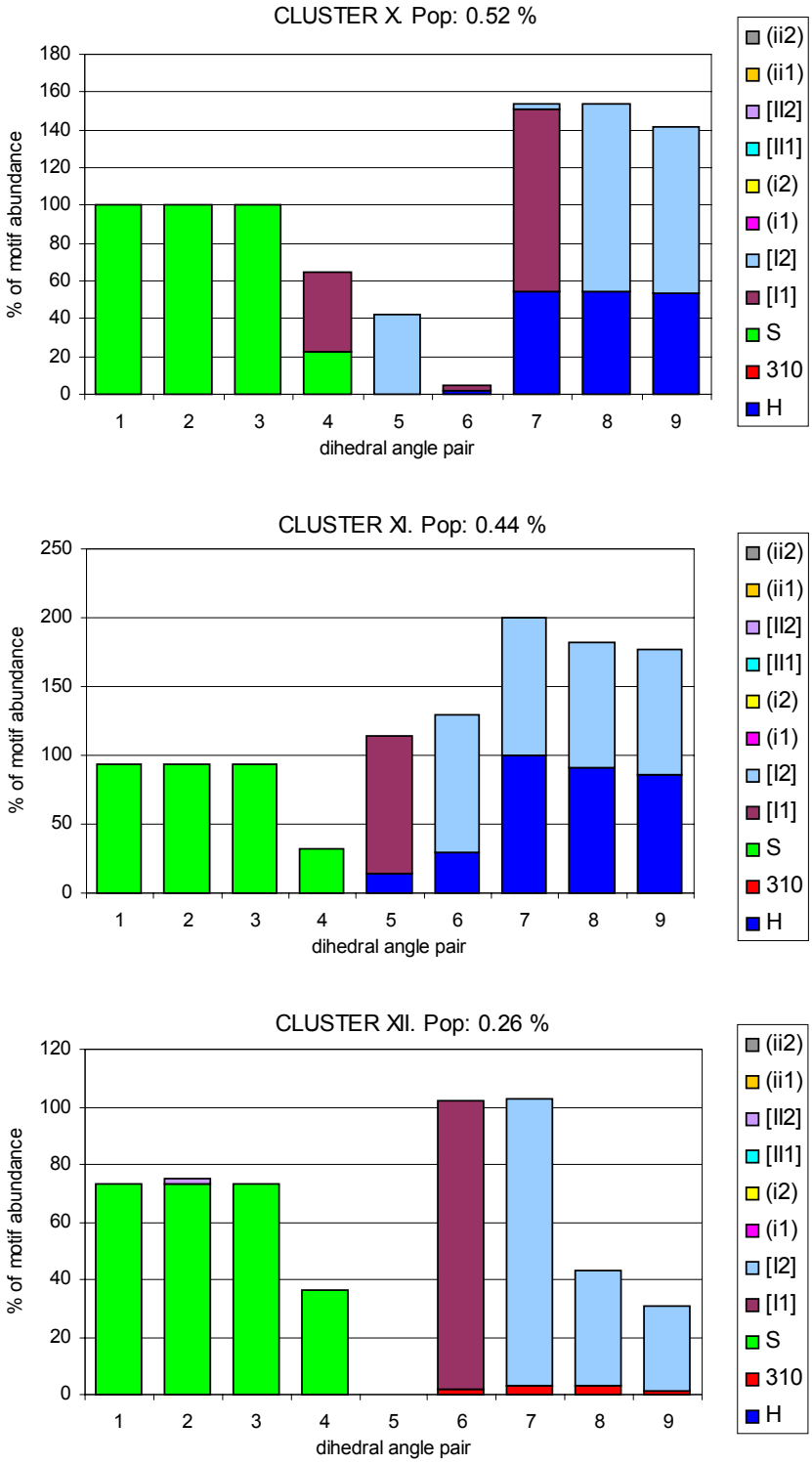

Figure 5.9. Clusters obtained for the MD trajectory of SP in water.

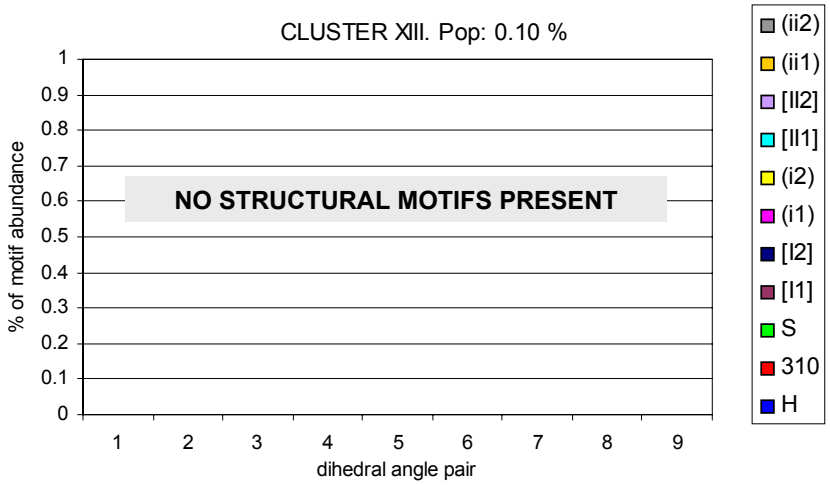

Figure 5.9. Clusters obtained for the MD trajectory of SP in water.

Table 5.7. Summary of the main structural features of the 13 clusters obtained using CLUSTERIT for the MD trajectory of SP in water. The second column shows the percentage of the total number of structures obtained in this MD trajectory that are contained within each cluster. The last column corresponds to the percentage of structures within each cluster that exhibit each motif. When the motif expands more than one residue with different percentages the interval is shown.

CLUSTER	% OF STRUCTURES CONTAINED	MOTIFS PRESENT	RESIDUES INVOLVED	% OF STRUCTURES CONTAINING THE MOTIF
I	51.8	β-strand type I β-turn	2-4 5-10	100 14-100
II	16.9	α-helical turn type I β-turn	5-7 5-8	10-13 89-100
III	8.8	β-strand type I β-turn	2-8 9-10	35-100 80
IV	6.7	β-strand α-helical turn type I β-turn	2-4 5-10 5-10	100 26-75 30-100
V	5.6	β-strand type I β-turn	2-5 9-10	93-100 76

CLUSTER	% OF STRUCTURES CONTAINED	MOTIFS PRESENT	RESIDUES INVOLVED	% OF STRUCTURES CONTAINING THE MOTIF
VI	3.3	β-strand 3_{10}-helical turn type I β-turn	2-4 5-10 5-10	100 17-45 47-100
VII	2.1	3_{10}-helical turn type I β-turn	5-8 5-10	41-90 15-100
VIII	2.0	β-strand type I β-turn	2-5 7-10	30-84 51-100
IX	1.3	β-strand type I β-turn type I β-turn	6-8 4-5 9-10	61 81 73
X	0.5	β-strand type I β-turn type I β-turn	2-5 5-6 8-10	22-100 42 88-100
XI	0.4	β-strand α-helical turn type I β-turn	2-5 6-10 6-10	31-94 14-100 91-100
XII	0.3	β-strand type I β-turn	2-5 7-10	37-73 30-100
XIII	0.1	none	--	--

Table 5.8. Summary of the local transitions with probability larger than 5% obtained for the MD trajectory of SP in water.

CLUSTERS		TRANSITIONS			REVERSIBILITY	STRUCTURES	
Origin	End	Total	% Local	% Global		Total	% Local
I	IV	1836	8.85	9.16	1	20735	51.83
	I	17728	85.5	44.32	1		
II	II	5874	86.93	14.68	1	6757	16.89
	VII	446	6.6	2.22	1.01		
III	III	3416	97.24	8.54	1	3513	8.78
IV	IV	682	25.32	1.7	1	2693	6.73
	I	1827	67.84	9.16	1		
V	V	2113	93.54	5.28	1	2259	5.65
VI	IV	80	6.01	0.42	0.92	1332	3.33
	VI	595	44.67	1.49	1		
	I	584	43.84	2.88	1.03		
VII	II	442	52	2.22	0.99	850	2.12
	I	63	7.41	0.32	0.97		
	VII	306	36	0.76	1		
VIII	VIII	449	55.23	1.12	1	813	2.03
	XI	90	11.07	0.47	0.92		
	II	63	7.75	0.31	1.05		
	I	127	15.62	0.62	1.05		
IX	III	55	10.62	0.27	1.04	518	1.29
	IX	437	84.36	1.09	1		
X	X	100	48.31	0.25	1	207	0.52
	VIII	16	7.73	0.08	1.07		
	IV	14	6.76	0.08	0.74		
	VI	37	17.87	0.17	1.23		
	I	28	13.53	0.14	0.93		
XI	VIII	98	55.06	0.47	1.09	178	0.44
	XI	50	28.09	0.12	1		
XII	VIII	24	23.08	0.14	0.77	104	0.26
	XI	7	6.73	0.03	1.75		
	XII	13	12.5	0.03	1		
	II	24	23.08	0.11	1.26		
	I	28	26.92	0.14	1		
XIII	V	15	37.5	0.08	0.94	40	0.1
	III	10	25	0.05	0.91		
	IX	3	7.5	0.01	3		
	II	4	10	0.02	1.33		
	XIII	8	20	0.02	1		

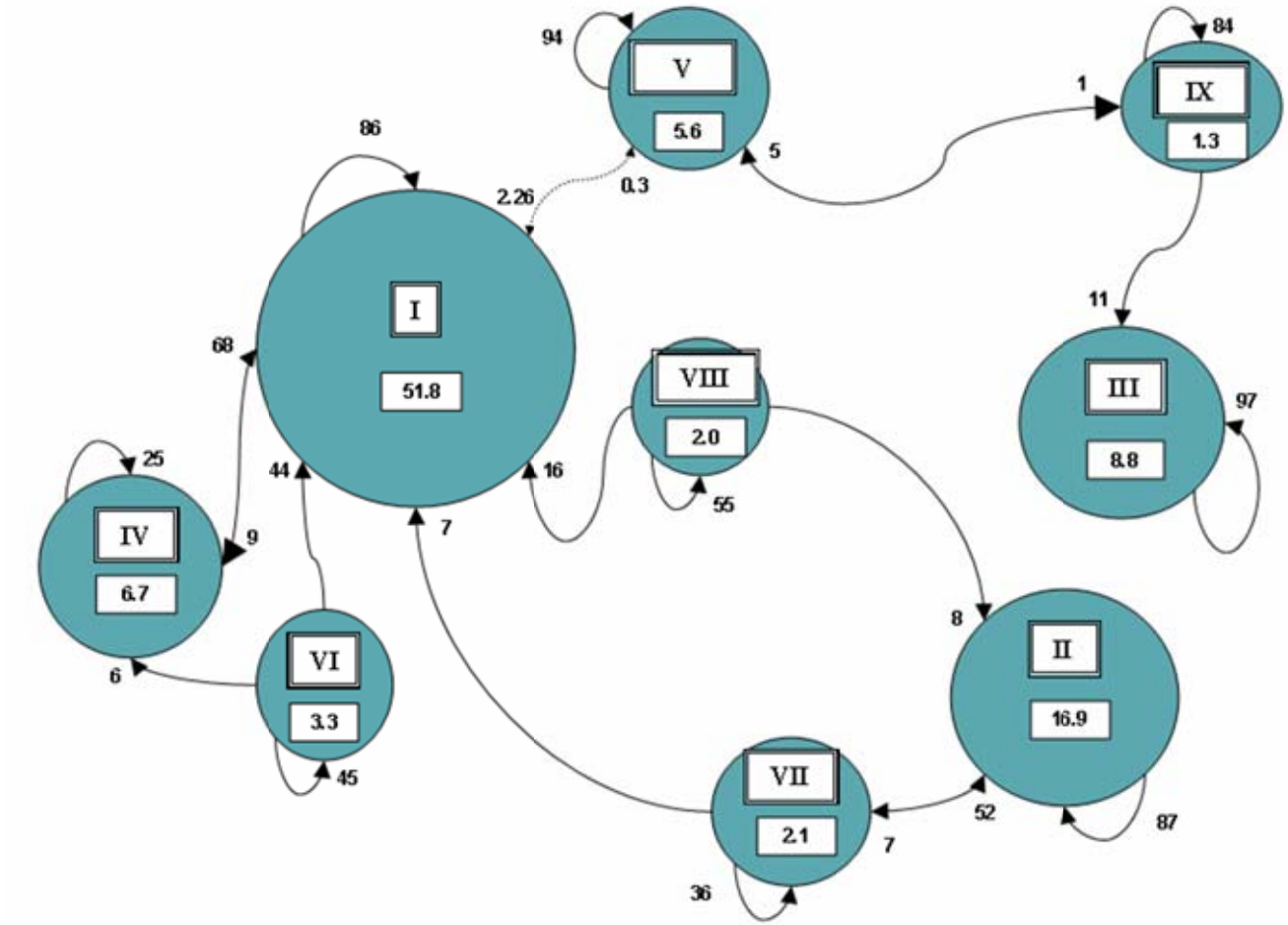

Figure 5.10. Transitions between the 9 largest clusters for the MD trajectory of SP in water.

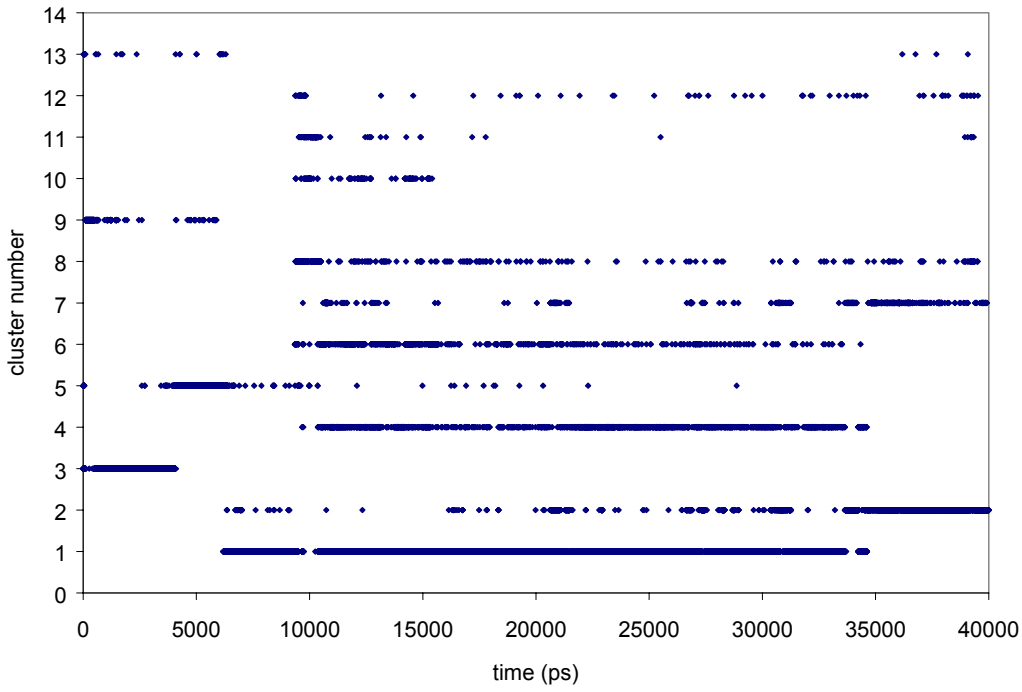

Figure 5.11. Evolution of clusters appearing along the MD trajectory of SP in water.

5.4.2.2. Molecular Dynamics of SPOH in water

A 40 ns MD trajectory of the peptide at 300 K was undertaken starting from its extended conformation soaked in a box of water molecules, using PBC and PME conditions as described in the methods section. The total energy and the density kept fairly constant at -9102 kcal·mol^{-1} and 0.945 g·cm^{-3}, respectively.

The average helical content for SPOH in water yielded 5.7% and was calculated as the sum of all the percentages of structures exhibiting α or 3_{10}-helical motifs and divided by 9, the number of residues that contain dihedral angle pairs. The helicity of each residue was computed by using a modified version of the CLASICO method as described in the methods section. In order to compare values of helicity obtained from the simulation with those obtained experimentally data was collected for 10 ns after the peptide had reached a folded conformation (10 ns) and the total number of snapshots containing helix was divided by the total number of structures (10,000 structures). Data is shown in Figure 5.5.A.

The CLASICO algorithm was used to analyze the structures of the MD simulation in water at 300 K in order to determine the conformational motifs attained by SPOH that are summarized in Table 5.6. The different conformations were labeled according to the conformational motifs exhibited and classified into 231 different patterns. Figure 5.7.B shows the evolution of new patterns sampled along time. At the beginning of the trajectory the profile exhibits a plateau at 5 ns after an initial steady increase of the number of patterns. This behavior can be associated with the sampling of new secondary structure structures from the extended conformation. The number of new patterns is very low until at nanosecond 17 the peptide samples an II2 motif located on the third residue, generating a wealth of new patterns from this point, until a second plateau is reached after 25 ns.

The folding process of the peptide can be analyzed in view of the evolution of patterns sampled. Since the simulation started from the extended conformation, the first patterns sampled correspond to structures with no conformational motifs or adopting dihedral angles of a β-strand. Subsequently, SPOH adopts a type I β-turn between residues 9 and 10 (457 ps) that unfolds quickly (724 ps), falling into a type I β-turn between residues 6 and 7 after 785 ps. This conformation appears to act as a *nucleation site* of the region that extends from residue 5 to 9, that folds lately to form two consecutive turns that will last for the last 39 ns of the MD trajectory with a combination of different turn types. These central turns adopt sporadically the form of a α- or 3_{10}-helix between residues 5 to 7 or between residues 6 to 8. The increase in the number of patterns from 17 ns corresponds to the sampling of an II2 motif in residue number 3. This motif is present together with the two central turns in the molecule mainly although sometimes appears with the 3_{10}-helix and more rarely with the α-helix.

In summary, the simulation points to the tendency of SPOH to attain a helical turn in the center of the molecule, however this turn is not stable and the molecule fluctuates around an ensemble of folded conformations characterized by the presence of two consecutive turns between residues from 5 to 9.

The structures of SPOH previously characterized were classified into clusters using the CLUSTERIT algorithm, described in the methods section. A criterion of $\Delta\overline{R} \geq 0.01$ (Figure 5.8) was adopted to stop the clustering process. Using this criteria 16 clusters remained (Figure 5.12). Table 5.9 summarizes the main structural features of the clusters found from the analysis of the MD trajectory at 300 K. The four most abundant clusters, represent 85% of the structures (shown in Figures 5.12.1 to 5.12.4) suggesting that the bulk of structures is grouped in a small number of clusters. The most abundant cluster (containing 35.5% of the total number of structures) exhibits β-strand dihedrals angle for residues 2 to 5 and a type I β-turn on residues 6 to 9. The second most abundant cluster (21.8%) exhibits β-strand values on residues 2 to 4 and two consecutives type I

β-turns extending from residues 5 to 8. Furthermore, 17% of the structures exhibit a 3_{10}-helical turn extending from residues 5 to 7. The third most abundant cluster (19.9%) exhibits a α-helical turn extending from residues 5 to 7, present in 17% of the structures of this cluster. The type I β-turn expands from residues 5 to 9 in a proportion going from 13 to 100%. Cluster IV groups structures presenting an II2 motif on residue 3 (72%) and type I β-turns extending from residues 6 to 8. The rest of clusters representing 15% of the structures exhibit less frequent structural features, like type I β-turns in two regions 5 to 7 and 9 and 10, or the β-strand (residues 2 to 4) in conjunction with a α-helical turn (residues 5 to 8), or the II2 motif (residue 3) together with a 3_{10}-helical turn. The type I' β-turn is rarely present for residues 6 and 7 and 8 and 9. Cluster XV and XVI, both accounting for 0.1% of the structures, group the structures that exhibit only β-strand or do not present any conformational motifs. To sum up, the peptide at 300 K can be described as a folded molecule exhibiting consecutive type I β-turns in the region expanding from residues 5 to 9 and with residues 2 to 4 exhibiting a β-strand or an II2 motif on residue 3. For residues 5 to 7 a α-helical turn or a 3_{10}-helical turn are the most probable structural features observed.

Transitions between clusters for the MD trajectory of SPOH were analyzed as described in the methods section and the data is presented in Table 5.10 and Figure 5.13. Only 9 clusters representing 98% of the structures and local transitions above 5% have been depicted for conciseness. Although transitions between the two most abundant clusters with local transitions less than 5%, are also shown for later discussion. The connections observed suggest that clusters can be grouped into two different classes. On the one hand, clusters I, IV, V, VI and VIII and on the other, clusters II, III, VII and IX. Both classes exhibit connections that are contained within each of the subgroups having few transitions between cluster I and II (less than 1% of their respective local transitions). For each snapshot in the MD trajectory of SPOH in water, its corresponding cluster has been assigned. The cluster number of each conformation has been plotted in Figure 5.14.

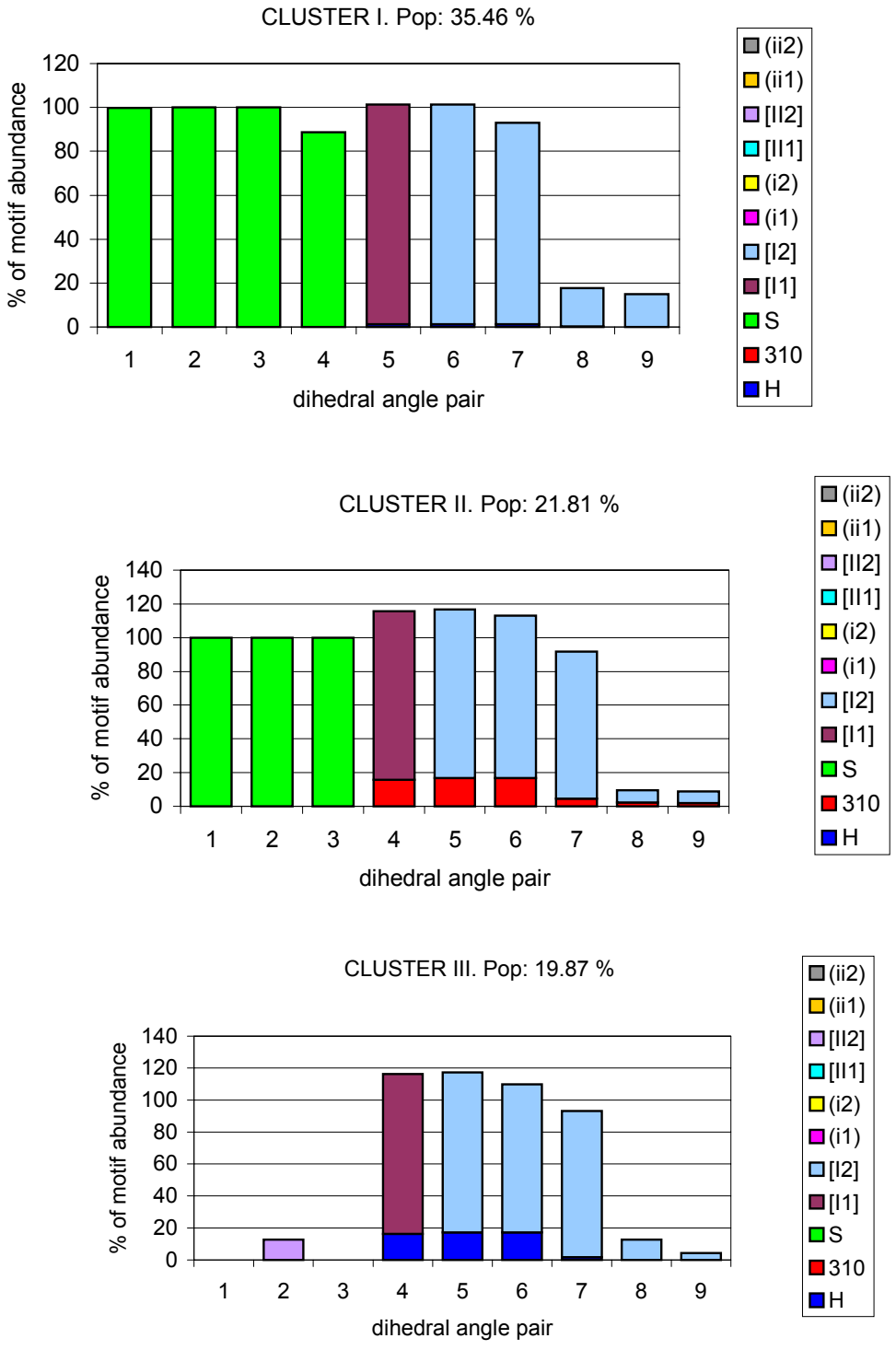

Figure 5.12. Clusters obtained for the MD trajectory of SPOH in water.

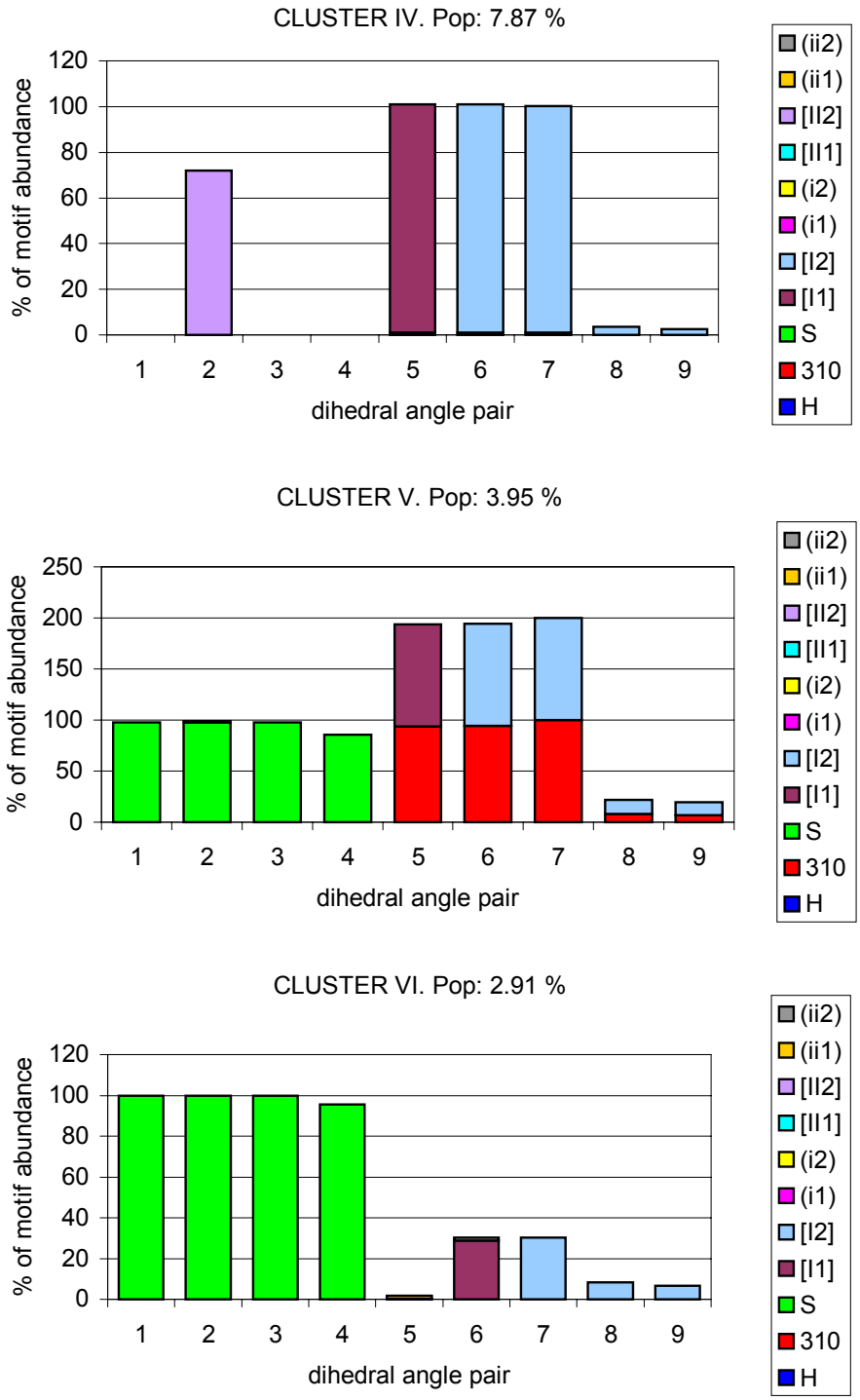

Figure 5.12. Clusters obtained for the MD trajectory of SPOH in water.

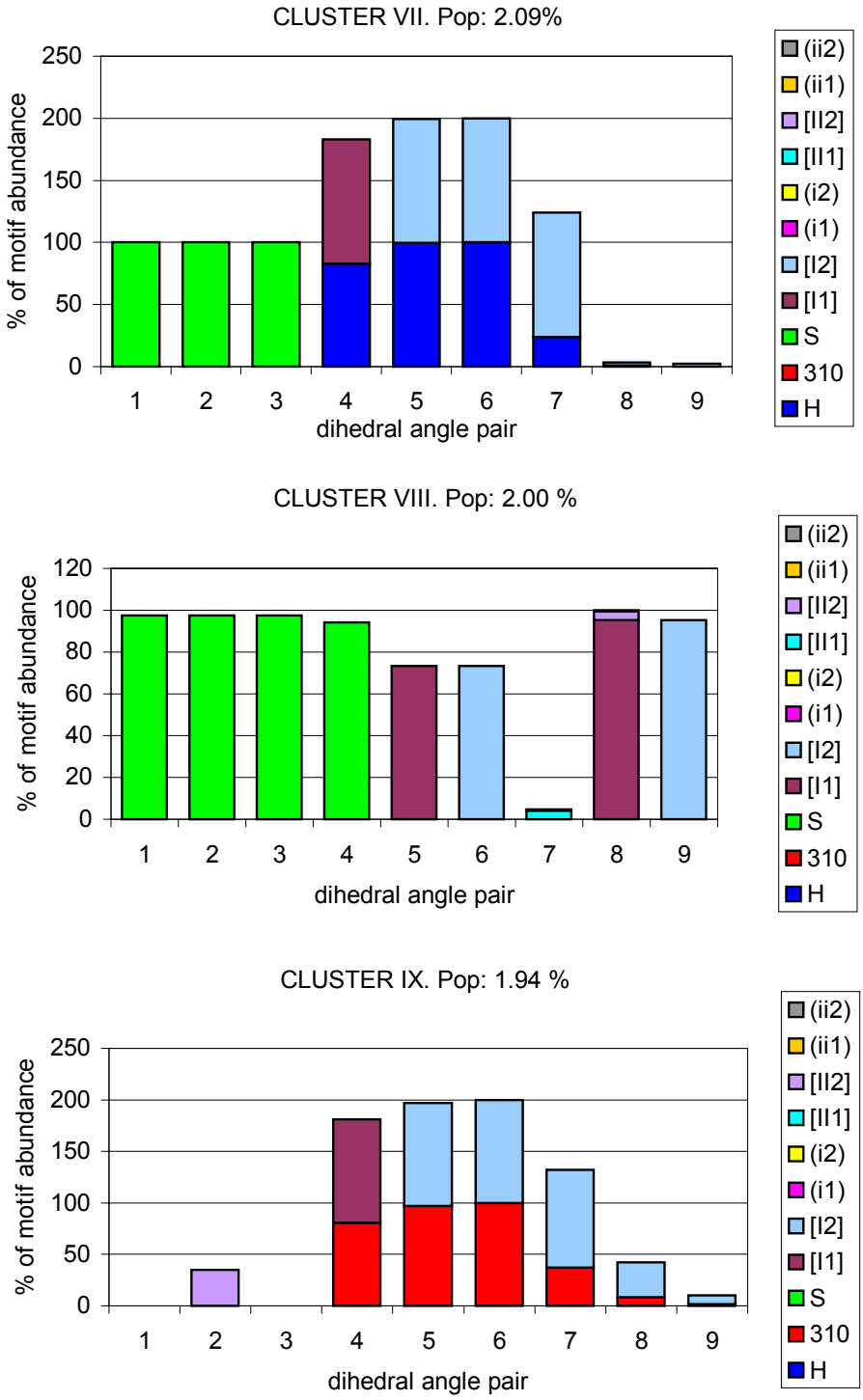

Figure 5.12. Clusters obtained for the MD trajectory of SPOH in water.

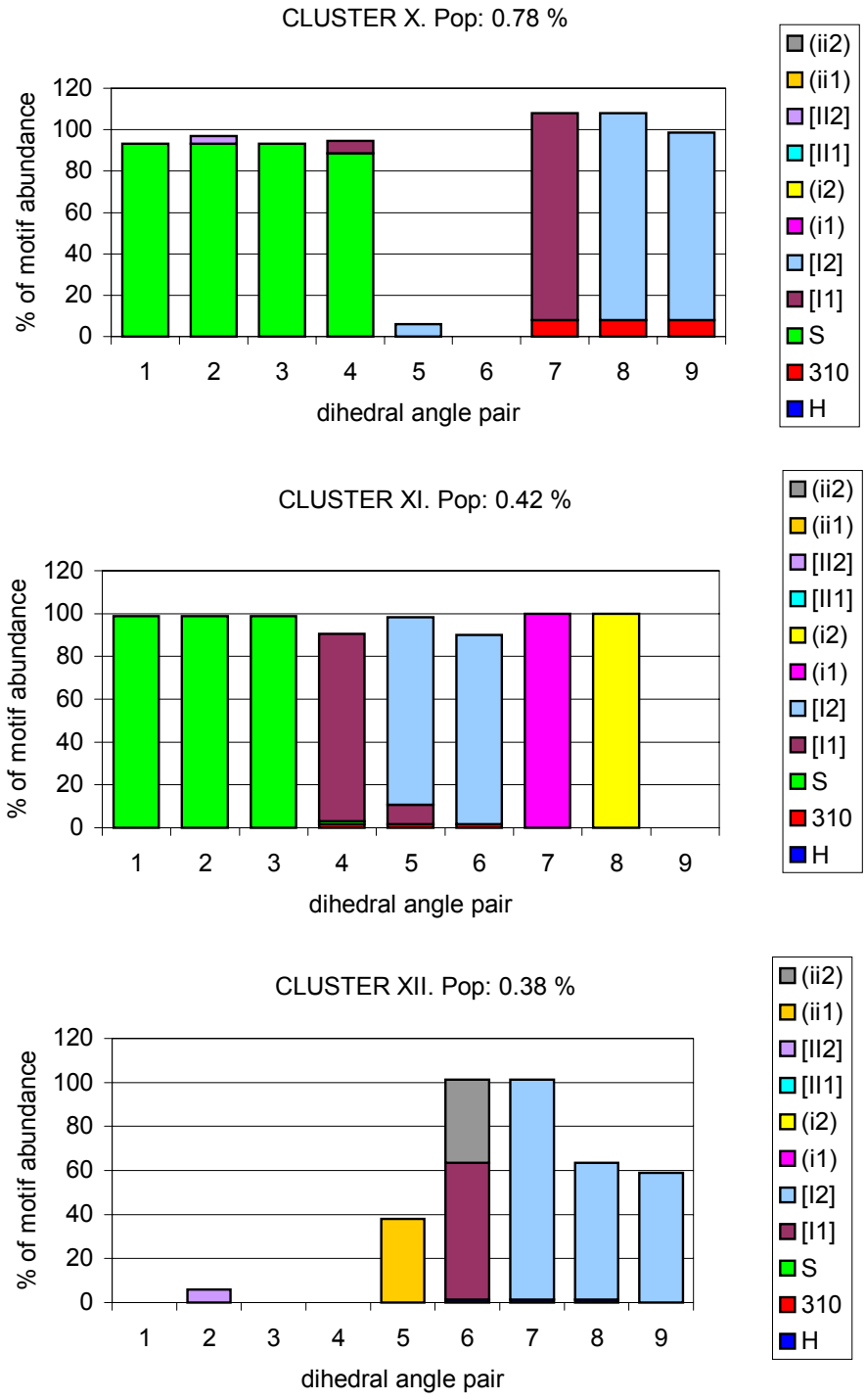

Figure 5.12. Clusters obtained for the MD trajectory of SPOH in water.

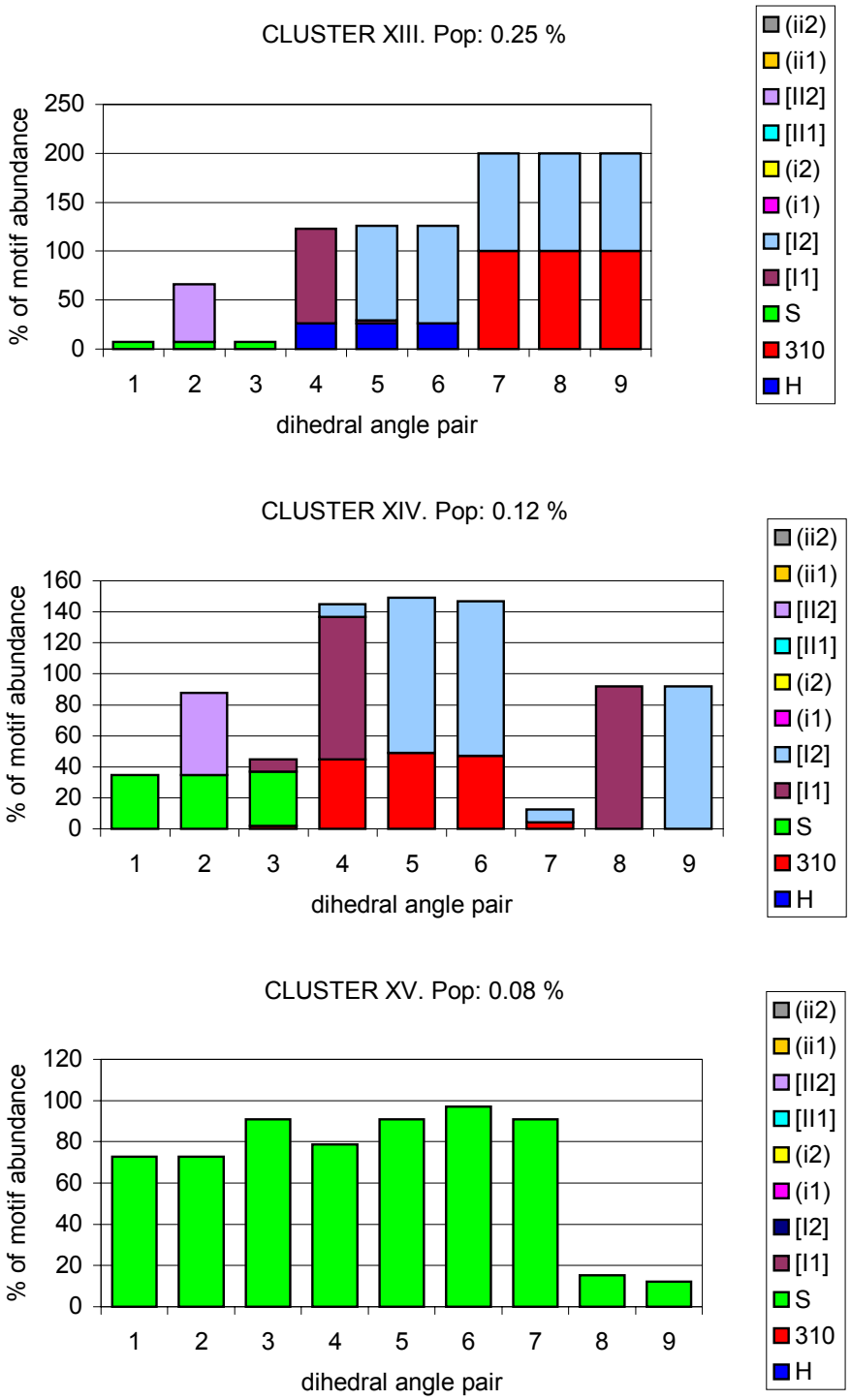

Figure 5.12. Clusters obtained for the MD trajectory of SPOH in water.

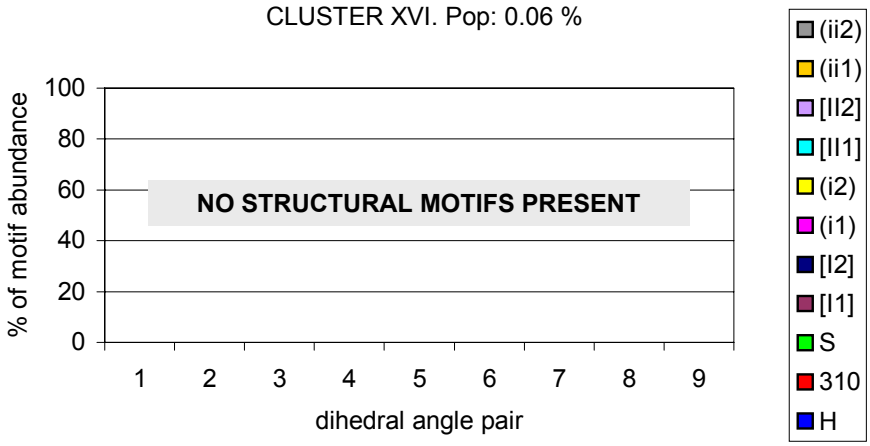

Figure 5.12. Clusters obtained for the MD trajectory of SPOH in water.

Table 5.9. Summary of the main structural features of the 16 clusters obtained using CLUSTERIT for the MD trajectory of SPOH in water. The second column shows the percentage of the total number of structures obtained in this MD trajectory that are contained within each cluster. The last column corresponds to the percentage of structures within each cluster that exhibit each motif. When the motif expands more than one residue with different percentages the interval is shown.

CLUSTER	% OF STRUCTURES CONTAINED	MOTIFS PRESENT	RESIDUES INVOLVED	% OF STRUCTURES CONTAINING THE MOTIF
I	35.5	β-strand type I β-turn	2-5 6-9	89-100 15-100
II	21.8	β-strand 3_{10}-helical turn type I β-turn	2-4 5-7 5-8	100 16-17 87-100
III	19.9	α-helical turn type I β-turn	5-7 5-9	16-17 13-100
IV	7.9	type I β-turn II2 motif	6-8 3	99-100 72
V	4.0	β-strand 3_{10}-helical turn type I β-turn	2-5 6-8 6-10	86-98 94-100 13-100
VI	2.9	β-strand type I β-turn	2-5 7-8	96-100 29-30
VII	2.1	β-strand α-helical turn type I β-turn	2-4 5-8 5-8	100 83-100 100
VIII	2.0	β-strand type I β-turn type I β-turn	2-5 6-7 9-10	94-98 73 95

CLUSTER	% OF STRUCTURES CONTAINED	MOTIFS PRESENT	RESIDUES INVOLVED	% OF STRUCTURES CONTAINING THE MOTIF
IX	1.9	3_{10}-helical turn type I β-turn II2 motif	5-8 5-9 3	37-100 34-100 35
X	0.8	β-strand type I β-turn	2-5 8-10	89-93 91-100
XI	0.4	β-strand type I β-turn type I' β-turn	2-5 5-7 8-9	99 88 100
XII	0.4	type I β-turn type I' β-turn	7-10 6-7	59-100 38
XIII	0.2	α-helical turn 3_{10}-helical turn type I β-turn II motif	5-7 8-10 5-10 3	26 100 97-100 59
XIV	0.1	β-strand 3_{10}-helical turn type I β-turn type I β-turn II motif	2-4 5-7 5-7 9-10 3	35 45-49 92-100 92 53
XV	0.1	β-strand	2-9	12-97
XVI	0.1	none	--	--

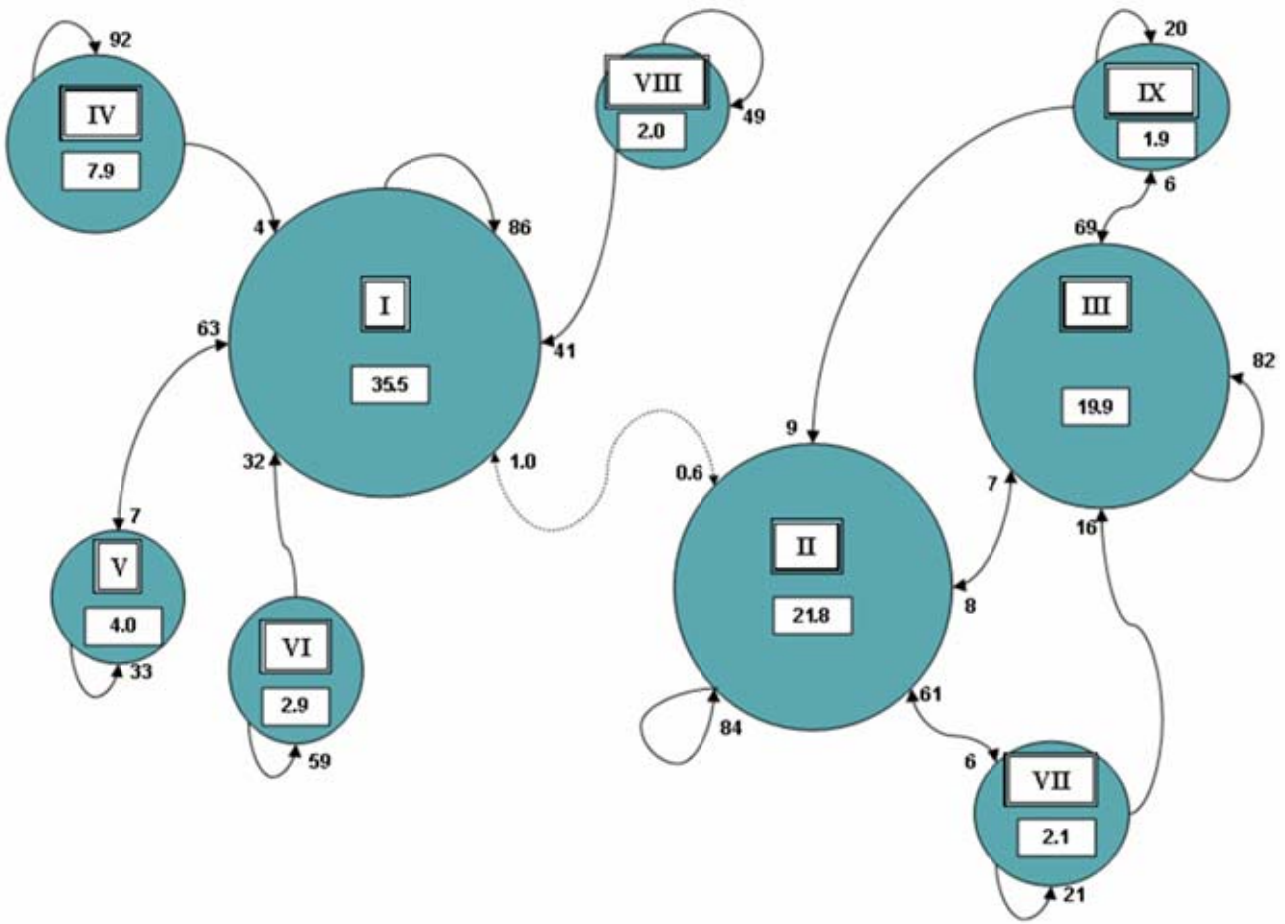

Figure 5.13. Transitions between the 9 largest clusters for the MD trajectory of SPOH in water.

Table 5.10. Summary of the local transitions with probability larger than 5% obtained for the MD trajectory of SPOH in water.

CLUSTERS		TRANSITIONS			REVERSIBILITY	STRUCTURES	
Origin	End	Total	% Local	% Global		Total	% Local
I	V	999	7.02	4.96	1.01	14222	35.46
	I	12198	85.77	30.42	1		
II	III	658	7.52	3.28	1	8746	21.81
	II	7326	83.76	18.27	1		
	VII	511	5.84	2.56	0.99		
III	III	6516	81.77	16.25	1	7969	19.87
	II	656	8.23	3.28	1		
	IX	519	6.51	2.62	0.97		
IV	IV	2912	92.27	7.26	1	3156	7.87
V	V	532	33.61	1.33	1	1583	3.95
	I	991	62.6	4.96	0.99		
VI	I	371	31.82	1.85	1	1166	2.91
	VI	683	58.58	1.7	1		
VII	III	135	16.11	0.69	0.95	838	2.09
	II	514	61.34	2.56	1.01		
	VII	179	21.36	0.45	1		
VIII	VIII	396	49.44	0.99	1	801	2
	I	325	40.57	1.61	1.01		
IX	III	533	68.51	2.62	1.03	778	1.94
	II	71	9.13	0.36	0.95		
	IX	157	20.18	0.39	1		
X	VIII	30	9.55	0.16	0.86	314	0.78
	I	104	33.12	0.51	1.02		
	X	158	50.32	0.39	1		
XI	II	21	12.43	0.1	1	169	0.42
	XI	143	84.62	0.36	1		
XII	XII	108	70.59	0.27	1	153	0.38
	IV	12	7.84	0.06	1		
	III	11	7.19	0.06	0.92		
	VI	16	10.46	0.07	1.14		

XIII	III	38	38	0.19	1	100	0.25
	II	14	14	0.07	0.88		
	IX	10	10	0.04	1.25		
	XIII	34	34	0.08	1		
XIV	III	17	34.69	0.09	0.89	49	0.12
	II	14	28.57	0.07	1		
	IX	4	8.16	0.02	1		
	XIV	10	20.41	0.02	1		
XV	VI	6	18.75	0.03	1.2	32	0.08
	XV	21	65.63	0.05	1		
	XVI	6	18.75	0.03	1		
XVI	IV	2	8.7	0.01	0.67	23	0.06
	III	3	13.04	0.01	1		
	VI	9	39.13	0.04	1.13		
	XV	6	26.09	0.03	1		

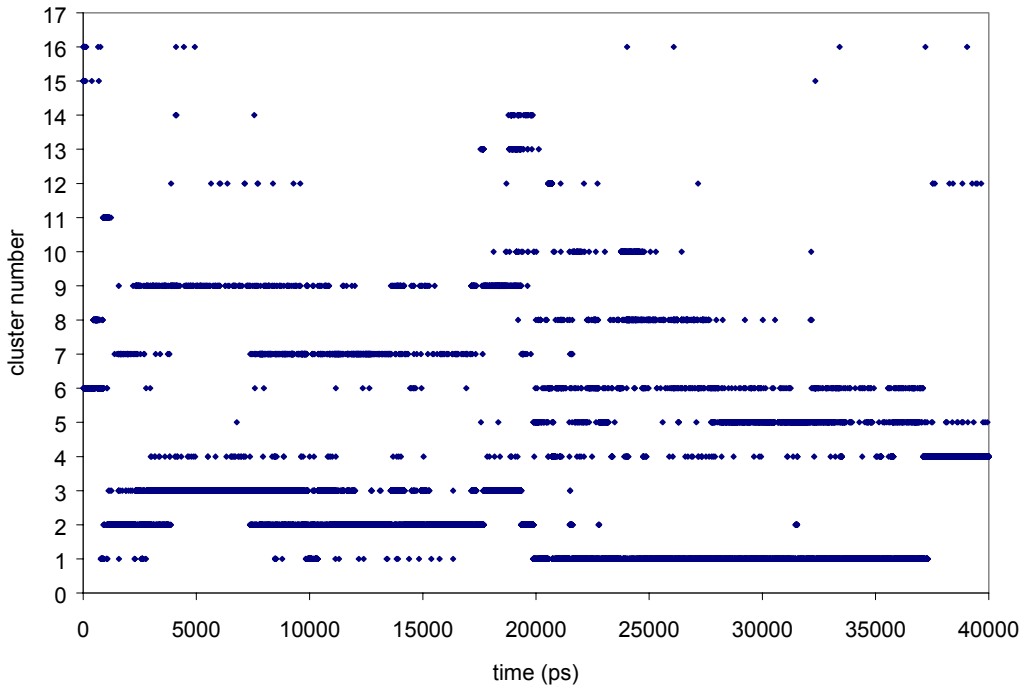

Figure 5.14. Evolution of clusters appearing along the MD trajectory of SPOH in water.

5.4.2.3. Molecular dynamics of SPOH in methanol

A 20 ns MD trajectory of the peptide at 300 K was undertaken starting from its extended conformation soaked in a box of methanol molecules, using PBC and PME conditions as described in the methods section. The total energy and the density kept fairly constant at 7832 kcal·mol^{-1} and 0.756 g·cm^{-3}, respectively.

The average helical content for SPOH in methanol yielded 8.5% and was calculated as the sum of all the percentages of structures exhibiting α or 3_{10}-helical motifs and divided by 9, the number of residues that contain dihedral angle pairs. The helical content for each residue was computed by using a modified version of the CLASICO method as described in the methods section. In order to compare values of helicity obtained from the simulation with those obtained experimentally data was collected for 10 ns after the peptide had reached a folded conformation (10 ns) and the total number of snapshots containing helix was divided by the total number of structures (10,000 structures). Data is shown in Figure 5.5.B.

The CLASICO algorithm was used to analyze the structures of the MD simulation in methanol with the charged N- and C-termini in order to determine the conformational motifs attained by SPOH that are summarized in Table 5.6. The different conformations were labeled according to the conformational motifs exhibited and classified into 228 different patterns. Figure 5.7.C shows the evolution of new patterns sampled along time. Until nanosecond 7 the growth is exponential and then the number of new patterns tends to grow slower. The patterns appearing at the first two ns (1-37) are rarely revisited along the rest of the trajectory whereas the patterns appearing from the 2 to 5 ns (38-81) are populated until the ns 16. From that point on a new group of patterns seem to be predominant (97-101, 197-223).

The folding process of the peptide can be analyzed in view of the evolution of patterns sampled. Since the simulation started from the extended conformation, the first patterns sampled correspond to structures with no conformational motifs or adopting dihedral angles of a β-strand (1-27). The pattern 28 contains a type I β-turn on residues 9 and 10 and β-strand dihedral angles for residues 2 to 5. Patterns from 27 to 37 contain a type I β-turn on residues 6 and 7 or/and 9 and 10 and type II β-turns on residues 8 and 9. Pattern 38 that is the most abundant pattern in the entire MD trajectory (18.05%) exhibits for the first time type I β-turns expanding from residues 6 to 10 and β-strand dihedral values from residues 2 to 5. This pattern seems to block the peptide in an ensemble of conformations that contain this pattern combined with the presence of α or 3_{10} helical motifs. From pattern 82 a group of patterns appear presenting β-strand dihedral values from

residues 2 to 4 and type I β-turns expanding from residues 5 to 10. These motifs are present on patterns 97 to 101 that are the most abundant for the 16 to 20 ns. Indeed pattern 101 is the third most abundant pattern (9.02%), and is described by the presence of β-strand dihedral angle values for residues 2 to 4 and type I β-turns expanding from residues 5 to 8. A small group of conformations appearing from patterns 195 to 219 contain a type II' β-turn on residues 9 and 10 apart from the presence of β-strand dihedral angle values and type I β-turns mentioned above. The most abundant of these patterns is pattern 197 (2.68%).

In summary, the simulation shows that the peptide folds in the first 2 ns, to adopt a fold that is fairly kept for the rest of the MD trajectory. The folding process evolves from having a β-strand on residues 2 to 5 to residues 2 to 4 and type I β-turns expanding from residues 6 to 10 to residues 5 to 10. The peptide sporadically exhibits a type II' β-turn on residues 9 and 10.

The structures of SPOH in methanol previously characterized were classified into clusters using the CLUSTERIT algorithm, described in the methods section. A criterion of $\Delta\overline{R} \geq 0.01$ (Figure 5.8) was adopted to stop the clustering process. Using this criteria 9 clusters remained (Figure 5.15). Table 5.11 summarizes the main structural features of the clusters found from the analysis of the MD trajectory of SPOH in methanol. The five most abundant clusters, represent 90% of the structures (shown in Figures 5.15, clusters I to V) suggesting that the bulk of structures is grouped in a small number of clusters. The most abundant cluster (containing 49.2% of the total number of structures) exhibits β-strand dihedrals angle for residues 2 to 5 and a type I β-turn on residues 6 to 10. The second most abundant cluster (22.2%) exhibits β-strand values on residues 2 to 4 and consecutives type I β-turns extending from residues 5 to 10. Furthermore, it exhibits a 3_{10}-helical turn extending from residues 5 to 8. The third most abundant cluster (8.0%) exhibits β-strand values on residues 2 to 5 and consecutives type I β-turns and 3_{10}-helical turns extending from residues 6 to 10. Cluster IV (5.6%) contains structures exhibiting β-strand values on residues 2 to 10 in variable proportions. Cluster V exhibits the same motifs as cluster III, but in this case 3_{10}-helical turns are replaced by α-helical turns. The rest of clusters (VI to IX) account for 11% of the structures. Cluster VI has β-strand values at residues 2 to 4, type I β-turns at residues 5 to 10 and α-helical turns at residues 5 to 7. In addition, cluster VI shows a type II' β-turn at residues 9 and 10. Cluster VII and VIII have as special feature that the type I β-turns and the 3_{10}-helical turns expand residues 7 to 10 and cluster IX is the cluster that does not contain any conformational motif.

Transitions between clusters for the MD trajectory of SPOH in methanol were analyzed as described in the methods section and the data is presented in Table 5.12 and Figure 5.16. Only 8 clusters representing 99.9% of the structures and local transitions above 5% have been depicted

for conciseness. Although transitions between the two most abundant clusters with local transitions less than 5%, are also shown for later discussion. For each snapshot in the MD trajectory of SPOH in methanol, its corresponding cluster has been assigned. The cluster number of each conformation has been plotted in Figure 5.17.

Table 5.11. Summary of the main structural features of the 9 clusters obtained using CLUSTERIT for the MD trajectory of SPOH in methanol. The second column shows the percentage of the total number of structures obtained in this MD trajectory that are contained within each cluster. The last column corresponds to the percentage of structures within each cluster that exhibit each motif. When the motif expands more than one residue with different percentages the interval is shown.

CLUSTER	% OF STRUCTURES CONTAINED	MOTIFS PRESENT	RESIDUES INVOLVED	% OF STRUCTURES CONTAINING THE MOTIF
I	49.2	β-strand type I β-turn	2-5 6-10	85-100 42-90
II	22.2	β-strand type I β-turn 3_{10}-helical turn	2-4 5-10 5-8	93 17-100 25-41
III	8.0	β-strand type I β-turn 3_{10}-helical turn	2-5 6-10 6-10	75-91 70-100 36-100
IV	5.6	β-strand	2-10	33-99
V	5.2	β-strand type I β-turn α-helical turn	2-5 6-10 6-9	57-61 82-100 17-63
VI	4.3	β-strand type I β-turn α-helical turn type II' β-turn	2-4 5-10 5-7 9-10	100 13-100 20-26 79
VII	3.6	β-strand type I β-turn	2-5 7-10	83-96 56-100
VIII	1.8	β-strand type I β-turn 3_{10}-helical turn	2-5 7-10 7-10	92-98 33-100 15-36
IX	0.04	none	--	--

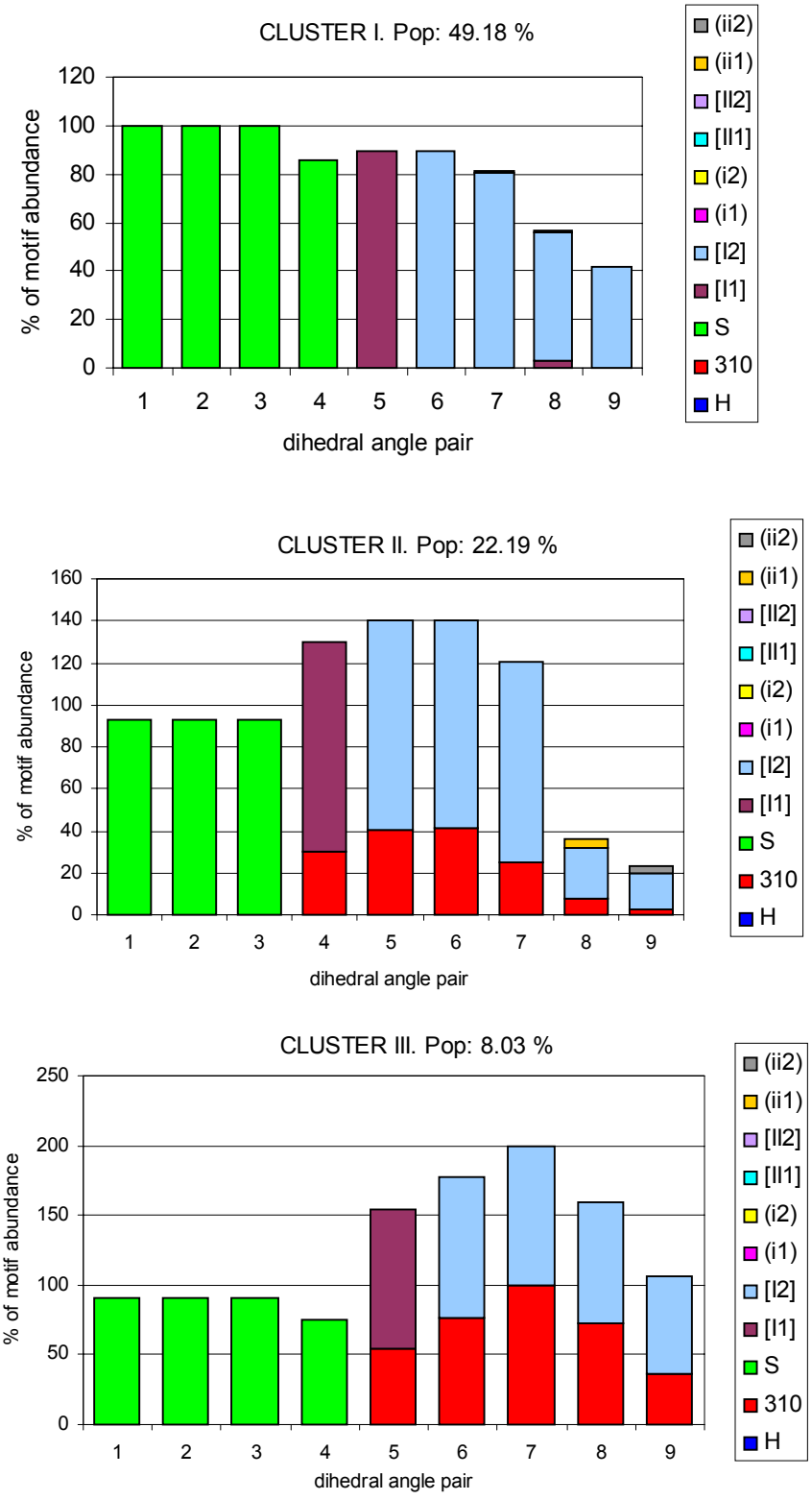

Figure 5.15. Clusters obtained for the MD trajectory of SPOH in methanol.

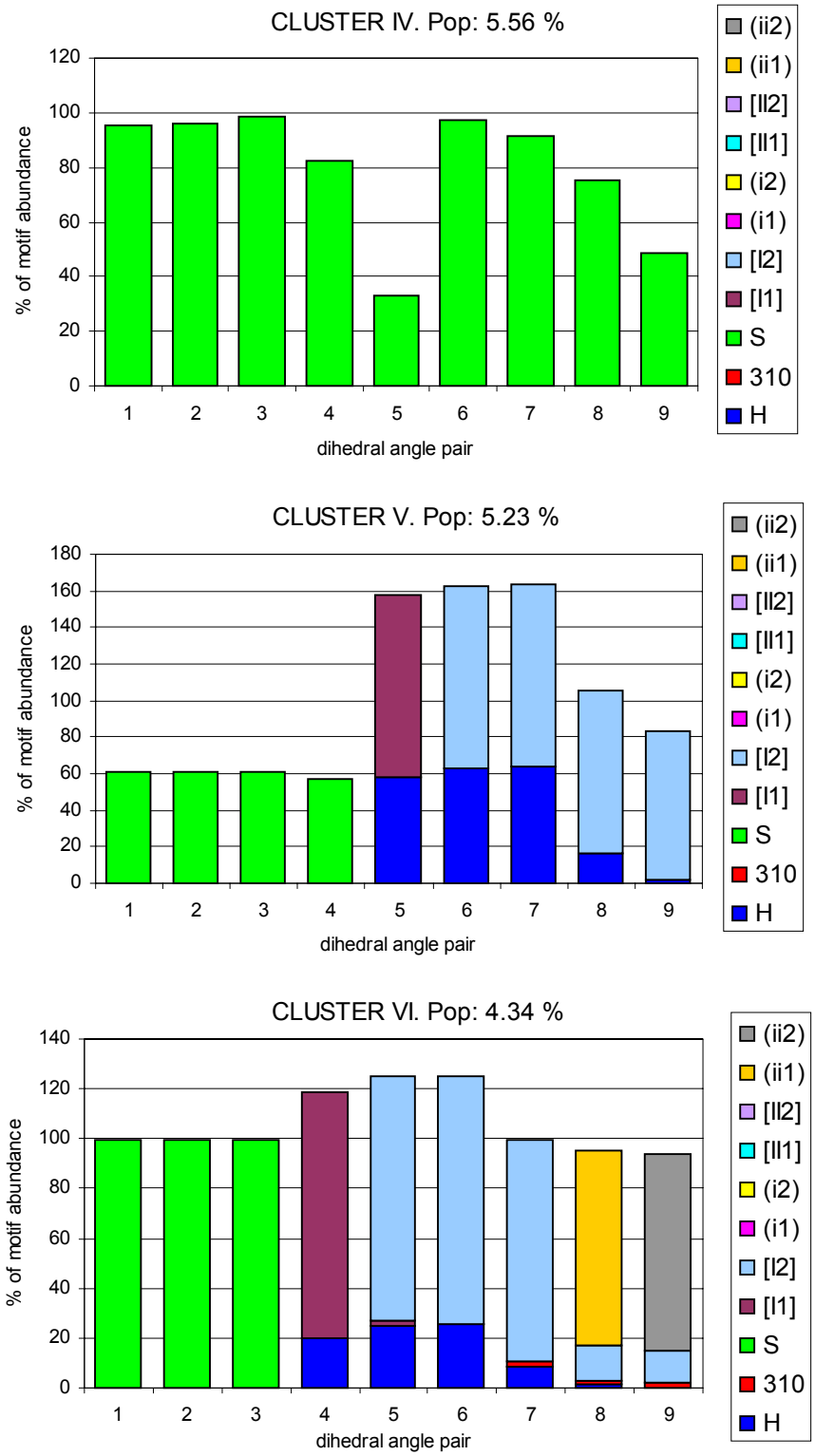

Figure 5.15. Clusters obtained for the MD trajectory of SPOH in methanol.

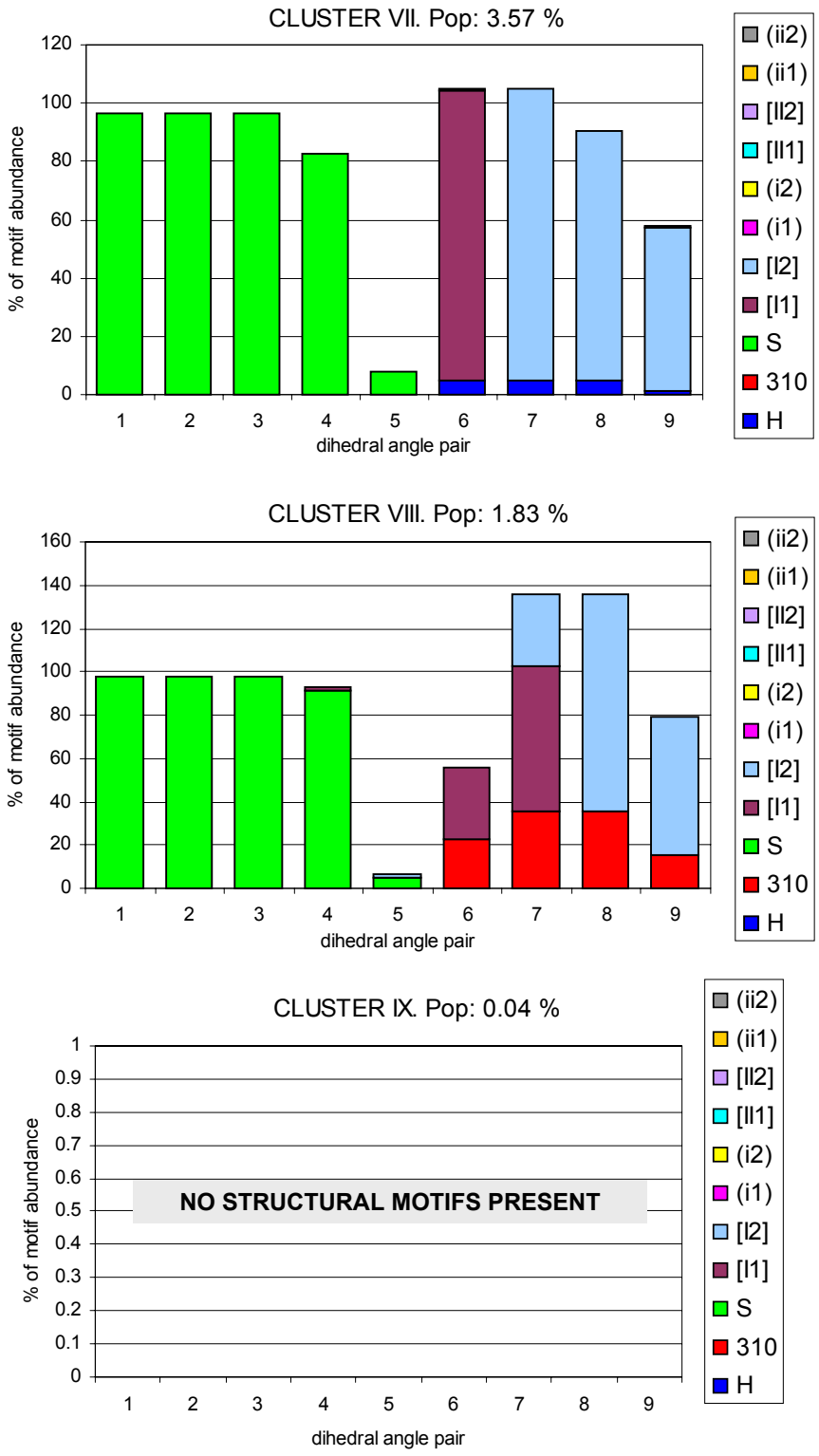

Figure 5.15. Clusters obtained for the MD trajectory of SPOH in methanol.

Table 5.12. Summary of the local transitions with probability larger than 5% obtained for the MD trajectory of SPOH in methanol.

CLUSTERS		TRANSITIONS			REVERSIBILITY	STRUCTURES	
Origin	End	Total	% Local	% Global		Total	% Local
I	III	682	6.85	6.76	0.99	9960	49.18
	I	8259	82.92	40.78	1		
II	VI	416	9.26	4.09	1.01	4494	22.19
	II	3911	87.03	19.31	1		
III	V	148	9.1	1.46	1.01	1627	8.03
	III	690	42.41	3.41	1		
	I	687	42.22	6.76	1.01		
IV	IV	991	87.93	4.89	1	1127	5.56
	I	120	10.65	1.18	1.02		
V	V	387	36.51	1.91	1	1060	5.23
	III	147	13.87	1.46	0.99		
	I	481	45.38	4.7	1.02		
VI	VI	447	50.91	2.21	1	878	4.34
	II	413	47.04	4.09	0.99		
VII	VII	396	54.7	1.96	1	724	3.57
	VIII	65	8.98	0.66	0.96		
	I	165	22.79	1.62	1.01		
VIII	VII	68	18.33	0.66	1.05	371	1.83
	VIII	86	23.18	0.42	1		
	III	30	8.09	0.27	1.25		
	I	160	43.13	1.64	0.92		
IX	IV	3	37.5	0.02	1.5	8	0.04
	I	5	62.5	0.05	0.83		

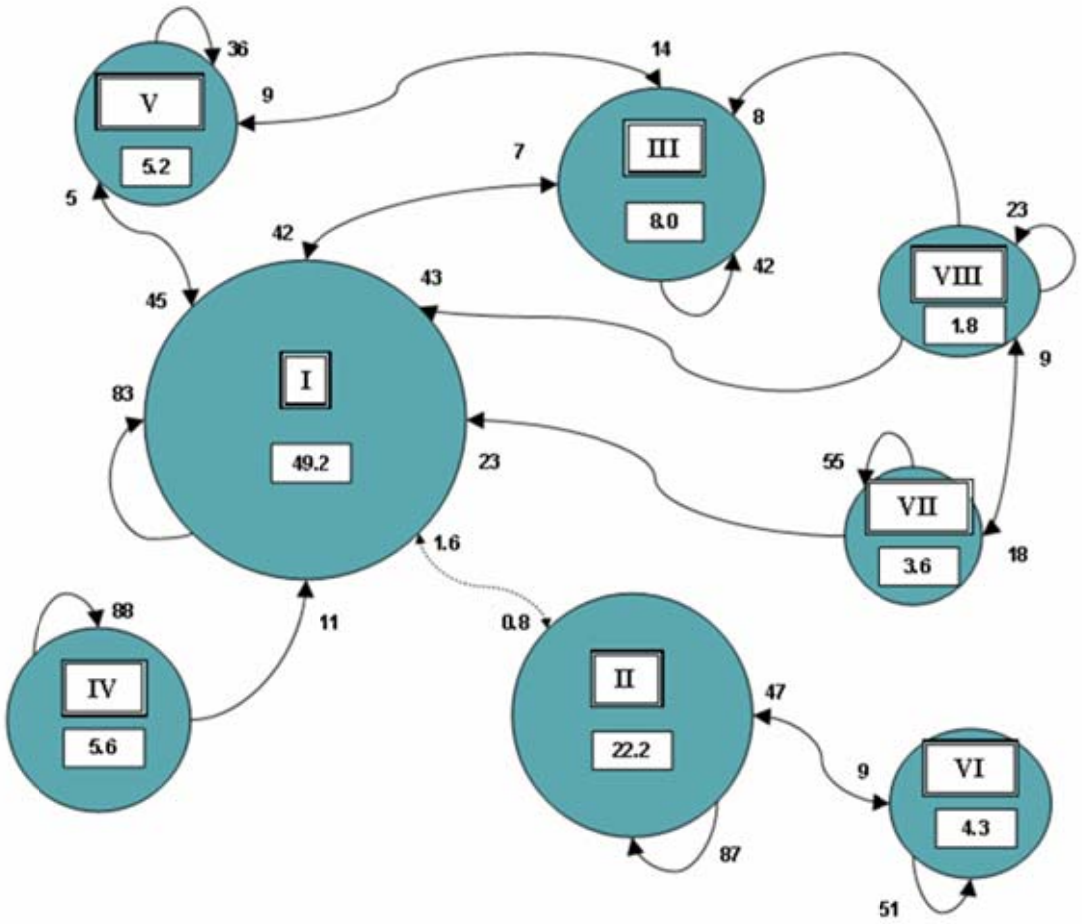

Figure 5.16. Transitions between the 8 largest clusters for the MD trajectory of SPOH in methanol.

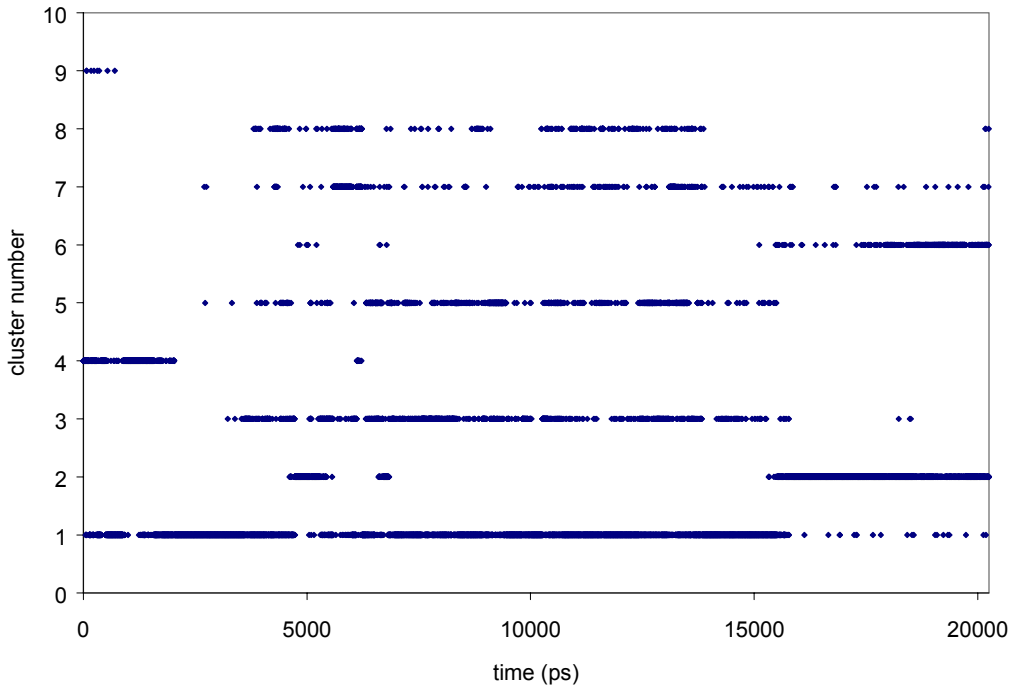

Figure 5.17. Evolution of clusters appearing along the MD trajectory of SPOH in methanol.

5.4.2.4. Molecular dynamics of SPOH in DMSO

The CLASICO algorithm was used to analyze the structures of the MD simulation in DMSO in order to determine the conformational motifs attained by SPOH that are summarized in Table 5.6. The average helical content for SPOH in DMSO yielded 0.0% as structures exhibiting α or 3_{10}-helical motifs are residual. The different conformations were labeled according to the conformational motifs exhibited and classified into 22 different patterns. Figure 5.7.D shows the evolution of new patterns sampled along the trajectory. At the beginning of the trajectory the profile grows until 17 patterns in 1.7 ns. Then for the rest of the MD trajectory, 18 ns, only 4 new patterns appear, thus indicating that the trajectory is reaching a plateau regarding the appearance of new type of conformations.

The folding process of the peptide in DMSO can be analyzed from the evolution of the patterns sampled. Since the simulation started from the extended conformation, the first patterns sampled correspond to structures exhibiting β-strand dihedral angles throughout all the peptide. Subsequently, SPOH adopts a very unstable type I β-turn at residues 8 and 9 at picosecond 67 (pattern 7). A new unstable type I β-turn appears at picosecond 182 (pattern 9) located at residues

9 and 10. Several other patterns (11-15) exhibit a type I β-turn at residues 8 to 10 and a 3_{10}-helical turn. The latter appears at picosecond 589 for 1 picosecond. All these conformational motifs constitute a rarity and only appear on the first half of the first nanosecond of the MD trajectory of SPOH in DMSO. The most abundant pattern in the first 15 ns of the MD trajectory are patterns 4 and 10 that are characterized by the presence of β-strand dihedral angles at residues 2 to 7 and 2 to 6, respectively. From nanosecond 15 the most abundant pattern is pattern 16 and 17 that only contain β-strand values at residues 2 to 4 and 2 to 5, respectively. Patterns 20 and 21 appear also at nanosecond 15 and exhibit β-strand values at residues 2 to 5 and 2 to 4 and a type II' β-turn at residues 9 and 10.

To sum up, the simulation points to a tendency to SPOH to attain an unfolded conformation in DMSO. The molecule forms very unstable type I and II' β-turns at residues 9 and 10 and only attains a very limited number of different patterns (22) in almost 20 ns of MD trajectory that compares poorly with the 228 patterns obtained in methanol in 20 ns of MD trajectory.

The structures of SPOH in DMSO previously characterized were classified into clusters using the CLUSTERIT algorithm, described in the methods section. A criterion of $\Delta\overline{R} \geq 0.01$ (Figure 5.8) was adopted to stop the clustering process. Using this criterion 10 clusters remained (Figure 5.18). Table 5.13 summarizes the main structural features of the clusters found from the analysis of the MD trajectory of SPOH in DMSO. The four most abundant clusters represent 99.4 suggesting that most of the structures are grouped only in 4 clusters. The three most abundant clusters (containing 69.6%, 20.4% and 8.93% of the total number of structures) exhibit β-strand dihedrals angle for residues 2 to 6, 2 to 5 and 5 to 7, respectively. Cluster IV that only accounts for 0.58% of the structures exhibits β-strand values on residues 2 to 8 and a type I β-turn between at residues 9 and 10. Cluster V (0.29%) is the cluster presenting no conformational motifs. Cluster VI and X exhibits β-strand values at residues 2 to 7 and a type I β-turn at residues 8 to 10. Furthermore, cluster X exhibits a 3_{10}-helical turn at residues 8 to 10. Cluster VIII exhibits β-strand dihedral angles at residues 2 to 5 and a type II' β-turn at residues 9 and 10.

Transitions between clusters for the MD trajectory of SPOH in DMSO were analyzed as described in the methods section and the data is presented in Table 5.14 and Figure 5.19. Only 6 clusters representing 99.9% of the structures and local transitions above 5% have been depicted for conciseness. However the most abundant transitions of cluster I, the largest cluster (69.6%), have also been depicted. For each snapshot in the MD trajectory of SPOH in DMSO, its corresponding cluster has been assigned. The cluster number of each conformation has been plotted in Figure 5.20.

Table 5.13. Summary of the main structural features of the 10 clusters obtained using CLUSTERIT for the MD trajectory of SPOH in DMSO. The second column shows the percentage of the total number of structures obtained in this MD trajectory that are contained within each cluster. The last column corresponds to the percentage of structures within each cluster that exhibit each motif. When the motif expands more than one residue with different percentages the interval is shown.

CLUSTER	% OF STRUCTURES CONTAINED	MOTIFS PRESENT	RESIDUES INVOLVED	% OF STRUCTURES CONTAINING THE MOTIF
I	69.6	β-strand	2-7	92-100
II	20.4	β-strand	2-5	31-100
III	8.9	β-strand	5-7	100
IV	0.6	β-strand type I β-turn	2-8 9-10	26-100 100
V	0.3	none	--	--
VI	0.14	β-strand type I β-turn	2-7 8-10	96-100 88-100
VII	0.06	β-strand	2-10	92-100
VIII	0.05	β-strand type II' β-turn	2-5 9-10	30-100 100
IX	0.01	β-strand type I β-turn	2-4 5-6	100 100
X	0.01	β-strand type I β-turn 3_{10}-helical turn	2-7 8-10 8-10	100 100 100

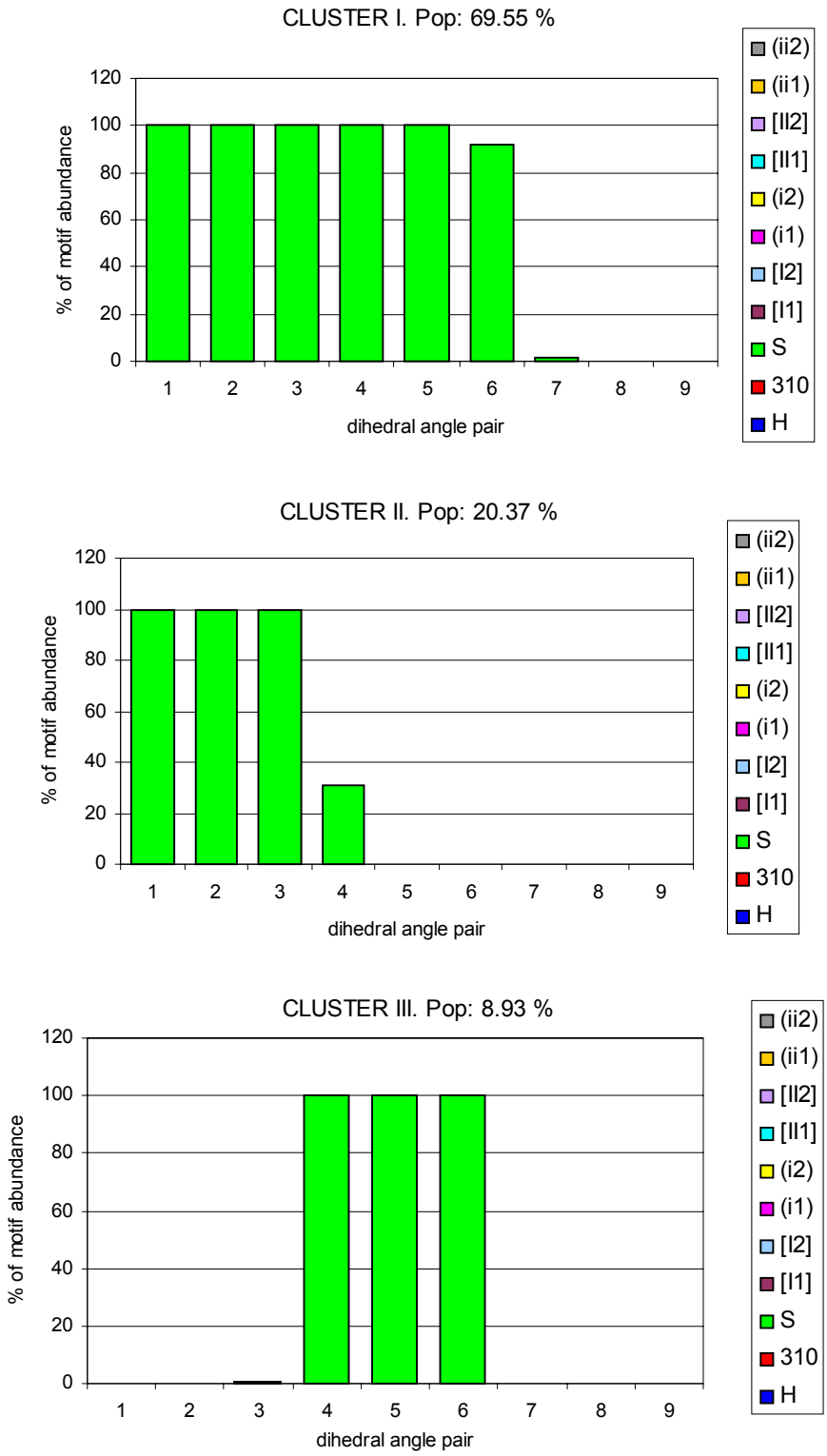

Figure 5.18. Clusters obtained for the MD trajectory of SPOH in DMSO.

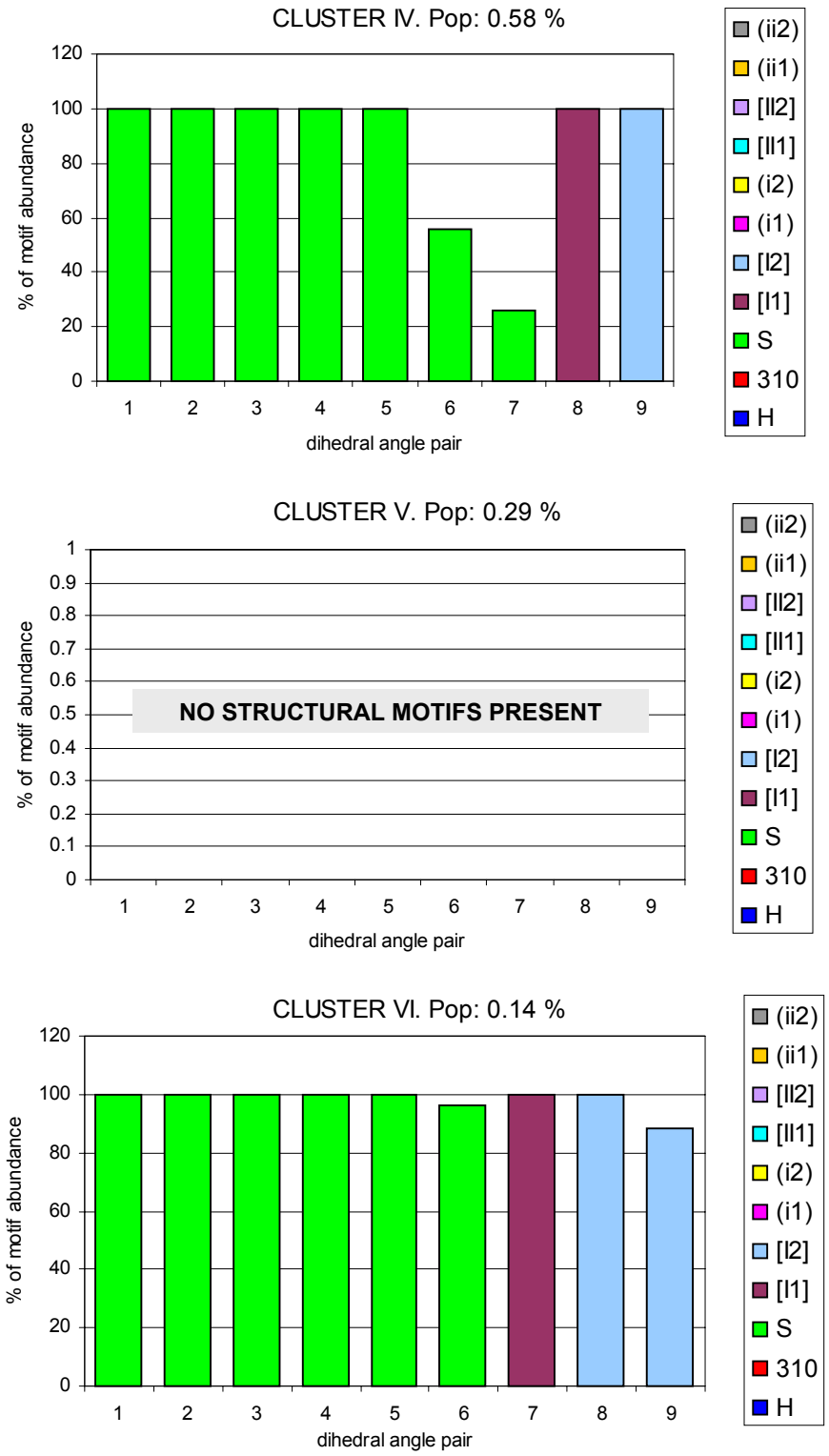

Figure 5.18. Clusters obtained for the MD trajectory of SPOH in DMSO.

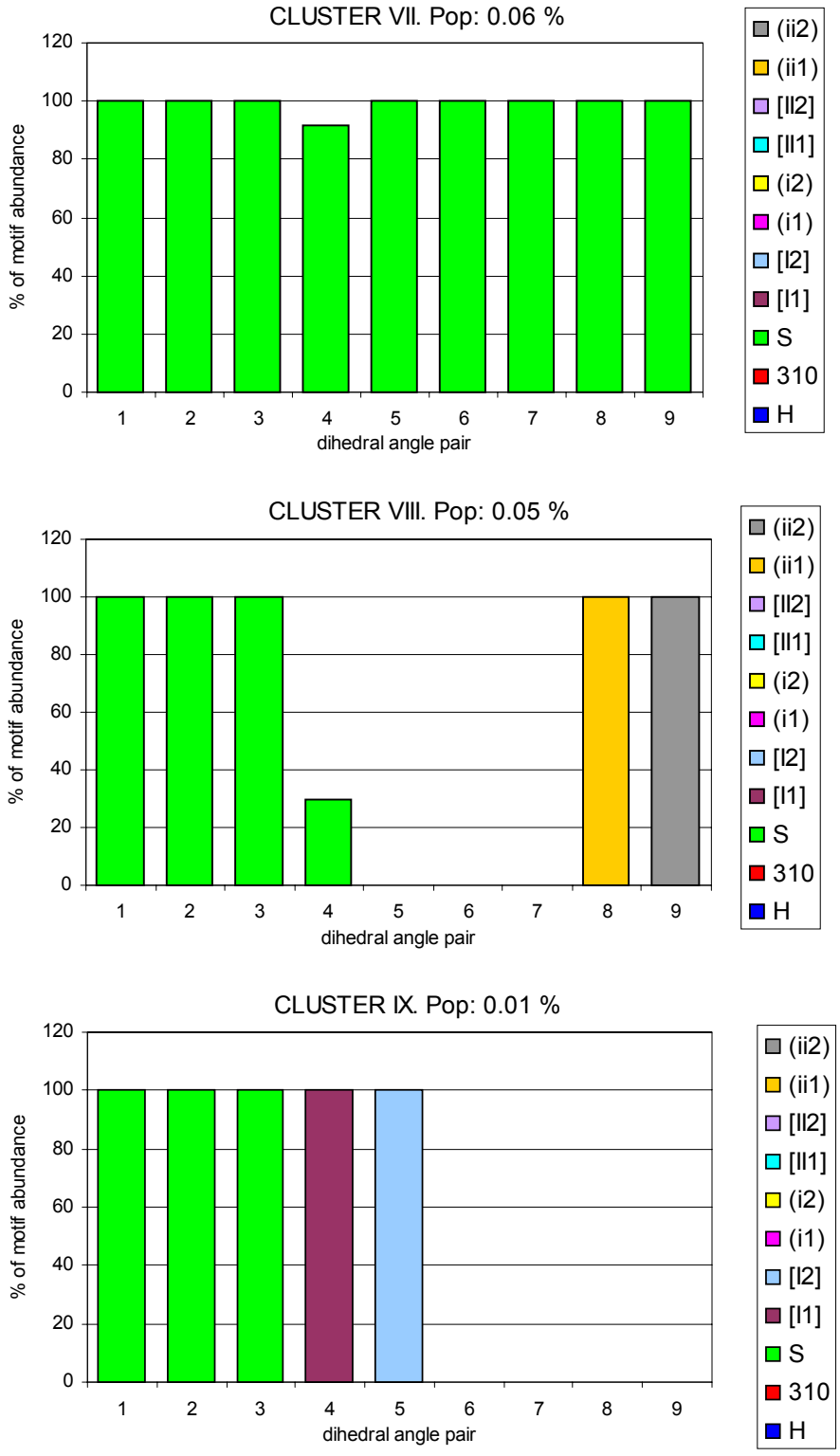

Figure 5.18. Clusters obtained for the MD trajectory of SPOH in DMSO.

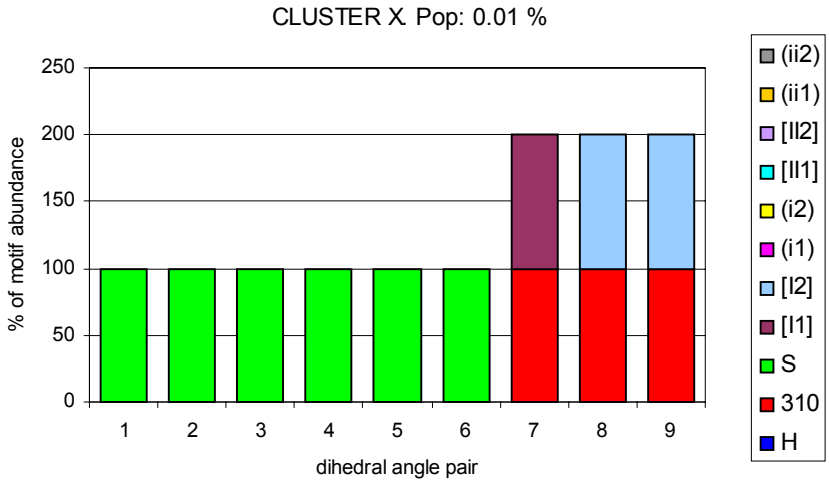

Figure 5.18. Clusters obtained for the MD trajectory of SPOH in DMSO.

Table 5.14. Summary of the local transitions with probability larger than 5% obtained for the MD trajectory of SPOH in DMSO.

CLUSTERS		TRANSITIONS			REVERSIBILITY	STRUCTURES	
Origin	End	Total	% Local	% Global		Total	% Local
I	I	12307	95.23	66.23	1	12923	69.55
II	II	3528	93.19	18.99	1	3786	20.37
II	I	244	6.44	2.63	1	3786	20.37
III	III	1320	79.52	7.1	1	1660	8.93
III	I	305	18.37	3.28	1	1660	8.93
IV	I	53	49.53	0.57	1.02	107	0.58
IV	IV	50	46.73	0.27	1	107	0.58
V	III	36	66.67	0.38	1.06	54	0.29
V	I	5	9.26	0.06	0.83	54	0.29
V	V	11	20.37	0.06	1	54	0.29
VI	I	6	23.08	0.08	0.75	26	0.14
VI	VI	14	53.85	0.08	1	26	0.14
VI	IV	5	19.23	0.05	1.25	26	0.14
VII	I	2	18.18	0.02	2	11	0.06
VII	VII	10	90.91	0.05	1	11	0.06
VIII	II	9	90	0.1	1	10	0.05
VIII	VIII	1	10	0.01	1	10	0.05
IX	I	1	100	0.01	0	1	0.01
X	II	1	100	0.01	1	1	0.01

Table 5.15. Maxima values for the probability distribution function for the dihedral angles of the MD trajectories of SP in water and of SPOH in water, methanol and DMSO.

ANGLE	SP IN WATER		SPOH IN WATER		SPOH IN METHANOL		SPOH IN DMSO	
	Angle value	Probab.	Angle value	Probab.	Angle value	Probab.	Angle value	Probab.
ψ_1	130, 140	25.62, 24.83	130, 140	21.42, 20.92	120	21.18	130	25.46
ω_1	180	39.36	180	37.65	180	40.00	180	41.09
ϕ_2	-60	33.34	-60	33.11	-60	31.97	-60	33.40
ψ_2	-20, 170	2.86, 26.62	-20, 170	1.92, 27.16	170	30.22	170	34.03
ω_2	180	37.11	180	35.80	180	37.54	180	38.77
ϕ_3	-130, -120, -60	6.05, 6.03, 23.63	-130, -120, -60, 40, 50	4.51, 4.40, 21.83, 3.47, 3.63	-130, -120, -60	2.85, 3.06, 28.95	-60	35.64
ψ_3	90, 160	2.50, 26.24	70, 160	4.60, 21.02	130, 140, 160	14.97, 15.35, 20.56	160	29.27
ω_3	180	40.41	180	38.96	180	41.33	180	35.71
ϕ_4	-60	30.09	-70, -60	31.31, 32.65	-70, -60	30.10, 32.14	-70, -60	31.56, 31.64
ψ_4	-20, -10, 170	1.32, 1.35, 28.93	90, 100, 170	5.82, 5.97, 24.33	170	27.72	90, 160, 170	2.43, 20.04, 19.66
ω_4	-170	36.11	-170	34.75	180	34.31	180	33.66
ϕ_5	-130, -50	2.18, 32.47	-130, -60	3.32, 29.19	-130, -60, -50	2.48, 27.80, 26.61	-140, -60	18.18, 10.09
ψ_5	-30, 170	25.73, 3.17	-30, -20, 90, 160	13.49, 13.08, 3.88, 6.63	-30, -20, 10, 20, 50, 110, 160	6.18, 6.30, 1.47, 1.46, 1.17, 9.38, 10.68	80, 90, 170	3.72, 3.61, 20.61
ω_5	180	47.66	180	35.56	-170	35.91	180	35.15
ϕ_6	-60	32.80	-60, -50	31.77, 30.69	-50	29.72	-130, -120, -70, -60	4.94, 5.08, 21.64, 21.68
ψ_6	-20, 160, 170	22.09, 2.09, 2.01	-20	26.65	-20	24.65	-10, 0, 160, 170	2.59, 2.74, 21.46, 20.76
ω_6	180	46.67	180	46.61	180	43.60	180	36.54
ϕ_7	-110, -60, 70	6.83, 20.20, 4.77	-120, -60	2.03, 26.93	-130, -50	2.08, 28.02	-60	32.45
ψ_7	-30, 160, 170	17.17, 2.09, 2.01	-30	20.41	-20, 160, 170	19.32, 1.95, 2.12	140	18.77

ω_7	180	37.79	180	41.54	180	42.55	180	41.89
ϕ_8	-120, -60	5.18, 19.43	-120, -70	7.48, 18.40	-110, -60	6.13, 21.73	-130	18.98
ψ_8	-10, 120, 140, 150	15.81, 2.86, 2.62,2.63	0	24.10	-10, 160, 170	19.92, 2.03, 2.23	-10	21.32
ω_8	180, -170	32.66, 32.89	-180, -170	36.34, 34.63	180	37.83	170	39.27
ϕ_9	-60, 80, 170,	7.04, 13.29, 1.71	-180, -70, 80	2.94, 2.98, 15.87	-180, -70, 80	3.64, 13.03, 3.05	80	27.94
ψ_9	10	15.55	10, 20	17.98, 17.82	-170, -80, 0, 70, 80	3.41, 2.56, 13.03, 2.04, 2.06	0, 10	17.84, 17.22
ω_9	-170	36.78	-170	38.50	180	37.54	-170	39.45
ϕ_{10}	-120, -60	2.17, 27.90	-120, -70	5.69, 19.52	-130, -120, -60	7.26, 7.75, 18.34	-70	22.99
ψ_{10}	-20	20.84	-10, 0, 90, 170	16.61, 15.93, 2.30, 2.40	-20, 120, 130	19.03, 1.51, 1.30	-10	16.53
ω_{10}	180	39.08	-180, -170	35.10, 33.85	180	34.22	-180, -170	32.73, 32.16
ϕ_{11}	-120, -70	7.68, 19.07	-130, -60	11.27, 13.75	-130, -70	10.87, 12.84	-140	31.16

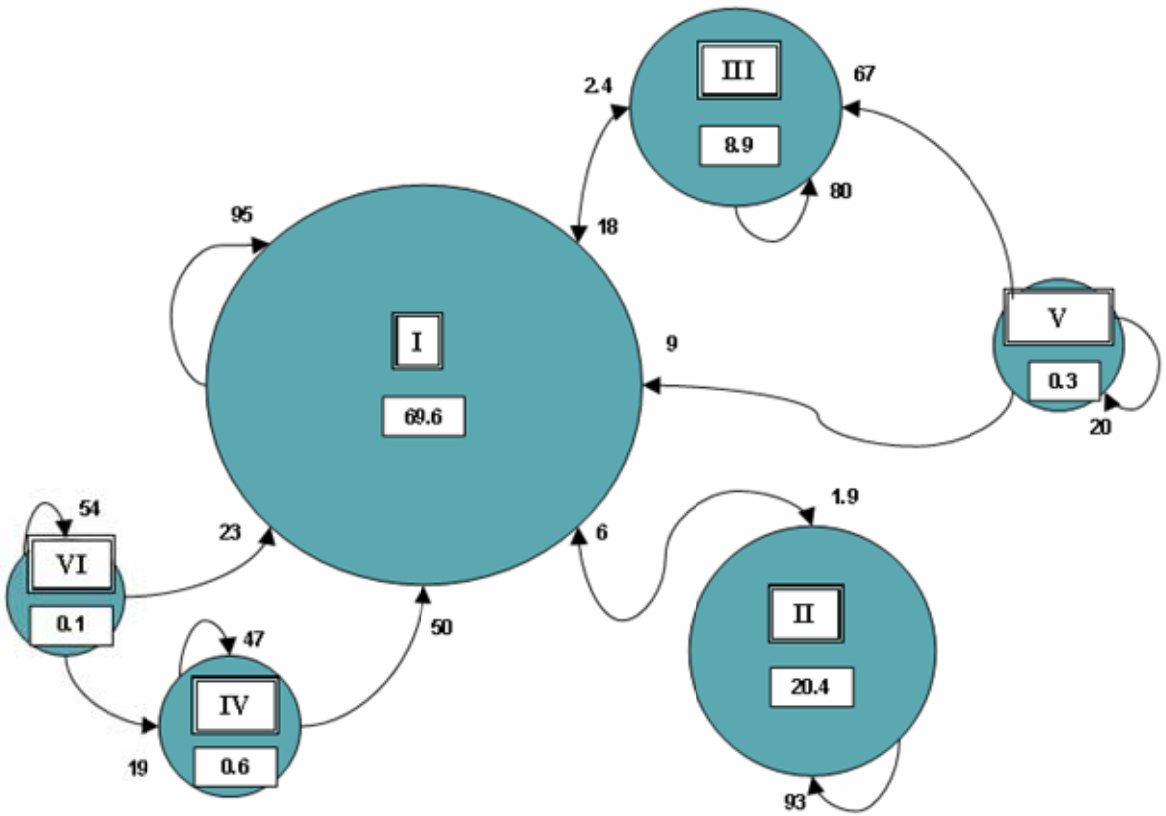

Figure 5.19. Transitions between the 6 largest clusters for the MD trajectory of SPOH in DMSO.

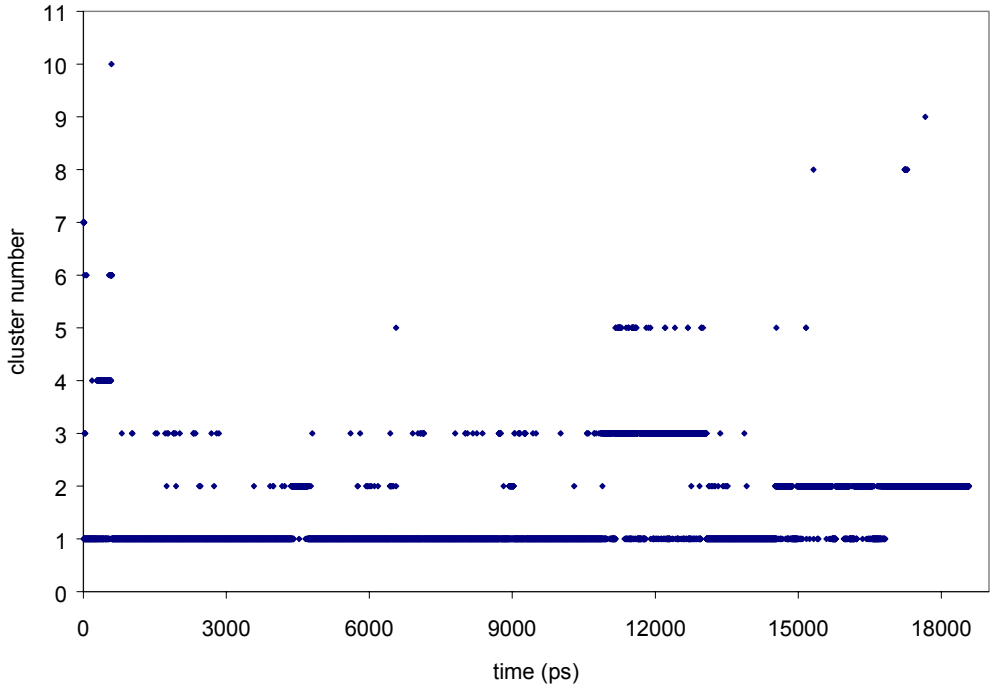

Figure 5.20. Evolution of clusters appearing along the MD trajectory of SPOH in DMSO.

5.6. Discussion

From the NOEs observed for SPOH in water and methanol (Figure 5.2), it can be inferred that the peptide does not show any strong interaction expanding 3 or 4 residues that could correspond to the presence of a 3_{10}- or α-helical turns, and only the NOEs for consecutive amide groups can be detected for the central part of the peptide, the region exhibiting a larger helical content. This must be the result of the peptide rapidly interconverting between α- and 3_{10}-helical motifs. Thus, in order to reduce the flexibility of the peptide and stabilize its secondary structures the use of a TFE/water mix could be a good choice as it has been reported in the literature (Bodkin et al., 1995). From the results of this study it could be inferred that SPOH would adopt a similar conformation to that obtained by Lee et al. (1999) on SP under a TFE/water mix, i.e. an extended conformation for the N-terminus and an α-turn for residues 5 to 9.

The assessment of the helical content estimated from the Hα conformational shifts (HαCS) can give an indication of the general structure of the peptide (Figure 5.3). Negative values of HαCS are indicative of helicity. From the results obtained in the present study for the SPOH in

water it can be inferred that the three first residues in the sequence are non helical and that from residue 5 the peptide adopts a structure with a certain degree of helicity (Figure 5.3). When the peptide is placed in methanol the same pattern applies with local deviations. Indeed, Arg^{1} and Leu^{10} have positive HαCS values whereas they are negative in water. For the region expanding residues 4 to 9 values are more negative in methanol than in water thus suggesting that the helix is more stable in methanol than in water. This is in agreement with what has been described by several authors that helices are more stable in alcoholic solvents than in water (Dwyer, 1998, Shimizu et al., 1999, Kinoshita et al., 2000). Thus, the average helical content yielded 10% in water and 23% in methanol. The helical content for the MD trajectories was also larger in methanol than in water (8.5% and 5.7%, respectively). The average helical content was 6.1% for SP in water showing no significant difference in respect to the MD trajectory of SPOH in water. Helical motifs for SPOH in DMSO are clearly disfavored as the average helical content obtained was 0.0%.

The helical content for residue was calculated dividing the HαCS by 0.38 ppm, the value corresponding to 100% helicity. For the MD trajectories of SPOH in water and methanol the helical content for each residue was calculated and plotted in Figures 5.4 and 5.5. In both cases, water and methanol, there is a general correspondence between the helicity computed for each residue in the NMR experiments and in the MD simulation. It is not possible to obtain the helicity on the MD trajectories for the end residues Arg^{1} and Met^{11} because there is not a pair of dihedral angles for these residues. The MD trajectory of SPOH in water yields helix from residues 5 to 10. In the NMR experiments the helix is deduced from residues 4 to 9 and at residue 11. This difference is due to the fact that we are obtaining an estimation of helicity by methods that do not share the same theoretical principles. The biggest discrepancy appears at Leu^{10} that is not helical on the NMR experiments and has more than 30% of helicity based on the MD estimation. This effect could be due to the high flexibility of Gly^{9} that could alter the helicity estimated for the following residue in the sequence.

The 40 ns MD simulation of SP and SPOH in water yielded 196 and 231 patterns, respectively. On the other hand, SPOH in DMSO only attained 22 different patterns in 20 ns (compared with 175 and 145 patterns obtained for SP and SPOH in water in 20 ns) indicating that within DMSO the peptide presents a rigid extended conformation. In methanol, SPOH exhibits a substantially more flexible behavior than in water, adopting 228 patterns in 20 ns of MD trajectory.

Regarding the conformational motifs SP and SPOH present under the different solvent conditions that have been summarized in Table 5.6, several differences arouse. In water, SPOH has a greater propensity to form the II2 motif than SP (9.2% vs. 1.1%). SP in water has a greater propensity to form type I β-turn at residue 5 (81.1%) than SPOH within the same conditions (46.5%). On the contrary, β-strand propensity is larger for SPOH (40.3%) than SP (14.5%) for the

same residue. Furthermore, residues 6 to 10 show a greater tendency to attain 3_{10}-helical turns for SPOH and on the opposite SP exhibits a greater proportion of α-helices for the same residues. Other minor differences can be also pointed out. Thus, SPOH in water exhibits a type II' type β-turn at residues 6 and 7, whereas SP in water exhibits the same conformational motifs at residues 9 and 10. Both SP and SPOH exhibit a type II β-turn at residues 8 and 9 but with different abundance (5.8% and 0.1%, respectively). Finally, SP shows a greater proportion of conformations with type I β-turn at residues 9 and 10 than SPOH in water (25.9% versus 11.9%, respectively).

On the other hand, when comparing the behavior of SPOH in water and methanol the molecule shares the general structural traits, although several differences can be pointed out. It has to be taken into account that some differences could be due to the different length of both MD trajectories (40 ns in water and 20 ns in methanol). First of all, β-strand dihedral angle values for residues 2 to 4 show a marked greater propensity in methanol than in water (95% versus 69%, respectively). Regarding residue 5 there is a greater tendency to attain β-strand dihedral angles in methanol than in water. For residues 6 and 7, the molecule in methanol has a clear preference to form 3_{10}-helical turns than to form α-helical turns (3 to 4 times) whereas in water the difference is lower (1.5 times greater preference for 3_{10}- than α-helical turns). For residues 8 to 10 the tendency to form helical turns is greater in methanol being the 3_{10}-helical turn the preferred type of helix in water and methanol. Residues 9 and 10 adopt type I β-turn in a greater proportion than in water (around 3 times). Therefore, for SPOH there is a balanced equilibrium between 3_{10}- and α-helical forms that is skewed towards 3_{10}–helical form in methanol. This is in agreement with the results on the study of α- and 3_{10}-helical transition through the use of potential of mean force reported by Smythe et al. (1995). The authors suggest that from thermodynamic data it can be deduced that α-helices are enthalpically stabilized and 3_{10}-helices are entropically favored. However, shorter 3_{10}-helices will also be favored enthalpically in nonpolar environments. This seems to be the case for SPOH when methanol is used as solvent. The fact that helices adopted by SPOH are favored in alcohol solvents seems to be in agreement with other studies indicating that helical turns are stabilized in peptides when solvent is changed from water to methanol. This has been rationalized by Kinoshita el al. (2000) on the basis of a greater work required for the cavity formation in methanol than in water due to the lower density of the alcohol, and as a consequence solvophobic atoms of a peptide can be exposed to the solvent more than in water and exposure of solvophilic atoms become less important. The solvation free energy in alcohol becomes less variable against conformational changes. The peptide molecule has a tendency to adopt the conformation with the lowest conformational energy with intramolecular hydrogen bonds such as the helical motifs. From experimental results (Hamada et al., 1995, Hamada, et al., 1997 and Hirota et al., 1998) it has been observed that alcohol induces peptides to form helical structures, and the degree of the induction increases with the increase in the size of the hydrocarbon group in alcohol (Ramirez-Alvarado et al., 1996). These authors suggest that the same could be applied for β-sheet if that is

the most stable structure. In fact, this is the case for the N-terminus of the peptide where methanol stabilizes the β-strand conformation of the peptide.

Finally, regarding the differences between SPOH in water and DMSO the behavior is markedly different. SPOH in DMSO adopts β-strand for residues 2 to 7. Residues 8 to 10 adopt sporadically type I β-turns and very rare events consist of type II' β-turns at residues 9 and 10. To sum up, the molecule mainly adopts an extended conformation and is fairly rigid, given the small number of different patterns appearing (22 patterns). This is in agreement with previous studies of vibrational spectroscopy undertaken by Vass et al. (1998) that pointed out the effect of DMSO in slowing down conformational interconversions and the decrease in the number of backbone conformers by distorting γ-turns and other weakly hydrogen bonded structures.

A more detailed comparison of the differences obtained from the use of different solvent conditions and between SP and SPOH can be done from the analysis of the dihedral angle distributions computed for the MD trajectories in study. Table 5.15 lists values of the maxima of the different dihedral angle distributions as well as their maximum probability value. Several differences between SP and SPOH in water were made evident. Dihedral angle ψ_2 shows a secondary peak at -20 only present in water for SP and SPOH and not present in methanol or DMSO for the MD trajectories of SPOH. Dihedral angle ϕ_3 exhibits two peaks for SP in water and for SPOH in methanol at -130º/-120º and at -60º and three peaks for SPOH in water at -130º/-120º, -60º and 40º/50º. On the other hand it exhibits only one peak at -60º for SPOH in DMSO. In all cases the most abundant peak is the one at -60º with probability going from 21% to 36%. For ψ_3 differences appear at the peak at 70º or 90º that is only present for SP and for SPOH in water and absent in methanol and DMSO. In methanol, SPOH exhibits a more marked peak at 130º/140º. In all cases, the most abundant peak corresponds to the peak at 160º. For ψ_4 a secondary peak appears at -20º only for SP and is absent for the rest of MD trajectories. A peak at 90º is only present for SPOH in water and DMSO and it is absent for the rest. However, in all cases the most abundant peak is located at 160º/170º. Marked differences start to appear from residue 5. Indeed, at ϕ_5 exhibits two peaks at -130º and -50º/-60º. In all cases but in DMSO, the most abundant peak is the one at -60º that corresponds to the type I β-turn. The dihedral angle ψ_5 varies enormously for the different MD trajectories. Thus, for SP in water it exhibits one predominant peak at -30º and a minor peak at 170º. For SPOH in water values are highly distributed exhibiting three peaks at -30º/-20º, at 90º and at 160º, containing the one at -30º almost half of the structures. For SPOH in methanol, the peak at -30º is the least important being the peak at 100º and 160º equally predominant. Finally, in DMSO the peak at -30º has disappeared and the only peaks appearing are at 80º/90º and 170º. Furthermore the peak at 170º is clearly the most abundant peak. Therefore, a gradual change is observed from SP in water to SPOH in DMSO for the decrease in the abundance of the peak at -30º and the increase for the peak at 170º. This change in the

abundance of the peak at -30º correlates with the gradual decrease of type I β-turn proportion from the 81% of SP in water to the absence for SPOH in DMSO that can be observed in Table 5.6 for the dihedral pair 4. Regarding residue 6, the ϕ_6 dihedral angle shows only one peak at -50º/-60º for all except the MD trajectory of SPOH in DMSO. The latter exhibits the predominant peak shifted to -70º and an additional peak at -130º/-120º. The ψ_6 dihedral angle shows a predominant peak at -20º and a secondary peak at 160º/170º for SP in water. For SPOH in water and methanol only the predominant peak at -20º, corresponding to the type I β-turn, is shared. For SPOH in DMSO, the predominant peak now is the one at 160º/170º corresponding to the β-strand, being the peak at -10º/0º residual. Indeed, this translates into SPOH in DMSO presenting only β-strand for the dihedral pair 5 (see Table 5.6), SPOH in water presently almost no β-strand motifs for the same dihedral pair and SP in water having almost 10% of the structures presenting β-strand dihedral angle values. Regarding residue 7, the ϕ_7 dihedral angle shows three peaks around -120º, -60º and 70º for SP in water. The peak at -120º and -60º is shared by the MD trajectories of SPOH in water and methanol. For all these experiments the predominant peak is the peak at -60º. For the MD trajectory of SPOH in DMSO only the peak at -60º is present. The ψ_7 dihedral angle exhibits two peaks for SP in water and for SPOH in methanol at -30º/-20º and 160º/170º and one peak for SPOH in water at -30º. In all cases the peak at -30º is the predominant one. On the contrary, the MD trajectory of SPOH in DMSO exhibits only one maximum at 140º. Regarding residue 8, ϕ_8 dihedral angle shows two peaks at -120º/-110º and at -70º/-60º, being the latter the most abundant peak for all but for the MD trajectory of SPOH in DMSO where only one peak at -130º is present. ψ_8 dihedral angle for the MD trajectory of SP in water exhibits three peaks at -10º, at 120º and 140º/150º, being the one at -10º the predominant one. In the case of the SPOH in water and in DMSO only one peak at 0º/10º is present. SPOH in methanol exhibits two peaks at -10º and 160º/170º. Regarding residue 9, ϕ_9 exhibits three peaks for SP in water, and for SPOH in water and methanol at -60º, 80º and 170º/180º, being the predominant one the one at 80º in all cases but for the SPOH in methanol where the one at -70º is the predominant one. SPOH in DMSO shows only one peak at 80º. Differences in the abundance of the peak at -60º/-70º of ϕ_9 dihedral angle account for the larger proportion of structures exhibiting type I β-turn for SPOH in methanol (50.1%) in comparison with SP in water (20.7%) and for SPOH in water (15.3%). ψ_9 dihedral angle exhibits one peak at 10º for all MD trajectories but one, SPOH in methanol. For the latter, additional secondary peaks appear at -170º, -80º and 70º/80º. However the maximum appears, as for the rest of MD trajectories studied with the peak at 0º. For residue 10, ϕ_{10} dihedral angle exhibits two peaks at -120º and -70º/-60º for all but for the MD trajectory of SPOH in DMSO that exhibits only the peak at -70º. ψ_{10} dihedral angle shows one peak at -20º for SP in water and for SPOH in DMSO. Three peaks are present at -10º, 90º and 170º for SPOH in water and two peaks at -20º and 120º/130º for SPOH in methanol. Finally, the ϕ_{11} dihedral angle shows two peaks at -130º/-120º and the most abundant at -70º/-60º for all but for the MD trajectory in DMSO. In the

latter case only one peak appears at -140º. The larger proportion of structures presenting 3_{10}-versus α-helical turns for SPOH in methanol for residues 6 to 10 cannot be explained by the distributions of the ψ dihedral angle being skewed towards 0º instead of -60º as the superimposition of the distributions for SPOH in water and methanol are highly concordant. Therefore, the larger proportion of structures presenting 3_{10}-helical turns in methanol must be related to the need for fulfilling this requirement for three consecutive residues and this fact cannot be derived by looking at local differences for dihedral pairs.

As a conclusion, we have seen that there are not marked differences between the MD trajectories of SP in water and for SPOH in water and methanol. Some of the differences have been translated into differences in the proportion of structures presenting a given conformational motif as it is the case for type I β-turn on residue 5. It has also been observed that differences in conformational motif proportion that affect several residues cannot always be translated into local differences in the probability function distribution of the implied dihedral angles as it has been the case for the larger proportion of structures presenting 3_{10}-helical turns in methanol. The MD trajectory of SPOH in DMSO presents a larger deviation in the probability function distributions of its dihedral angles than the differences observed within the dihedral angle distributions of the rest of the MD trajectories. This fact is in agreement with the differences that are observed when looking at the conformational motifs proportions (Table 5.6).

In order to compare the results of the present study with the NMR structures in TFE/water (Lee et al., 1999) and in SDS (Keire et al., 1986), patterns corresponding to these structures were calculated and compared with the three more abundant patterns obtained in the MD trajectories of SP in water and SPOH in water, methanol and DMSO (Table 5.16).

The NMR structure obtained in SDS presents a type II β-turn involving residues 4 and 5 and a type I β-turn involving residues 9 and 10. Though the pattern was not sampled during the MD simulations, there are 3 patterns in DMSO containing a type I β-turn at residues 9 and 10, having the rest of the molecule with variable β-strand segments accounting for 0.57% of the molecules. Regarding the structure derived from the NMR study in TFE/water, the conformation proposed agrees well with the structural motifs sampled in the MD simulations in all cases with the exception of the DMSO. Main differences consist in the number of consecutive type I β-turns present, running from residues 5 to 9 in the NMR structure and from residues 5 to 8 (for the two most abundant patterns for SP in water) and 5 to 10 (for the third most abundant pattern for SP in water). For the MD of SPOH in water and methanol the same patterns are observed only differing in that residues 5 or 6 can adopt either β-strand or type I β-turn conformations.

Table 5.16. Summary of secondary structure motifs present in the structures obtained by NMR experiments and the three most abundant patterns for the MD trajectories of SP in water and SPOH in water, methanol and DMSO. Percentages from the total structures of each trajectory are shown in brackets for the most abundant patterns.

RESIDUE NUMBER		2	3	4	5	6	7	8	9	10
NMR SP in TFE/water					I1	I2	H/I2	H/I2	H/I2	
NMR SP in SDS				II1	II2				I1	I2
MD of SP in water	1st (28.82%)	S	S	S	I1	I2	I2	I2		
	2nd(12.11%)				I1	I2	I2	I2		
	3rd (6.33%)	S	S	S	I1	I2	I2	I2	I2	I2
MD of SPOH in water	1st (32.06%)	S	S	S	S	I1	I2	I2		
	2nd(6.18%)	S	S	S	I1	I2	I2	I2		
	3rd (4.34%)				I1	I2	I2	I2		
MD of SPOH in methanol	1st (18.05%)	S	S	S	S	I1	I2	I2	I2	I2
	2nd(9.84%)	S	S	S	S	I1	I2	I2		
	3rd (9.02%)	S	S	S	I1	I2	I2	I2		
MD of SPOH in DMSO	1st (%)	S	S	S	S	S	S			
	2nd(%)	S	S	S						
	3rd (%)				S	S	S			

Comparison of the cluster analysis obtained from the MD trajectory of SP in water and the MD trajectory of SPOH in water, methanol and DMSO suggests that the criteria used to end the clustering process $\Delta\overline{R} > 0.01$ is not affected by the size of the ensemble of patterns to classify (Figure 5.8). Thus, for the MD of SPOH in DMSO although there are only 22 patterns to classify, $\Delta\overline{R}$ is larger than 0.01 when 10 patterns are still remaining. This number is of the same order of magnitude as for the rest of MD trajectories analyzed in the present study with the numbers of patterns to classify around 200. The criteria above mentioned yields in all instances a discrete number of clusters, around 10, irrespective of the initial size of the sample to classify. Thus, the method could be easily automated.

When we look to the clusters we can see differences between the different MD trajectories analyzed. Thus, the structures obtained for the MD of SPOH in water were grouped into clusters where 3_{10}- and α-helical motifs were equally predominant with clusters II and III, containing 21.81% and 19.87% of the structures, being the most abundant clusters containing 3_{10}- and α-helical motifs, respectively. Regarding the MD trajectory of SP in water, the most abundant cluster containing a 3_{10}-helical turn (51.83%) is bigger than the most abundant cluster containing a α-helical turn (16.89%). The third most abundant cluster for SP in water is the cluster containing β-strand dihedral angle values on residues 2 to 8 and containing a single type I β-turn motif at residues 9 and 10. This cluster accounting for 8.78% of the structures is only present in the MD trajectory of SPOH in DMSO but only accounts for 0.58% of the structures. This probably constitutes the most remarkable feature distinguishing SP from SPOH. Regarding the MD of

SPOH in methanol, clusters containing 3_{10}-helical motifs, clusters II (22.19%), III (8.03%) and VIII (1.83%) are more abundant than clusters containing α-helical motifs, clusters V (5.23%), VI (4.34%) and VII (3.57%). Finally, the MD trajectory of SPOH in DMSO has clusters I, II, III and VII exhibiting only β-strand dihedral angle values. These clusters account for 98.9% of the total number of structures of the MD trajectory. An analog to these clusters does not exist for the MD trajectory of SP in water, and accounts only for 0.08% and 5.56% for the MD trajectories of SPOH in water and methanol, respectively.

The study of transitions between consecutive conformations provides a detailed analysis of the relations of vicinity in the conformational space among the different groups of structures. From the study of the most frequent transitions between the different clusters in the MD trajectory of SP in water, it can be inferred that clusters can be grouped into three different classes (Figure 5.10). The largest one is formed by clusters I, IV, VI and VIII. Cluster I contains a β-strand at residues 2 to 4 and type I β-turn at the region running from residues 5 to 10. Cluster IV and VII share in common with cluster I both the β-strand in region 2 to 4 and the type I β-turn at residues 5 to 10. In addition, cluster IV and cluster VI exhibit consecutive α-helical turns and 3_{10}-helical turns extending from residues 5 to 10, respectively. On the other hand, cluster VIII shows a β-strand motif going from residues 2 to 5 and a type I β-turn going from residues 7 to 10.

Another subgroup of clusters is constituted by clusters II and VII. Cluster II exhibits a type I β-turn expanding residues 5 to 8 and a α-helical turn at residues 5 to 7. The main difference in respect to cluster I is the absence of the β-strand motif at the N-terminus of the peptide. This later feature is shared by cluster II and VII. Cluster VII differs from cluster II in the type of helix type that exhibits, 3_{10} instead of α-helix, and that the type I expands from residues 5 to 10, instead of 5 to 8 for cluster II.

The last subgroup of clusters is formed by cluster III, V and IX. All these clusters share in common the presence of a type I β-turn at residues 9 and 10. In addition clusters III and V exhibit a β-strand for residues 2 to 8 and 2 to 5, respectively. Cluster IX, in addition to the type I β-turn at the C-terminus shows another type I β-turn at residues 4 and 5 and a β-strand at residues 6 to 8.

From the study of the evolution of the cluster appearance along the MD trajectory of SP in water one can check the correctness of the subgroups that have been created by the analysis of cluster transition (Figure 5.11). For the MD trajectory, clusters III, V and IX are the first clusters to appear and possibly constitute intermediate folding states. Only cluster V appears after the first 5 nanoseconds, although as a sporadic conformation, probably resultant from partial unfolding of the molecule. From nanosecond 6 the predominant clusters are I, IV, VI and to a lesser extent cluster VIII. Clusters II and VII are the predominant clusters from nanosecond 34 until the end of the MD

trajectory. Clusters that are predominant at each stage of the MD trajectory are in agreement with the subgroups of clusters obtained in the MD trajectory. Thus, indicating that the existence of the subgroups of clusters is explained by the existence of different stages in the folding process. Therefore, the first stage corresponds to a partial folded conformation presenting β-strand dihedral angles in a large proportion of the N-terminus and a type I β-turn at the C-terminus. Cluster I, IV, VI and VIII all share in common the presence of β-strand dihedral angles for residues 2-4 or 2-5. This motif disappears in the last part of the MD trajectory (nanoseconds 34 to 40). The MD trajectory should be extended in order to determine whether the lost of this conformational motif is a temporary situation or is a more stable conformation under the experimental conditions in use. The last part of the MD trajectory is then populated by conformations that only have the type I β-turn at residues 5 to 8 or 5 to 10 and a 3_{10}- or α-helical turn at residues 5 to 8 or 5 to 7.

From the study of the most frequent transitions between the different clusters in the MD trajectory at 300 K two different subgroups of clusters can be distinguished (Figure 5.13). On the one hand, clusters I, IV, V, VI and VIII and on the other, clusters II, III, VII and IX. Between both subgroups transitions only occur from cluster I to cluster II, the two most abundant and account for only a small proportion of their local transitions (0.6 and 1% respectively).

Structures belonging to cluster I are characterized by exhibiting a β-strand between residues 2 to 5 and consecutive type I β-turns in the segment 6 to 9. Clusters IV, V and VIII share in common type I β-turns on residue 6, but not on residue 5, as is the rest of clusters presenting such conformational motif. Structures that belong to cluster VI exhibit only a type I β-turn on residues 7 and 8, and accordingly correspond to a partially unfolded group of structures. Clusters V, VI and VIII are unstable as there are frequent jumps back to the main cluster of the subgroup, cluster I. On the other hand, cluster IV seems to be quite stable as there are numerous jumps onto itself, on 92% of the cases.

Clusters II and III are the most populated clusters of this subgroup (21.8 and 19.9%, respectively). Both, clusters II and III are also the most stable clusters within this subgroup as they jump onto themselves on 84% and 82% of their transitions. Moreover, cluster II jumps with the same frequency to cluster VII and III. Transitions from cluster II to cluster III require both the unfolding of the β-strand of the N-terminal and passing from a 3_{10}- to a α-helical turn, whereas transitions from cluster II to cluster VII only represent the transition from a 3_{10}-helical turn to a α-helical turn.

From the study of the evolution of the cluster appearance along the MD trajectory of SPOH in water one can check the correctness of the subgroups that have been created by the analysis of cluster transition (Figure 5.14). Clusters VI, VIII, XV and XVI are the first clusters to appear in the

MD trajectory. Clusters XV and XVI are only present in less than 0.1% of the structures and contain structures that exhibit only β-strand dihedral angles along the peptide or that do not exhibit any of the conformational motif that have been considered in the present study, respectively. Cluster XVI appears later in the MD trajectory indicating sporadic unfolding of the peptide. Cluster VI and VIII represent partially unfolded states of the peptide exhibiting β-strand dihedral angles at residues 2 to 5 and one or two non-consecutive β-turns at the C-terminus of the peptide. These two clusters are only predominant at the first nanosecond and after the first 20 nanoseconds. In addition, cluster VIII becomes rare after nanosecond 27. After the first nanosecond 4 clusters become predominant: clusters II, III, VII and IX. These clusters constitute a subgroup of clusters that have been determined by the study of the transitions due to the fact that transitions occurring on these clusters are contained within this group (see Figure 5.13). These clusters are characterized by the presence of a helical turn (3_{10} or α) at residues 5 to 7 or 5 to 8. However, on the N-terminus β-strand dihedral angles can be present on residues 2 to 4 (for clusters II and VII) or absent or substituted by an II2 motif (for cluster III and IX, respectively). Clusters II and III are the most stable clusters of this subgroup (84% and 82% of autotransitions) whereas clusters VII and IX are less stable clusters (21 and 20% of their autotransitions). After nanosecond 20, clusters I, V, VI and VIII become the predominant clusters. These clusters together with cluster IV constitute the second subgroup of clusters that have been identified by the study of transitions (see Figure 5.13). All these clusters, except for cluster IV, share in common the presence of β-strand dihedral angles at residues 2 to 5 instead of at residues 2 to 4 as it was the case for clusters II and VII. As a consequence the type I β-turns start in all cases at residue 6 or 7. In this part of the MD trajectory cluster I act as a great basin as it is the most abundant and stable cluster (86% of autotransitions). The only cluster containing helical turns is cluster V (3_{10}) probably indicating that the presence of the β-strand dihedral angle value at residue 5 unfavors the formation of helical turns. Finally, cluster IV is the most abundant cluster for the last 3 ns of the MD trajectory. Cluster IV has as an II2 motif at residue 3 and a type I β-turn at residues 6 to 8. As a conclusion the peptide rapidly folds into the conformation containing a β-strand in the N-terminus and a helical turn in the C-terminus. When the MD trajectory reaches nanosecond 20 the β-strand extend to residue 5 partially disturbing the helical turn on the C-terminus. The last 3 nanoseconds of the MD trajectory are dominated by a conformation not presenting β-strand but an II2 motif and a type I β-turn at residues 6 to 8.

The study of the most frequent transitions between the different clusters in the MD trajectory of SPOH in methanol suggests that clusters can be grouped into three different classes (Figure 5.16). The largest one is formed by clusters I, III, V, VII and VIII. Cluster I contains a β-strand at residues 2 to 5 and a type I β-turn at the region running from residues 6 to 10. Clusters III and V share in common with cluster I a β-strand at residues 2 to 5 and a type I β-turn at residues 6 to 10. In addition, clusters III and V exhibit 3_{10}- and α-helical turns at residues 6 to 10, respectively.

Clusters VII and VIII share in common with cluster I the β-strand at residues 2 to 5. However, they exhibit type I β-turns running from residues 7 to 10, instead of 6 to 10 for cluster I. Furthermore, cluster VIII exhibits 3_{10}-helical turns from residues 7 to 10. Another subgroup of clusters is formed by cluster II and VI. Clusters II and VI differ from cluster I in that they exhibit a β-strand at residues 2 to 4 instead of residues 2 to 5. They also differ from cluster I in the type I β-turn region that starts at residue 5 instead of residue 6. Cluster II and VI exhibit a 3_{10}- and α-helical turns at residues 5 to 8, respectively. In addition, cluster VI shows a type II' β-turn at residues 9 and 10, but it is not a very stable cluster as half of the transitions are into the same cluster and the other half of the transitions end in cluster II. Cluster II is more stable, having 87% of autotransitions. The last subgroup of clusters is formed by cluster IV exhibiting a β-strand expanding residues 2 to 10 and with 88% of autotransitions indicating that the cluster is stable.

From the study of the evolution of the cluster appearance along the MD trajectory of SPOH in methanol one can check the correctness of the subgroups that have been created by the analysis of cluster transition (Figure 5.17). Clusters I, IV and IX are the predominant clusters at the beginning of the MD trajectory. Clusters IV and IX are the clusters containing only β-strand dihedral angles or not containing any conformational motifs, respectively. Cluster I contains β-strand at residues 2 to 5 and a type I β-turn at residues 6 to 10. Clusters III, V, VII and VIII become also predominant together with cluster I from nanosecond 3 to nanosecond 16. All these clusters share in common the β-strand at residues 2 to 5 and a type I β-turn at residues 6 to 10 or 7 to 10. They differ in the presence of 3_{10}-helical turns (cluster III and VIII) and α-helical turns (cluster V) and in the helices starting at residue 6 (cluster III and V) or at residue 7 (cluster VII and VIII). Thus, from the plot depicting transitions between clusters we have assigned a subgroup of clusters formed by cluster I, III, IV, V, VII and VIII. The difference of the residue where the helices leads to a stronger relation between clusters VII and VIII and between clusters III and V. Both groups are related to cluster I that acts as the great basin. Cluster IV, the cluster only containing β-strand dihedral angles appearing at the first two nanoseconds of the MD trajectory is a stable cluster (88% of autotransitions) and transitions only occur with cluster I that is the only cluster together with cluster IX appearing at the beginning of the MD trajectory. Cluster II and VI are the predominant clusters in the MD trajectory from the nanosecond 15. Both clusters form a subgroup of clusters from the analysis of transitions and they differ from the rest of clusters in that the β-strand region expands residues 2 to 4 instead of residues 2 to 5. Whereas cluster II is quite similar to the rest of the predominant cluster presenting a type I β-turn at residues 5 to 10 and 3_{10}-helical turn at residues 5 to 8, clusters VI exhibits a particular turn, type II' β-turn at residues 9 and 10 apart from the type I β-turn and α-helical turn at residues 5 to 7.

From the study of the most frequent transitions between the different clusters in the MD trajectory of SPOH in DMSO we can establish the existence of three different subgroups of

clusters (Figure 5.19). One is formed by clusters I, IV and VI. Cluster I contains a β-strand at residues 2 to 7. Clusters IV and VII share in common with cluster I the β-strand in region 2 to 7. In addition, they exhibit a type I β-turn at residues 9 and 10. Another subgroup of clusters is constituted by cluster II. Cluster II exhibits a β-strand expanding residues 2 to 5 and is a stable cluster as autotransitions amount for 93% of the total number of transitions. The last group of clusters is formed by clusters III and V. Cluster III exhibits a β-strand at residues 5 to 7. Cluster V is the cluster that does not show any conformational motif.

From the study of the evolution of the cluster appearance along the MD trajectory of SPOH in DMSO one can check the correctness of the subgroups that have been created by the analysis of cluster transition (Figure 5.20). On the first nanosecond two clusters are predominant clusters I and IV. Cluster IV exhibits a β-strand expanding residues 2 to 8 and a type I β-turn at residues 9 and 10. Cluster VI appears sporadically and differs from cluster IV in that the β-strand expands residues 2 to 7 and the type I β-turn is located at residues 8 to 10. From that point on, cluster I is the only predominant cluster until nanosecond 11 where cluster III and to a lesser extent cluster V become also populated. The peptide undergoes a transition from a β-strand at residues 2 to 7 to a β-strand at residues 5 to 7 or to a structure presenting no conformational motif from nanoseconds 10 to 13. At nanosecond 14 the peptide adopts a β-strand at residues 2 to 5 (cluster II). Only clusters I, II and III are stable. Cluster IV and VI act as folding intermediates of cluster I and cluster V is a folding intermediate of cluster III. Thus, the subgroups determined by the analysis of transitions justify the predominance of clusters at each stage of the MD trajectory.

The existence of a stereochemical code (Anfinsen, 1973) that could lead from the amino acid sequence to a well defined 3D-conformation has led to a wealth of studies attempting to obtain specific rules for secondary structure prediction from protein sequence (see Gunasekaran et al. 1998 for a list). Peptides have been described as flexible molecules in aqueous solvent based on the difficulty to detect any structural motifs by the use of NMR spectroscopic techniques. Thus, in order to determine the bioactive conformation, i.e. the conformation that will bind to the receptor and exert its biological function, authors have used solvents that are known to stabilize structural motifs, as TFE/water mixes. The analysis of the sequence could give further insight into whether the conformation stabilized by the use of less polar solvents is relevant for the biological activity by looking if the structure of the peptide could be *stereochemically codified* in its sequence. Gunasekaran et al., (1998) reported a study on a set of 250, largely non-homologous, high-resolution proteins structures from the Brookhaven Data Bank in order to determine the propensities of different amino acids at the different positions flanking and contained within the helices. From the analysis of the dihedral angles of the residue ending the helix, they group helices in two types: left-handed (α_L)-terminated and extended (E)-terminated. Their study reinforces the hypothesis that Gly acts as helix terminator in the case of α_L-terminated helices presenting the

motif α_R-α_R-α_R-α_L motif where a succession of three residues in right-handed α-helical conformations is followed by a screw sense reversal at the C-terminal end of the helix. When looking what residues are found at the T+1 position, being T the helix terminator residue Gly they found that His, Asn, Leu and Phe had the greatest propensity. Given the fact, that SP has the Gly^9-Leu^{10} sequence at the C-terminus we have investigated whether the sequence could act as a C-capping motif. The helical capping has also been studied in peptides, and the propensities that are found in peptides are the same that those found in proteins and the effect of Gly as a helix terminator is a common property in both types of molecules (Chakrabartty et al, 1993, Thomas et al., 2001). Thus, we could infer that the Gly^9-Leu^{10} sequence could act ending the helix. From the study of the probability distribution function of dihedral angles (see Annex section and Table 5.15) and from the summary of secondary structure motifs (Table 5.6) we can conclude that the helical motif is substantially disrupted by the presence of Gly^9-Leu^{10} because in all cases there is a clear decrease in the percentage of structures presenting a type I β-turn from Phe^8 to Gly^9 (70.1% to 27.9% for SP in water, 87.6% to 15.3 for SPOH in water and 83.3% to 50.1% for SPOH in methanol). Serrano et al. (1992) proposed that Gly in the terminator position (T) and with a left-handed conformation is largely exposed to solvent. Thus, the introduction of a less polar solvent, like methanol as has been argued above, favors the intramolecular interactions, as in helices, and unfavors the conformation that exposes the polar groups of the backbone to the solvent, left-handed conformation. This would explain the smaller decrease in type I β-turn motif for SP in methanol and also the observation that the ϕ_9 dihedral angle presents as the predominant peak the peak at -70º instead of the peak at 80º as it is the case for SP in water. This environment-dependent conformation of Gly^9 has been observed in other peptides like alamethicin. Indeed, Gibbs et al. (1997) carried out a MD trajectory of alamethicin in methanol. Whereas the peptide adopts a regular α-helix in the crystal structure, in methanol alamethicin establishes 3_{10}-helix hydrogen bonds at a motif containing Gly-Leu and this confers some flexibility and allow for the bending of the peptide around this position. This would be paralleled by SP and SPOH Gly^9-Leu^{10} motif and suggest the existence of a hinge region at the C-terminus of these peptides that could play a critical role in the induced fit of the peptide to its receptor providing flexibility to their structure.

The α_L terminated helix, also known as Schellman motif (Schellman, 1980) is further characterized by the existence of two hydrogen bonds: a 6 $\rightarrow$ 1 hydrogen bond between the N-H group of residue T+1 (Leu^{10} in SP) and the C=O group of residue T-4 (Gln^5) and a 4 $\rightarrow$ 1 hydrogen bond between the N-H group of residue T (Gly^9)and the C=O group of residue T-3 (Gln^6) (Aurora et al., 1994). We have also calculated the probability of having these two additional interactions in the MD trajectory of SP in water. We have found that both interactions are highly abundant (44.5% and 41.4%, respectively) (Table 5.17). Hydrogen bonds were considered when fulfilling the criteria: O···H-N angle lower than 60º and less than 4 Å for the distance between the O and N atoms of the

carbonyl and the amide groups of the backbone. The existence of these interactions between backbone atoms of Leu^{10} and Gln^{5} and of Gly^{9} and Gln^{6} directs the C-terminus of SP, residues Gly^{9}-Leu^{10}-Met^{11}, to residues Gln^{5}-Gln^{6}. This fact has been suggested by Chassaing et al. (1986) for SP in methanol.

Regarding the N-terminus of SP it is remarkable the existence of two Pro, a highly conformationally restricted peptide. MacArthur and Thornton (1991) described the Pro-X-Pro sequence as a sequence favoring an extended conformation. The first Pro and the X residue, where X can be any of the natural amino acids except for Pro, are predominantly adopting a β-strand conformation, whereas the second Pro populates indistinctly the α and β conformations. They also found this sequence never occurring in the centre of α-helices but at the beginning or just before the turn of the helix. In addition, other authors have postulated that Pro residues located in the first turn of helices act as N-capping residues thus stabilizing helices (Richardson et al., 1988). In the case of SP and SPOH, Pro^{2}–Lys^{3} adopts an extended or β-strand conformation as the predominant motif and Pro^{4} can adopt both type I β-turn and β-strand dihedral angles. This is in total agreement with the results obtained by MacArthur and Thornton, thus further suggesting that the peptide has its predominant conformation *stereochemically* determined at both the extended conformation at the N-terminus and the ends of the helical motif at the C-terminus.

Table 5.17. Most abundant backbone hydrogen bonds present in the MD trajectory of SP in water. The definition of hydrogen bond considered is > 120º for the ONH angle and a distance less than 4 Å between N and O atoms.

H-BOND NO.	ATOMS	% OCCUPIED	DISTANCE (Å)	DEVIATION	ANGLE (º)	DEVIATION
I	NH(Phe^{7})…CO(Pro^{4})	78.0	3.07	0.22	20.99	10.71
II	NH(Phe^{8})…CO(Gln^{5})	62.4	3.27	0.28	32.34	15.23
III	NH(Gly^{9})…CO(Gln^{5})	51.0	3.11	0.27	34.17	15.36
IV	NH(Leu^{10})….CO(Gln^{5})	44.5	3.14	0.26	27.29	13.94
V	NH(Phe^{8})…CO(Pro^{4})	42.2	3.32	0.39	22.55	13.93
VI	NH(Gly^{9})…CO(Gln^{6})	41.4	3.37	0.32	28.85	12.39
VII	NH(Leu^{10})…CO(Phe^{8})	20.5	3.35	0.33	47.50	10.99
VIII	NH(Met^{11})…CO(Gln^{5})	19.9	3.44	0.33	25.85	14.52
IX	NH(Met^{11})…CO(Phe^{8})	17.8	3.30	0.32	25.48	14.71
X	NH(Gly^{9})…CO(Phe^{7})	16.9	3.41	0.32	50.49	8.26
XI	NH(Phe^{8})…CO(Gln^{6})	16.5	3.05	0.35	32.17	15.37
XII	NH(Met^{11})…CO(Gly^{9})	15.8	3.26	0.30	51.34	7.84
XIII	NH(Leu^{10}…CO(Phe^{7})	14.5	3.22	0.30	31.65	15.34
XIV	NH(Phe^{7})…CO(Gln^{5})	13.0	3.18	0.25	51.92	7.38

5.7. Conclusions to chapter 5

The present study is a combined approach using NMR and MD studies on the amidated (SP) and the free acid form (SPOH) of substance P. The aim is to characterize structurally both peptides under different solvent conditions. The ^{1}H-NMR experiments were carried out on SPOH in water and methanol. From these experiments it is suggested that the peptide does not adopt a rigid conformation. The MD studies suggest that both SP in water and SPOH in water and methanol adopt an ensemble of conformations characterized by the presence of an extended N-terminus affecting the 3 first residues and from that point onwards the peptide would adopt a flexible helix that would interconvert between α- and 3_{10}-helical conformations. These results are in agreement with the results that had been previously obtained for SP in a TFE/water mix and for SP in methanol. Some authors have suggested that helical peptides are plastic structures and could be in rapid interconversion of a wide range of helix-like conformers as a function of their molecular environment (Topol et al., 2001). Results obtained in the present study agree with this picture for SP and SPOH.

On the other hand, Gly^{9} would induce a left-handed helix termination at the C-terminus. The end of the helix at the C-terminus would be folded in a Schellman motif pointing the C-terminus to the central part of the peptide (Gln^{5}-Gln^{6}). The helix would fry from that point onwards (Gly^{9}), being methanol the solvent where SPOH exhibits a greater propensity for helix continuation at Gly^{9}. Gly residue terminating a left-handed helix is largely exposed to solvent. The introduction of a less polar solvent, like methanol would favor intramolecular interactions, as in helices, and unfavors the conformation that exposes the polar groups of the backbone to the solvent, i.e. left-handed conformation. In addition, we suggest that the Gly^{9}-Leu^{10} sequence in SP could act in the same manner as in alamethicin introducing flexibility at the C-terminus of the peptide. This could play a critical role in the induced fit of the peptide to its receptor allowing for the unfolding of the Schellman motif directing the C-terminus to the receptor.

Regarding the N-terminus of SP, the existence of the Pro-X-Pro sequence favors an extended conformation. Pro^{2} and Lys^{3} residues are predominantly adopting a β-strand conformation, whereas Pro^{4} can adopt α-helical and β-strand conformations. This is in total agreement with what had been described for the Pro-X-Pro motif. Furthermore, this motif had been proposed to be at the beginning or just before the turn of the helix and given the known function of Pro as N-capping residue this suggest that the presence of this sequence has a clear structural function. Thus, Pro^{2}, Pro^{4}, Gly^{9} and Leu^{10} would play a critical role in conferring the structural properties of SP. This is in agreement of the existence of a stereochemical code formulated by Anfinsen (1973). Thus, the absence of a unique conformation in water of the peptide cannot be

thought of it as not having structure. On the contrary, the peptide would adopt a restricted group of conformations presenting flexible motifs that would interconvert easily.

On the other hand, SPOH has also been studied through MD with explicit DMSO. The peptide is extended and rigid under such conditions and this is consistent with studies that have pointed out DMSO as responsible for the disruption of unstable hydrogen bonds and the reduction in the number of backbone conformations.

We have used in the present work a methodology developed *in house* for classification (CLASICO) and clustering of structures based on information theory (CLUSTERIT) that efficiently group structures upon their structural similarity. This method has proven to be a useful tool in the analysis of the evolution of a peptide through an extended MD. The use of this tool has also allowed for the study of the transitions that take place along the MD trajectories. This methodology could be used in peptides or proteins without any size restriction and could be easily automated.

5.8 References to chapter 5

Aurora, R., Srinivasan R. and Rose, G.D. *Science*, 264, 1126-1130, (1994).

Bodkin, M.J. and Goodfellow, J.M. *Biopolymers*, 39, 43-50, (1996).

Brooks,C.L.,III and Nilsson, L. *J. Am. Chem. Soc.*, 115, 11034-11035, (1993).

Case, D.A., Pearlman, D.A., Cadwell, J.W., Cheatham III, T.E., Ross, W.S., Simmerling, C.L., Darden, T.A., Merz, K.M., Stanton, R.V., Cheng, A.L., Vincent, J.J., Crowley, M., Ferguson, D.M., Radmer, R.J., Seibel, G.L., Singh, U.C., Weiner, P.K. and Kollman, P.A. (1997), *AMBER 5*, University of California, San Francisco.

Chakrabartty, A., Doig, A.J. and Baldwin, R.L. *Proc. Natl. Acad. Sci. USA*, 90, 11332-11336, (1993).

Chassaing G., Convert O. and Lavielle S., *Eur. J. Biochem.*, 154, 77-86, (1986).

Cornell, W.D., Cieplak, P., Bayly, C.I., Gould, I.R., Merz, K.M. Jr., Ferguson, D.M., Spellmeyer, D.C., Fox, T., Caldwell, J.W. and Kollman P.A. *J. Am. Chem. Soc.*, 117, 5179-5197, (1995).

Coutinho, E., Kamath, S., Saran, A. and Srivastava, S. *J. Biomol. Struct. Dyn.,* 16(3) 747-755 (1998).

Daura, X., Gademann, K., Schäfer, H., Jaun, B., Seebach, D. and van Gunsteren, W.F. *J. Am. Chem. Soc.*, 123, 2393-2404, (2001).

Daura, X., Jaun, B., Seebach, D., van Gusteren, W.F. and Mark, A.E. *J. Mol Biol.*, 280, 925-932, (1998).

Daura, X., van Gunsteren, W.F. and Mark, A.E. *Prot. Struct. Funct. Genet.* 34, 269-280, (1999)

Duan, Y. and Kollman, P.A. *Science.* 282, 740-744, (1998).

Duan, Y., Wang, L. and Kollman, P.A. *Proc. Natl. Acad. Sci. USA*, 95(17), 9897-902, (1998).

Dwyer, D.S. *Biopolymers*, 49, 635-645, (1999).

Erne, D., Rolka, K. and Schwyzer, R. *Helv. Chim. Acta*, 69, 1807-1816 (1986).

Fournier, A., Couture, R., Regoli, D., Gendreau, M. and St-Pierre, S. *J. Med. Chem.*, 25, 64-68, (1982).

Fox, T. and Kollman, P.A. *J. Phys. Chem. B*, 102, 8070-8079, (1998).

Frisch, M. J., Trucks, G. W., Schlegel, H. B., Gill, P. M. W., Johnson, B. G., Robb, M. A., Cheeseman, J.R., Kieth, T.A., Petersson, G.A., Montgomery, J.A., Raghavachari, K., Al-Laham, M.A., Zakrzewski, V.G., Ortiz, J.V., Foresman, J.B., Cioslowski, J., Stefanov, B.B., Nanayakkara, A., Challacombe, M., Peng, C.Y., Ayala, P.Y., Chen, W., Wong, M.W., Andres, J.L., Replogle,

E.S., Gomperts, R., Martin, R.L., Fox, D.J., Binkley, J.S., DeFrees, D.J., Baker, J., Stewart, J.P., Head-Gordon, M., Gonzalez, C., Pople, J.A. (1995), *GAUSSIAN94***,** Gaussian, Inc., Pittsburgh, PA.

Gunasekaran, K, Nagarajaram, H.A., Ramakrishnan, C. and Balaram, P. *J. Mol. Biol.*, 275, 917-932, (1998).

Hamada, D. and Goto, Y. *J. Mol Biol.*, 269, 479-487, (1997).

Hamada, D., Kuroda, Y., Tanaka, T and Goto, Y. *J. Mol. Biol.*, 254, 737-746, (1995).

Hirota, N., Mizuno, K. and Goto, Y. *J. Mol. Biol.*, 275, 365-378, (1998).

Hummer, G., García, A.E. and Garde, S. *Prot. Struct. Funct. Genet.*, 42, 77-84, (2001)

Jorgensen, W.L. *BOSS, version 4.2*; Yale University: New Haven, CT, 2000.

Jorgensen, W.L., Maxwell, D.S. and Tirado-Rives, J. *J. Am. Chem. Soc.*, 118, 11225-11236, (1996).

Kinoshita, M., Okamoto, Y. and Hirata, F. *J. Am. Chem. Soc.*, 122, 2773-2779, (2000).

Lee, S., Suh, Y.H., Kim, S. and Kim, Y. *J. Biomol. Struct. Dyn.*, 17(2), 381-391 (1999).

Lide, D.R. *Handbook of Chemistry and Physics.* 76th Edition. CRC Press, Inc. 1995 Boca Raton. pp. 8-64.

Lide, D.R. *Handbook of Chemistry and Physics.* 76th Edition. CRC Press, Inc. 1995 Boca Raton. pp. 14-15.

Liu, H. Y.; Muller-Plathe, F.; van Gunsteren, W. F. *J. Am. Chem. Soc.*, 117, 4363-4366, (1995).

Manavalan P. and Momany, F.A. *Int. J. Pept. Protein Res.*, 20, 351-365, (1982).

Manavalan, P. and Momany, F.A. *Pept. Synth. Struct. Proc. Am. Pept. Symp. 7th*, 713-716, (1981).

Mehlis B., Rueger, M., Becker, M., Bienert, N., Niedrich, H. and Oehme, P. *Int. J. Pept. Protein Res.*, 15, 20-28 (1980).

Mehlis, B., Boehm, S., Bechker, M. and Bienert, M. *Biochem. Biophys. Res. Commun.*, 66, 1447-1453, (1975).

Miyazawa, T., *Kagaku Kyoiku*, 32, 18-21, (1984).

Murokoshi, T., Yangisava, M. Kitada, C., Fujino, M., and Otsuka, M. *Eur. J. Pharmacol.* 90, 133-137, (1983).

Nikiforovich, G.V., Balodis,I Yu and Cipens, G. *Bioorg. Khim.* 7, 645-654, (1981).

Patel, A.B., Srivastava, S. , Phadke, R.S., *J. Biomol. Struct. Dyn.*, 19,129-138, (2001)

Ramirez-Alvarado, M., Blanco, F.J., Serrano, L. *Nature Struct. Biol.,* 3, 604-612, (1996).

Richardson, J.S. and Richardson, D.C. *Science*, 240, 1648-1652, (1988).

Rizo, J., Blanco, F.J., Kobe, B., Bruch, M. and Gierasch, L.M. *Biochemistry*, 32, 4881-4894, (1993).

Rolka, K., Erne, D. and Schwyzer R. *Helv. Chim. Acta*, 69, 1807-1816, (1986).

Schellman, C. In *Protein folding* (Jaenicke, R.,ed.), pp. 53-61, Elsevier/North-Holland, New York.

Schwyzer, P., Erne D. and Rolka, K. *Helv. Chim. Acta*, 69, 1789-1797, (1986).

Serrano, L., Sancho, J., Hirshber, M. and Fersht, A.R. *J. Mol. Biol.*, 227, 544-559, (1992).

Shimizu, S. and Shimizu, K. *J. Am. Chem. Soc.*, 121, 2387-2394, (1999).

Shukla, D.R. and Mahajan, S. *Proteins*, 85-95, (1991).

Smythe, M.L., Huston, S.E. and Marshall, G.R. *J. Am. Chem. Soc.*, 117, 5445-5452, (1995).

Sumner S.C., Gallagher, K.S., Davis, D.G., Covell, D.G., Jernigan, R.L. and Ferretti, J.A. *J.Biomol. Struct. Dyn.*, 8, 687-707, (1990).

Topol, I.A., Burt, S.K., Deretey, E., Tang, T.H., Perczel, A., Rashin, A. and Csizmadia I.G. *J. Am. Chem. Soc.,* 123, 6054-6060, (2001).

Vass, E., Láng, E., Samu, J., Majer, Zs., Kajtár-Peredy, M., Mák, M., Radics, L., Hollósi, M. *J. Mol. Struct.*, 440, 59-71, (1998).

Wiliams, R.W. and Weawer, J.L. *J. Biol. Chem.*, 265, 2505-2523, (1990).

Wishardt, D.S. and Sykes, B.D. *Methods Enzymol.*, 239, 363-392, (1994).

Wüthrich, K. *NMR of Proteins and Nucleic Acids;* John Wiley & Sons: New York, 1986.

Wymore, T. and Wong, T.C., *Biophys. J.*, 76, 1199-1212, (1999).

Young, J. K., Anklin, C., Hicks, R.P. *Biopolymers*, 34, 1449-1462, (1994)